Engineering Journal

American Institute of Steel Construction

Second Quarter 2011 Volume 48, No. 2

Performance of the Unified Block Shear Equation for Common Types of Welded Steel Connections

STEVEN A. OOSTERHOF and ROBERT G. DRIVER

ABSTRACT

Block shear describes a steel connection failure mode in which a combination of tensile and shear failures along perpendicular planes results in a block of material being displaced from a member. This behavior has been observed to govern the design of many bolted connections and has been well researched, resulting in design equations of various forms. Certain arrangements of welded connections are also susceptible to block shear. This paper reports on the potential application of a "unified" block shear equation, proposed by Driver et al. (2006) for bolted connections, to various welded connections. Experimental results for welded steel lap plate connections loaded concentrically in tension are examined. The results of these tests are used to describe the connection behavior and to evaluate the performance of several design equations, including the proposed "unified" equation. The application of the unified equation to welded connections of slotted hollow structural sections (HSS) and to coped beams supported at their ends by a clip angle welded to the beam web.

Keywords: block shear, coped beams, slotted HSS connections, welded connections.

Block shear describes a failure mode observed in some steel connections in which a combination of tensile and shear failures along perpendicular planes results in a block of material being displaced from a member. This behavior has been observed to govern the design of many bolted connections, because the removal of material for bolt holes outlines a block of reduced net area along which failure may occur. The problem of block shear in bolted connections has been well researched, resulting in design equations of various forms.

In addition to bolted connections, however, certain arrangements of welded connections are also susceptible to block shear. As described subsequently, this failure mode has been observed to govern in both experimental and analytical studies of welded connections, wherein a block of material defined by a perimeter adjacent to the weld toes defines the failure region. Research in this area is limited, and current North American design specifications do not explicitly address this case. The direct application of existing design criteria often results in inaccurate capacity predictions.

Steven A. Oosterhof, Ph.D. candidate, Department of Civil and Environmental Engineering, University of Alberta, Edmonton, AB, Canada (corresponding). E-mail: sao@ualberta.ca

Robert G. Driver, Ph.D., P.Eng., Professor and Associate Chair, Department of Civil and Environmental Engineering, University of Alberta, Edmonton, AB, Canada. E-mail: rdriver@ualberta.ca

This paper reports on the potential application of the "unified" block shear equation, proposed by Driver et al. (2006) for bolted connections, to various welded connections. Experimental results for welded steel lap plate connections loaded concentrically in tension are examined. The results of these tests are used to describe the connection behavior and to evaluate the performance of several existing design equations, including the unified equation. The application of the unified equation to welded connections of slotted hollow structural sections is also presented and discussed. Finally, the unified equation is considered for the case of coped beams supported at their ends through a clip angle welded to the beam web.

EXISTING BLOCK SHEAR DESIGN EQUATIONS

AISC 2005 Specification

Although the current block shear provisions in North American design specifications do not explicitly address the case of welded connections, the equations provided can reasonably be so applied. In the 2005 AISC *Specification for Structural Steel Buildings* (AISC, 2005), hereafter referred to as AISC 2005, a nominal block shear capacity, R_n, is calculated to account for rupture along the tension face and simultaneous yielding or rupture of the shear face(s), as given by the lesser of the following two equations:

$$R_n = 0.6F_yA_{gv} + U_{bs}F_uA_{nt} \quad (1)$$

$$R_n = 0.6F_uA_{nv} + U_{bs}F_uA_{nt} \quad (2)$$

where

F_y = specified minimum yield stress
F_u = specified minimum tensile strength
A_{gv} = gross area subject to shear
A_{nv} = net area subject to shear
A_{nt} = net area subject to tension
U_{bs} = reduction coefficient; taken as 1.0 for uniform tensile stress and 0.5 for nonuniform tensile stress

If this method is applied to typical welded connections, Equation 1 governs because the absence of bolt holes causes the net and gross areas to be equal. A resistance factor of 0.75 is applied for load and resistance factor design.

Unified Block Shear Equation

Based on an extensive experimental database compiled from the literature by Kulak and Grondin (2001), Driver et al. (2006) demonstrated that a "unified" block shear equation can be used for a wide variety of bolted connection types to provide capacity predictions that are more consistent with experimental observations than other methods, thus resulting in more consistent structural reliability. The unified block shear equation takes the following form:

$$R_n = 0.6\frac{F_y + F_u}{2}A_{gv} + U_t F_u A_{nt} \quad (3)$$

where

U_t = equivalent tensile stress factor

The equivalent stress factor accounts for nonuniform stress distributions that develop as a result of eccentric loading or asymmetrical blocks, and thus its value depends on the connection type being considered (Driver et al., 2006).

The unified equation has been adopted into the current edition of the Canadian standard, CAN/CSA-S16-09 *Design of Steel Structures* (CSA, 2009), hereafter referred to as CSA-S16-09. The standard contains a table of U_t values for a selection of connection types and specifies a value of 1.0 for symmetrical blocks with concentric loading. A resistance factor of 0.75 is used with the unified equation.

CONCENTRICALLY LOADED LAP PLATE CONNECTIONS

The case of concentrically loaded welded steel lap plate connections is examined because of its frequent occurrence in applications such as trusses and braced frames in buildings. Fifteen specimens tested to failure were considered: 11 from research reported by Topkaya (2007) and an additional 4 carried out by Oosterhof and Driver (2008) as part of the current research. The latter tests, described in the following section, serve to expand the available data set, providing a unique sample of materials and geometries designed to fail at significantly higher loads than those observed by Topkaya.

Experimental Program

A comprehensive description of the test specimens, material properties, test setup, instrumentation, and test procedures

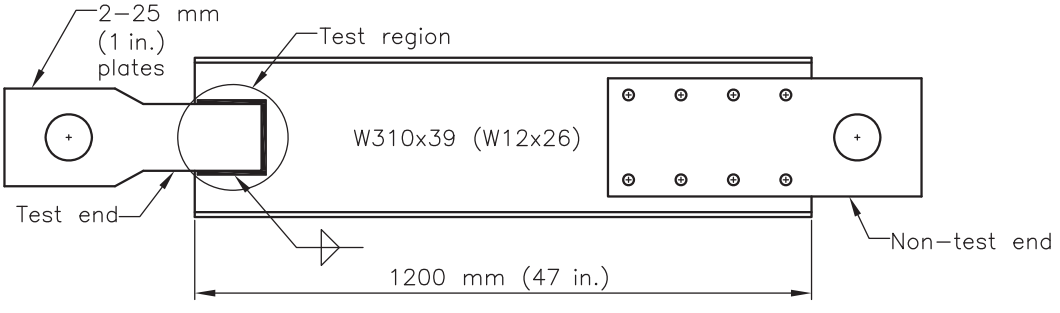

Fig. 1. General arrangement of test specimens.

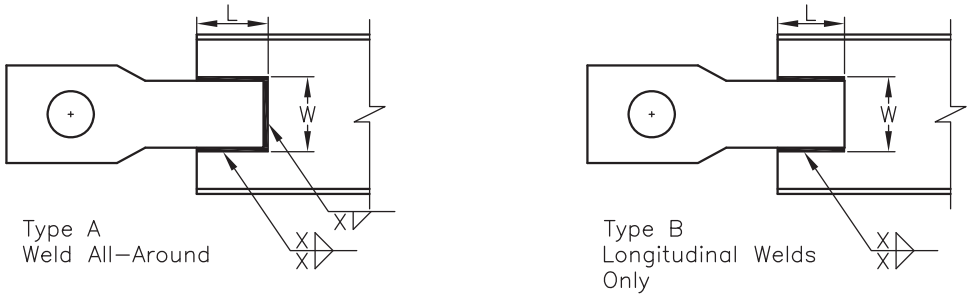

Fig. 2. Test region parameters.

Table 1. Summary of Welded Lap Plate Specimen Parameters and Test Results									
Specimen ID	Weld Type†	Weld Size (mm)	As-built		Block Material Thickness (mm)	Material Properties		Test Failure Load (kN)	Displacement at Failure (mm)
			Length, L† (mm)	Width, W† (mm)		F_y (MPa)	F_u (MPa)		
W1	A	10	146.5	150.4	6.2	379	472	1006	5.9
W2	B	12	144.7	152.2	6.2	379	472	941	4.1
W3	A	10	201.4	103.7	6.2	379	472	1005	6.0
W4	B	10	200.1	100.0	6.2	379	472	963	4.7
Data reported by Topkaya (2007)									
1	A	7	50	60.3	4	309	402	216	—
2	A	7	95.3	57.5	4	309	402	314	—
3	A	7	98.3	77.5	4	309	402	347	—
4	A	7	150.3	78.6	4	309	402	430	—
5	A	7	49.3	98.8	4	309	402	295	—
6	A	7	96	97.8	4	309	402	395	—
7	A	7	150	99.9	4	309	402	475	—
8	A	7	47.3	148.8	4	309	402	386	—
9	A	7	96	148.2	4	309	402	467	—
10	B	7	101.3	56.4	4	309	402	306	—
11	B	7	149.3	98.2	4	309	402	433	—
† Refer to Figure 2; Note: 1 in. = 25.4 mm; 1 ksi = 6.895 MPa; 1 kip = 4.448 kN									

for the experimental program is reported by Oosterhof and Driver (2008). The following provides a summary of the main parameters.

Description of Test Specimens

Figure 1 shows the general arrangement of the test specimens, which consisted of two lap plates fillet welded to either side of the web of a wide-flange section. The connection was designed to be loaded concentrically in tension and to fail by tearing of a block of material from the 5.8-mm (0.23-in.)-thick web of the wide-flange tension member, in the area labeled "test region" in the figure. The bolted "non-test end" of the specimen was designed with a wide gauge to induce a relatively uniform stress distribution, as would be expected in a longer tension member. Figure 2 defines the parameters in the test region that differentiate the test specimens, namely, connection geometry and weld arrangement. Connection block length-to-width ratios, L/W, of approximately 2:1 and 1:1 were chosen, with the lengths and widths being measured to include the legs of the fillet welds. Connection plates were either welded all-around (type A) or only longitudinally (type B). As-built dimensions are summarized in Table 1.

Material Properties

All material meets the requirements of ASTM A572 Grade 50 and CAN/CSA-G40.21 Grade 350W steel. Tension coupon tests were performed to determine the relevant material properties of the webs of the tension members—all cut from the same piece—with mean values obtained as follows: $F_y = 379$ MPa (55.0 ksi), $F_u = 472$ MPa (68.5 ksi) and $E = 206{,}800$ MPa (30,000 ksi). The mean rupture strain was 32.1% on a 50-mm gauge length.

Test Procedure

The specimens were loaded in tension in a 6600-kN (1.5 million-lb) universal testing machine (4000 kN in tension). All tests were conducted using stroke control at a rate of 0.5 mm/min (0.02 in./min). Specimens were loaded beyond their maximum capacity until the block of failed material was pulled completely apart from the web or until the applied load had decreased significantly from its peak value. Further details are provided by Oosterhof and Driver (2008).

Test Results

All four test specimens failed in block shear. Figure 3a shows typical whitewash flaking patterns formed during loading, providing an indication of strain and, indirectly, stress distributions. Rupture of the tension surface of the block preceded that of the shear surfaces in all specimens. Material rupture was typically initiated at the ends of the longitudinal welds (near the corners of the lap plates), as shown in Figure 3b. The tear then propagated toward the center of the specimen under continued loading. For all specimens, it was observed that tension failure occurred on a curved, and often irregular, surface. Figure 3c shows a specimen after complete rupture of the block.

Load versus block displacement curves for each test are shown in Figure 4. These curves show consistent loading and unloading patterns and clearly identifiable yield and ultimate loads. The observed failure mode was quite ductile, with block displacements at the ultimate load ranging from

(a) *(b)* *(c)*

Fig. 3. Typical yield and rupture patterns: (a) typical strain distribution pattern; (b) tear development on tension face; (c) failed connection.

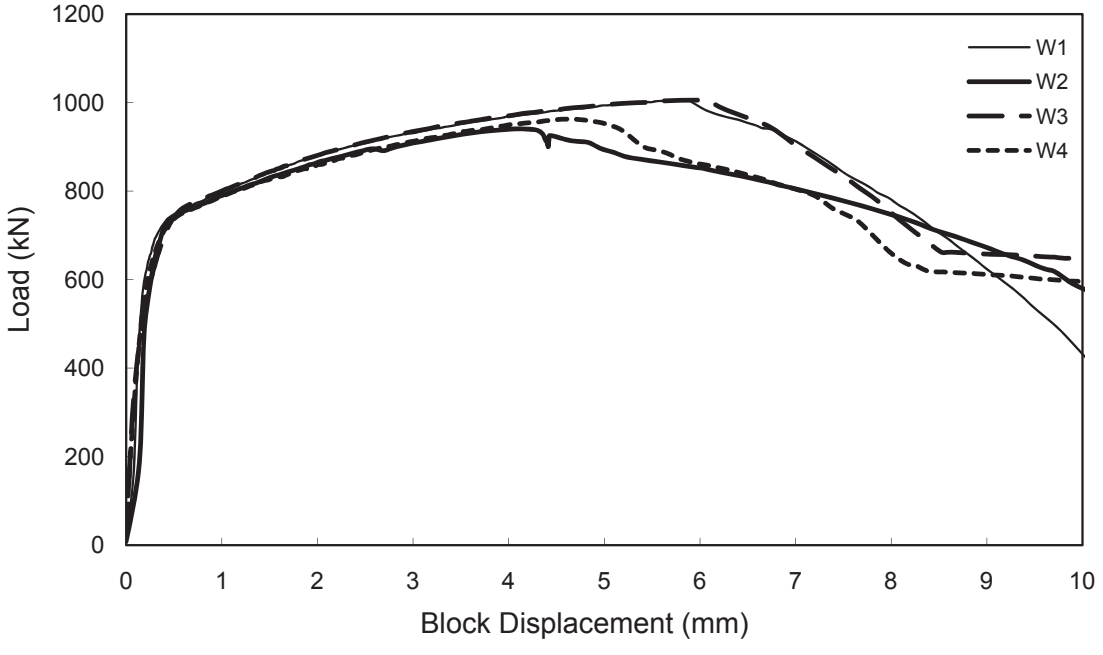

Fig. 4. Load versus block displacement curves for tested lap plate connections.

Table 2. Test-to-Predicted Ratios for Concentrically Loaded Lap Plate Connections							
Experimental Program	Number of Tests	AISC 2005		Topkaya's Equation		Unified Equation $U_t = 1.25$	
		Mean	COV	Mean	COV	Mean	COV
Oosterhof and Driver (2008)	4	1.14	0.029	0.93	0.029	0.99	0.032
Topkaya (2007)	11	1.26	0.042	1.01	0.042	1.07	0.045
Weighted Statistics	15						
Mean		1.20		0.97		1.03	
Coefficient of variation		0.036		0.036		0.039	
Maximum		1.34		1.07		1.15	
Minimum		1.10		0.90		0.94	

10 to 16 times those at first yield. The type A specimens exhibited slightly greater ductility than type B, although this small difference is not considered to be of consequence in this study. A summary of the ultimate failure loads is shown in Table 1, along with the results from the similar tests by Topkaya (2007).

Discussion of Observed Behavior

The curved failure surface observed on the tension faces of all failed members, as seen in Figure 3c, is an important characteristic differentiating the behaviors of welded and bolted connections. The block shear failure perimeter in bolted connections typically follows a straight line between bolt holes, because the removed material defines a reduced net area that is most susceptible to failure. Conversely, the curved failure surface observed in the welded connections increases the physical perimeter of the block, effectively engaging a greater area of material than considered in existing capacity equations. This is considered to be the primary reason the welded connections tested had significantly higher block shear capacities than those calculated by equations derived for bolted connections, as discussed in the following sections.

Performance of Existing Capacity Equations

Table 2 summarizes the test-to-predicted ratios for the AISC 2005 provisions, the unified equation (discussed in the next section) and an equation proposed by Topkaya (2007) for block shear of welded connections. In applying these equations, the block perimeter is taken as lying adjacent to the weld toes that define the potential failure surface. The tests performed by Oosterhof and Driver (2008) resulted in significantly higher failure loads than those performed by Topkaya (2007), and, as indicated in Table 2, the larger-scale specimens have appreciably lower test-to-predicted ratios. Recognizing the significance of the apparent difference in behavior between the two sets of specimens, the weighted mean test-to-predicted ratios are also shown in Table 2, giving 50% weight to the 4 larger-scale tests and 50% to the 11 smaller-scale tests. Test-to-predicted ratios for the individual tests are presented by Oosterhof and Driver (2008).

Figure 5a shows that AISC 2005 consistently underestimates block shear capacity for this type of welded connection. While this is conservative, the inaccuracy is significant and may lead to inefficient designs.

Having observed this incongruity, Topkaya (2007) proposed the following design equation based on physical tests and numerical analyses, which provides significantly improved results:

$$R_n = \frac{F_u}{\sqrt{3}} A_{gv} + 1.25 F_u A_{gt} \quad (4)$$

where all variables have been defined previously. (Note that $1/\sqrt{3}$ is expressed as 0.6 in Equations 1, 2 and 3.) According to Topkaya, the coefficient 1.25 in the second term of this equation accounts for triaxial stress effects on the tensile plane, resulting in significantly higher capacities than those predicted by preexisting design equations. However, Figure 5 suggests that while Equation 4 is accurate for the specimens tested in the research program of Topkaya (2007), it may overestimate the strengths of large-scale connections, as evidenced by the fact that the capacities of the four specimens tested by Oosterhof and Driver (2008) are overestimated by up to 10%.

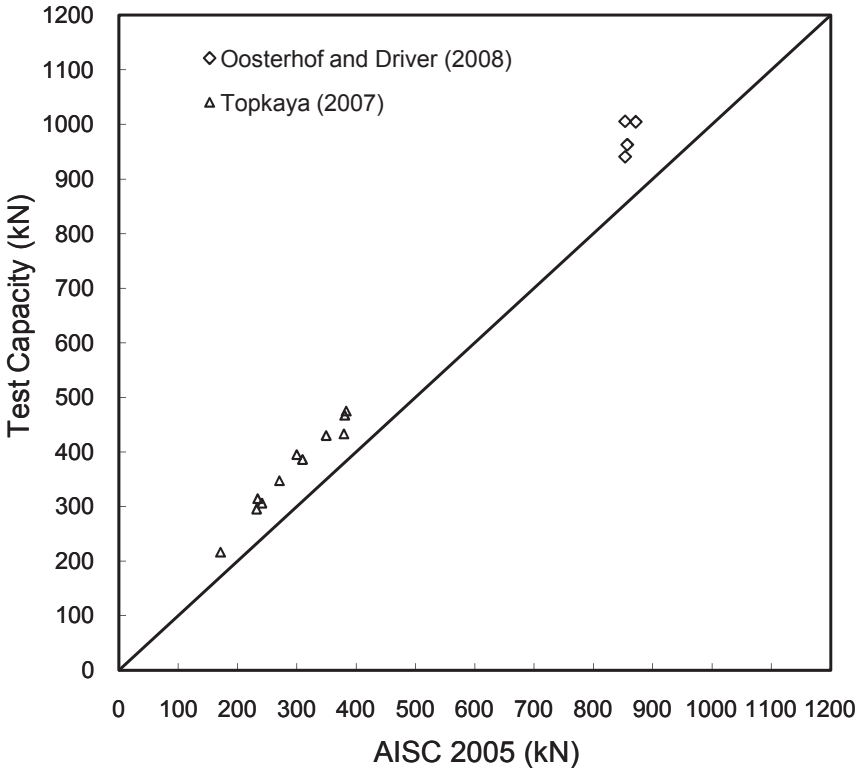

(a)

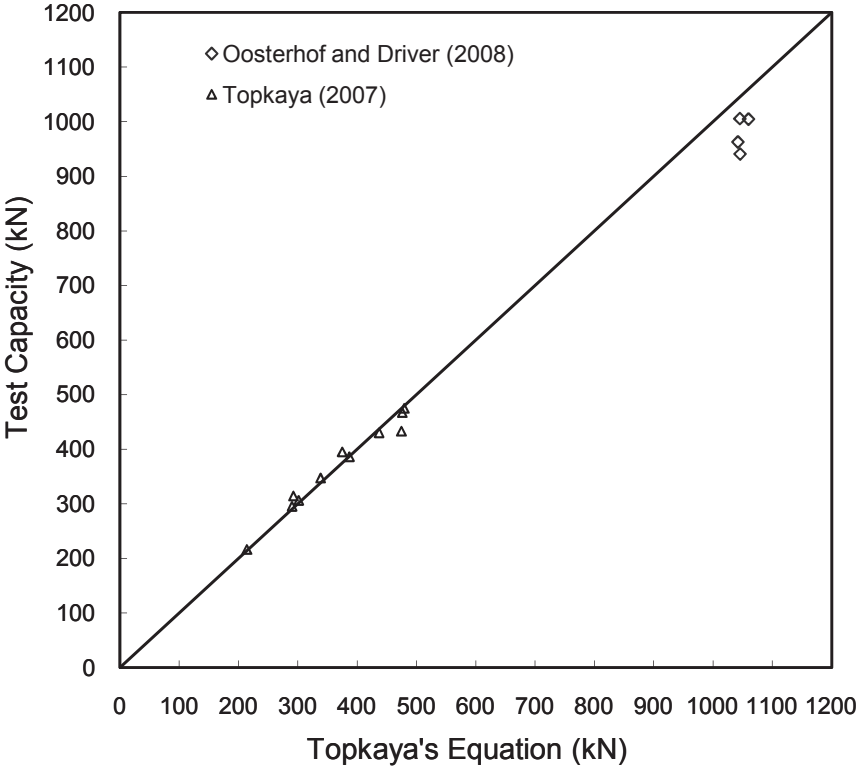

(b)

Fig. 5. Comparisons of design equations and experimental results for welded lap plate connections.

Performance of Unified Equation

Equivalent Stress Factor

The unified equation (Equation 3) has been shown by Driver et al. (2006) to address inconsistencies in block shear strength predictions associated with existing design specifications. The equivalent stress factor, U_t, allows the equation to be adjusted to account for the presence of nonuniform stress distributions present among various connection configurations. For the welded connections studied in this investigation, Oosterhof and Driver (2008) propose that a value of $U_t = 1.25$ is appropriate for design, because it produces test-to-predicted ratios near unity for the tests considered. This proposal implies that the capacity of the tension plane, which was observed to initiate failure, is expected to increase from the nominal value by about 25% due to a combination of triaxial stress effects and a nonlinear failure path. (Test results show that these effects dominate over a possible capacity decrease that would be caused by the nonuniformity of the stress field.) The resulting capacity equation is consistent with Equation 4, proposed by Topkaya (2007), which also includes a factor to increase tension resistance by 25%.

It is shown in Figure 5 that the application of the unified equation to welded lap plate connections, as proposed by Oosterhof and Driver (2008), achieves considerably improved predictions of the test results as compared to AISC 2005 and slightly more consistent agreement for the two individual sets of test data than the equation proposed by Topkaya (2007).

Reliability Study

Principles of limit states design (or load and resistance factor design) include the statistical determination of failure probability, which can be controlled by the selection of a target reliability index, β. To achieve the target level of safety, an appropriate resistance factor, ϕ, is applied to reduce the predicted capacity. For this study, the resistance factor was calculated based on the method of Ravindra and Galambos (1978), using the same approach as that discussed in detail by Franchuk et al. (2004).

The relevant parameters required to calculate the resistance factor are the material, geometry and professional factors (ρ_M, ρ_G and ρ_P, respectively), and their associated coefficients of variation (V_M, V_G and V_P, respectively). The material and geometry factors are the ratios of mean

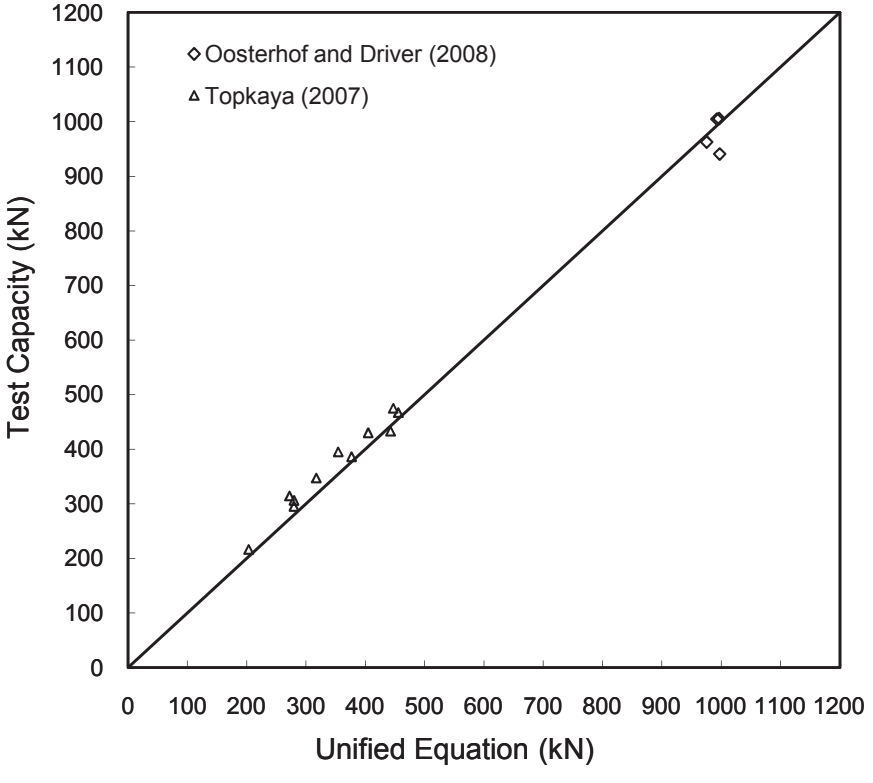

(c)

Fig. 5 (cont.). Comparisons of design equations and experimental results for welded lap plate connections.

Table 3. Summary of Reliability Parameters: Lap Plate Connections			
Parameter	**Value**		
ρ_M	1.05		
ρ_G	1.00		
ρ_P	1.03		
V_M	0.063		
V_G	0.050		
V_P	0.039		
ϕ	0.70	0.75	0.80
β	5.1	4.6	4.1

measured-to-nominal values. The professional factor is the mean test-to-predicted strength ratio for available test results, with the implied presumption that the tests are broadly representative of cases encountered in practice.

The predicted block shear resistance of a steel connection is a function of both the yield and ultimate strengths of the material, and in both cases the mean strengths are generally greater than the nominal values. For the material parameters used in the reliability study, it is conservative to use the values for the static yield strength because the material factor for yield strength is lower and the coefficient of variation higher than those for the ultimate strength. For plates ranging in thickness from 10 to 20 mm (0.4 to 0.8 in.), Schmidt and Bartlett (2002) propose values of 1.07 and 0.054 for the static yield strength material factor and associated coefficient of variation, respectively (values for thinner plates were not reported). For the static yield strength of webs of rolled W-shapes, they recommend values of the material factor and coefficient of variation of 1.05 and 0.063, respectively. Thus, because the two cases give similar material parameters, a slightly conservative approach that can be considered generally suitable for this type of lap plate connection is to use the values for the webs of rolled shapes, providing the lower material factor and the higher coefficient of variation.

The parameters affecting the block shear geometry factor are the material thickness and block perimeter. Block perimeter variability for these welded connections is likely increased somewhat from that of bolted connections, because it depends on both the fabricated size of the lap plates and the weld dimensions. Insufficient data are currently available to determine the overall geometry factor and coefficient of variation for welded lap plate connections. As such, values reported by Hardash and Bjorhovde (1984) for bolted gusset plates are used: geometry factor equal to 1.00 and coefficient of variation equal to 0.050. The proposed geometry factor is believed to be conservative; for example, Zhao and Hancock (1995) reported a value of 1.47 for the weld throat geometry factor in a similar reliability study indicating larger weld sizes than nominal (likely a combination of leg size and face reinforcement). Data reported by Callele et al. (2009) and others also reflect the tendency of welds to be deposited slightly oversized. The variability of the weld size as deposited may be somewhat greater than reflected in the value of the coefficient of variation used, although the weld leg size would constitute the smaller part of the total block perimeter. The geometry factor is also lower and the coefficient of variation higher than the values reported for bolted connections by Franchuk et al. (2004) of 1.017 and 0.039, respectively.

The professional factor is the mean test-to-predicted ratio, with the predicted values determined using measured material and geometric properties. It thus acts as an indication of the level of agreement between the design equation and experimental results. As shown in Table 2, the mean test-to-predicted ratio for the unified equation is 1.03, and the coefficient of variation of these ratios is 0.039.

Using the parameters discussed previously, reliability indices are determined for resistance factors of 0.70, 0.75 and 0.80 for comparison. For connections, the traditional target reliability index is 4.5, although, increasingly, values falling between 4.0 and 4.5 are being considered adequate. Reliability indices of 5.1, 4.6 and 4.1 are obtained for resistance factors of 0.70, 0.75 and 0.80, respectively. Considering the larger-scale tests alone, the reliability indices are 4.8, 4.3 and 3.9, respectively. Based on the results of the reliability analysis, the resistance factor of 0.75 that has been recommended for bolted connections is also considered appropriate for use with the unified equation for the design of concentrically loaded welded lap plate connections. A summary of reliability parameters is shown in Table 3.

SLOTTED HSS-TO-GUSSET PLATE CONNECTIONS

Hollow structural sections (HSS) are commonly connected to gusset plates by cutting a slot into the end of the HSS member, inserting the gusset plate and fillet welding, either along the longitudinal edges only or all around, as shown in Figure 6. These slotted HSS connections are ubiquitous in HSS truss and bracing members. It is possible for this type of connection to fail by block shear of the HSS member when loaded in tension, as most recently reported by Martinez-Saucedo and Packer (2009).

Comparisons to Welded Lap Plate Connections

Conceptually, a slotted HSS member welded to a gusset plate is similar to the case of the welded lap plate connections discussed earlier in that both involve concentric loading resulting in the failure of a nominally rectangular block of material defined by the weld toe perimeter on the

connecting element. It was reported based on experimental programs completed by Zhao and Hancock (1995) and Zhao et al. (1999) that block shear failure initiated at the ends of the longitudinal welds farthest from the HSS end, suggesting a failure process similar to that observed in the welded lap plate connections. One notable difference between these two cases, however, is the boundary conditions near the planes of failure. That is, in slotted HSS connections, the gusset plate is connected to a closed HSS section with return walls. Additional significant differences between the two cases include the material properties of HSS sections and the removal of material for the slot from within the block perimeter.

Previous Studies on Slotted HSS-to-Gusset Plate Connections

Martinez-Saucedo and Packer (2009) examined the performance of the unified equation for the block shear failure mode in slotted HSS connections. They reported the results of eight experimental tests—two that failed in block shear, four that failed circumferentially and two that experienced local buckling. This study, along with others before it, identified the limitations of applying existing design equations (namely, Equations 1 and 2) for block shear to this case. Using the results of finite element analyses, Martinez-Saucedo and Packer (2009) recommended the use of the unified equation (Equation 3) with $U_t = 1.0$ for cases where block shear is the governing failure mode. A new design equation to calculate net section capacity for the circumferential failure mode, accounting for shear lag, was also presented.

Research programs conducted by Zhao and Hancock (1995), Korol (1996), Zhao et al. (1999), Wilkinson et al. (2002), and Martinez-Saucedo et al. (2006) include tests of a total of 88 HSS connections. Ling et al. (2007) performed a study on existing test data, adding data of their own from an experimental program on very high strength tubes with a yield strength near 1400 MPa (203 ksi). They proposed modifications to existing design equations, but did not consider the unified equation, as is done later. Capacity prediction of very high strength steel members is beyond the scope of this paper.

The numerical study performed by Martinez-Saucedo et al. (2006) examines the behavior of these connections; however, it is not included in the reliability study discussed later because of the lack of fabrication variability inherent to finite element modeling.

Performance of AISC 2005 Equations

Table 4 shows test-to-predicted ratios comparing existing and proposed design equations to the test results of Zhao and Hancock (1995), Zhao et al. (1999), Wilkinson et al. (2002), and Martinez-Saucedo et al. (2006). [The 11 test results from Korol (1996) are not included in Table 4 or the subsequent reliability study because measured ultimate and yield strengths were not available.] The predicted values used to determine the ratios presented in the table are based on a

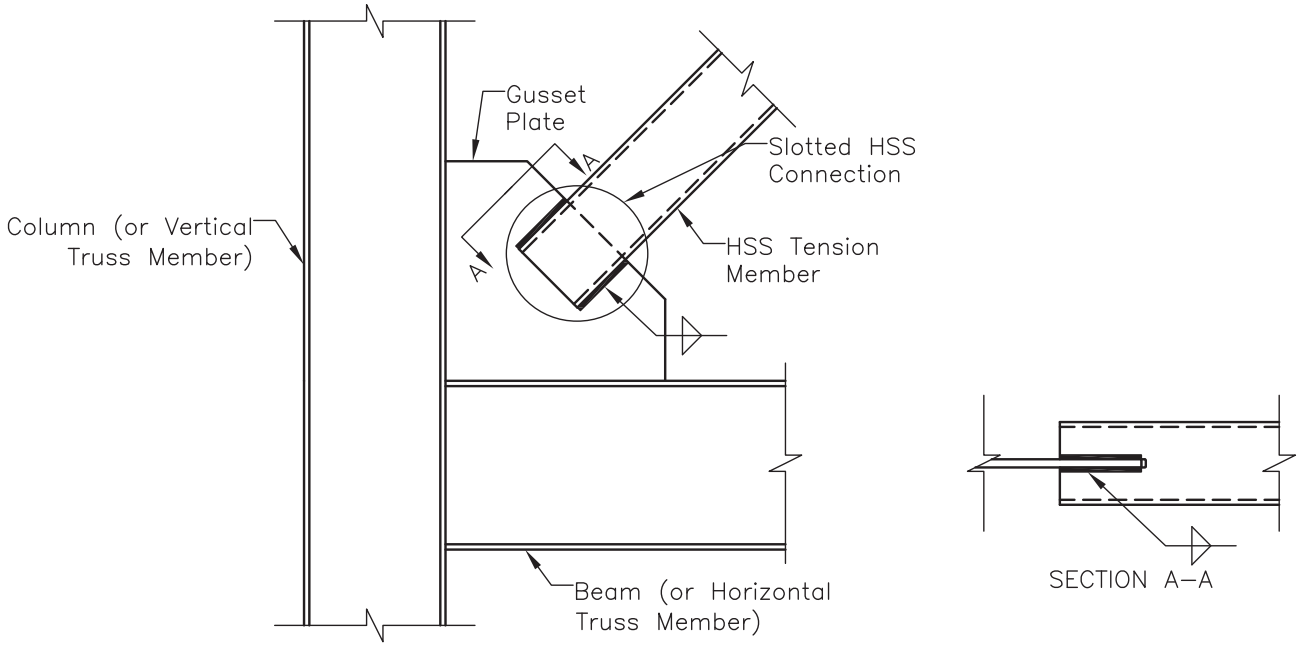

Fig. 6. Schematic of slotted HSS connection.

Table 4. Test-to-Predicted Ratios for Slotted HSS Connections									
Experimental Program	Number of Tests	AISC 2005[a]		Unified Equation[a] $U_t = 1.0$		Unified Equation[a] $U_t = 1.25$		Unified Equation[b] $U_t = 1.25$	
		Mean	COV	Mean	COV	Mean	COV	Mean	COV
Zhao and Hancock (1995)									
Weld type A†	24	1.06	0.05	1.02	0.05	0.97	0.05	1.13	0.05
Weld type B†	24	1.13	0.08	1.10	0.07	1.06	0.07	1.06	0.07
Zhao et al. (1999)									
Weld type A†	12	1.06	0.06	1.04	0.04	0.97	0.04	1.18	0.04
Weld type B†	12	1.12	0.07	1.09	0.06	1.05	0.06	1.05	0.06
Wilkinson et al. (2002)									
Weld type B†	3	1.06	0.04	1.01	0.03	0.98	0.03	0.98	0.03
Martinez-Saucedo et al. (2006)									
Weld type A†	1	0.89	—	0.89	—	0.85	—	0.97	—
Weld type B†	1	1.01	—	1.01	—	0.99	—	0.99	—
Combined Statistics	77								
Mean		1.09		1.06		1.01		1.09	
Coefficient of Variation		0.070		0.065		0.070		0.072	
Maximum		1.31		1.26		1.22		1.29	
Minimum		0.89		0.89		0.85		0.92	

† Refer to Figure 2; [a] Net tension area including slot width for type A; [b] Net tension area excluding slot width

block that includes the weld leg dimension, and the material properties used are those measured and reported by the respective researchers. These studies included both type A and type B specimens (i.e., welded all-around or longitudinally only, as defined in Figure 2). For type B specimens, the area subject to tension includes the weld leg dimensions of the two longitudinal welds only, because of the presence of the slot. The slot width is included as part of the tension area for type A specimens, assuming that the weld material effectively bridges the slot.

The design equations from AISC 2005 are again found to generally underestimate connection capacity, as was the case for lap plate connections. The mean test-to-predicted ratio for all tests is 1.09, which is closer to unity than the value of 1.20 obtained for the lap plate tests. As was suggested earlier, underestimation of the tensile component of the block capacity in welded connections appears to be the main reason for the high test-to-predicted ratios. Because typical slotted HSS connection geometry causes a decreased portion of load to be carried on the tension face compared to lap plate connections, the lower mean test-to-predicted ratio, albeit with a value still greater than unity, is expected.

Performance of the Unified Equation

Equivalent Stress Factor

Two equivalent stress factors for use in the unified equation (Equation 3) are considered: the recommendation of $U_t = 1.0$ by Martinez-Saucedo and Packer (2009) and the recommendation made for lap plate connections of $U_t = 1.25$ to account for the expected increased contribution of the tension face. Results in Table 4 show that while both versions of the unified equation improve capacity predictions, $U_t = 1.25$ achieves test-to-predicted ratios closer to unity with a similar coefficient of variation. This supports the intuitive similarity between the cases of the slotted HSS and lap plate connections. Therefore, for the design of slotted HSS connections against block shear failure, the unified equation as shown in Equation 3, with $U_t = 1.25$, does appear appropriate and is therefore considered in the following comparisons and the reliability study discussed in the next section. However, because the contribution of the tension face is relatively small for typical geometries, using a value of $U_t = 1.0$ is a reasonable and slightly more conservative alternative that results in similar capacity predictions and level of safety.

Observing the results in Table 4, a consistent correlation between test-to-predicted ratio and weld type is evident. Type A specimens in each experimental program have a lower mean test-to-predicted ratio than do type B specimens, for all capacity equations considered. However, with the exception of the single type A test of Martinez-Saucedo et al. (2006), which is discussed later, ratios for both weld types are found to be sufficiently close to unity when the unified equation is used.

Figure 7a shows the relationship between test capacities and capacity predictions using the unified equation with U_t = 1.25 for the block shear failures of slotted HSS connections. Generally, the data plot very close to the diagonal line that represents a test-to-predicted ratio of unity. The result of the type A test of Martinez-Saucedo et al. (2006) (test-to-predicted ratio of 0.85) is considered significant because it represents one of only two large-scale test results available. The other of these tests (type B) shows excellent agreement with the unified equation capacity prediction (test-to-predicted ratio of 0.99). These two test specimens are similar in geometry and failure load, but the capacity prediction for the type A test is significantly greater because the area of the tension surface of the block includes the width of the slot bridged by the weld metal. This results in a significant overprediction of capacity in this case.

However, using this same approach for the other 36 tests considered, test-to-predicted ratios near, albeit slightly below, 1.0 were achieved for type A specimens. Based on these observations, it appears that depositing a type A weld around the end of the gusset plate that completely and consistently engages the full tension face of the block (i.e., with no reduction for the slot) may not be readily achievable—a situation that is clearly exacerbated if the slot is significantly longer than the length of gusset plate inserted into the HSS. Moreover, it is possible that engaging the full tension face of the block is more difficult to achieve for large-scale connections than for smaller ones.

Until more large-scale tests similar to those conducted by Martinez-Saucedo et al. (2006) are available, as a conservative approach it is considered prudent to exclude the width of the slot (while still including the width of the fillet weld legs at the end of the longitudinal welds) when calculating the net area in tension for both types A and B connections. As indicated in Table 4, this increases the test-to-predicted ratio using the unified equation for the test in question from 0.85 to 0.97 and the ratio for all tests from 1.01 to 1.09. This effect is shown graphically in Figure 7b. The fact that the mean test-to-predicted ratio for all type A specimens increases to 1.16 indicates that entirely neglecting the slot width is very conservative and could be revisited when additional large-scale type A test data are available.

Table 5. Summary of Reliability Parameters: Slotted HSS Connections

Parameter	Value		
ρ_M	1.18		
ρ_G	1.00		
ρ_P	1.09		
V_M	0.097		
V_G	0.05		
V_P	0.072		
ϕ	0.70	0.75	0.80
β	5.5	5.0	4.6

Reliability Study

A reliability study was completed to examine the performance of the unified equation (with U_t = 1.25) for predicting the capacity of slotted HSS connections. The method used is discussed in the section on lap plate connections.

Material parameters for the HSS members are taken from Schmidt and Bartlett (2002). For ultimate strength, recommended values of the material factor and associated coefficient of variation are 1.18 and 0.063, respectively; for yield strength, the recommended values are 1.35 and 0.097, respectively. It is conservative to take the lower-bound material factor and upper-bound coefficient of variation; thus, values of 1.18 and 0.097 are selected.

The relevant geometric parameters for slotted HSS connections are the HSS wall thickness and block perimeter. For HSS thickness, Schmidt and Bartlett (2002) report values of the geometry factor and associated coefficient of variation of 0.973 and 0.011, respectively. No statistics are currently available on appropriate geometric parameters that include the variability of the block perimeter of slotted HSS connections. As discussed in the section on lap plate connections, values of 1.00 and 0.05 are assumed to be appropriate—in the absence of better statistical data—for the geometric parameters.

The professional factor is 1.09 (the mean test-to-predicted ratio for the unified equation, excluding the slot width for the determination of the net area in tension, as reported in Table 4), and the associated coefficient of variation is 0.072.

Using these factors, reliability indices of 5.5, 5.0 and 4.6 are obtained for resistance factors of 0.70, 0.75 and 0.80, respectively. Based on these results, the resistance factor of 0.75 recommended for lap plate connections is also considered appropriate for design of slotted HSS connections. The associated reliability index of 5.0 is considered sufficiently high to account for the uncertainty in the selection of geometric parameters. (Note that the reliability index obtained by including the slot width in the predicted capacities of type A specimens is 4.5.) A summary of all reliability parameters is shown in Table 5.

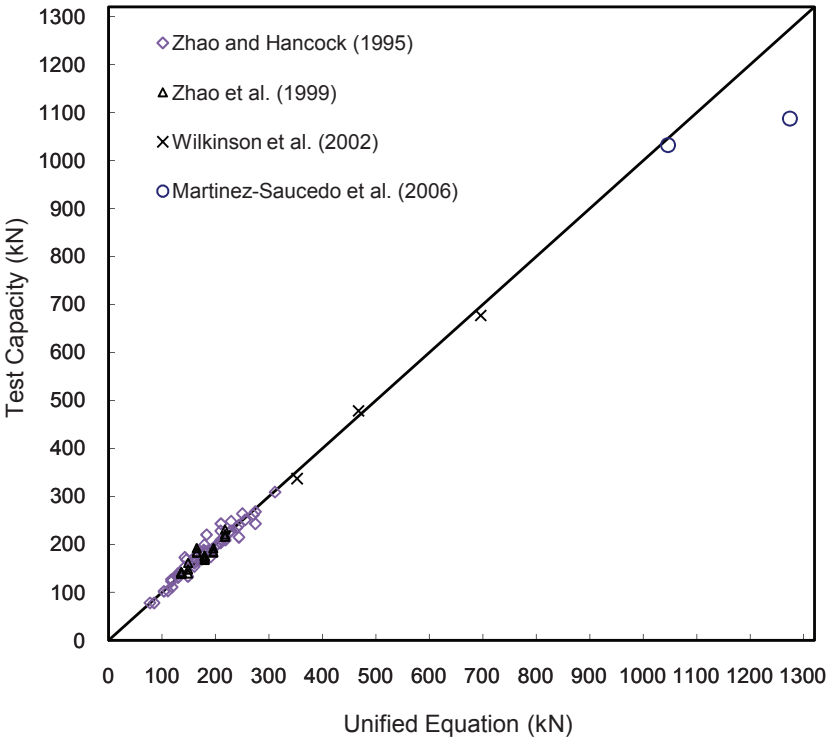

(a)

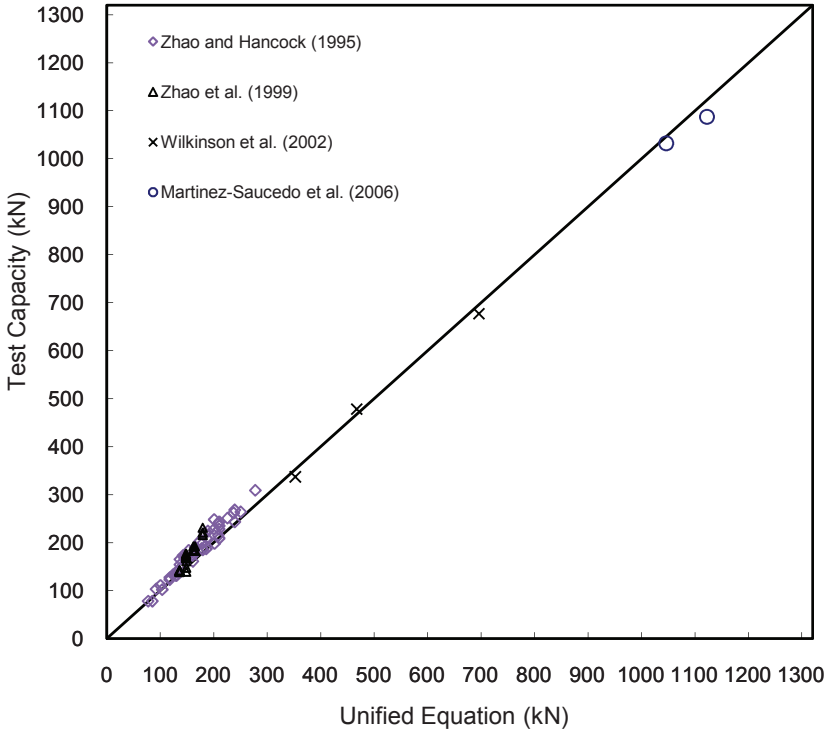

(b)

Fig. 7. Comparisons of design equations and experimental results for slotted HSS connections: (a) including slot width in net area in tension; (b) excluding slot width from net area in tension.

Table 6. Test-to-Predicted Ratios for Coped Beams with Welded Clip Angles								
	Including Web Buckling Tests				Excluding Web Buckling Tests			
	AISC 2005	Unified Equation			AISC 2005	Unified Equation		
		$U_t = 0.3$	$U_t = 0.7$	$U_t = 0.9$		$U_t = 0.3$	$U_t = 0.7$	$U_t = 0.9$
Mean	1.02	1.38	1.08	0.98	1.07	1.40	1.12	1.02
Coefficient of variation	0.10	0.09	0.09	0.09	0.07	0.07	0.06	0.07
Maximum	1.18	1.60	1.23	1.11	1.18	1.55	1.22	1.11
Minimum	0.81	1.14	0.91	0.80	0.91	1.23	0.97	0.88

COPED BEAMS WITH WELDED CLIP-ANGLE CONNECTION

Another common type of welded connection that can be susceptible to block shear is that of a coped beam with a clip-angle connection to its web, as depicted in Figure 8. An important distinction between this case and those discussed earlier is the eccentric loading condition on the block, resulting in stress concentrations that reduce connection capacity.

Previous Studies on Block Shear Capacity of Coped Beams

The block shear behavior of coped beams with bolted connections has been researched by Franchuk et al. (2003, 2004). The results of that study led to the recommendation of the unified equation for design, with $U_t = 0.9$ for one row of bolts and $U_t = 0.3$ for two rows. Yam et al. (2006a, 2006b) and Wei et al. (2010) examined the case of coped beams with welded double-clip-angle connections, including 22 physical tests and a parametric study using finite element modeling. A total of 10 tests failed by block shear. Although eight of the test beams exhibited local web buckling at failure, the researchers report that prior to this, a significant "block shear type" deformation occurred in all cases, indicating that the block shear capacity had been approached, or perhaps even reached. As such, these test results are included in this study. Results excluding the tests in which web buckling occurred are also reported for comparison, although it should be noted that all of the tests where web buckling did not occur had small connection eccentricities, making it impractical to assess the effect of eccentricity on block shear capacity using only these data. One test failed in the weld and three were not loaded to failure; these four tests are not included in the following discussion.

Performance of Existing Capacity Equations

Table 6 shows test-to-predicted ratios comparing existing and proposed design equations to the test results from Yam et al. (2006a) and Wei et al. (2010). AISC 2005 does not state whether U_{bs} should be taken as 1.0 or 0.5 in Equation 1 for this case. Taking this connection to be similar to the case of "single-row beam end connections," as shown in the AISC 2005 Commentary, values shown in Table 4 assume a value of 1.0 for U_{bs}.

Based on experimental results and subsequent finite element analyses, Yam et al. (2006b) proposed the use of Equation 1 from AISC 2005 with the inclusion of additional factors on both the shear and tension terms that are functions of the connection geometry and, in the case of the tension term, the ultimate strength of the material. These terms were developed from their test results to obtain a mean test-to-predicted ratio near unity and to minimize the coefficient of variation. Although the equation proposed by Yam et al. (2006b) achieves excellent agreement with their test results, it is desirable to use a simpler approach that is consistent with that used for other types of connections; thus, the performance of the unified equation is examined in the following section. Furthermore, the previous research did not perform a reliability study to quantify the statistical level of safety achieved by the design equation.

Performance of the Unified Equation

Equivalent Stress Factor

The unified equation has been shown by Franchuk et al. (2004) to provide good results for bolted connections in

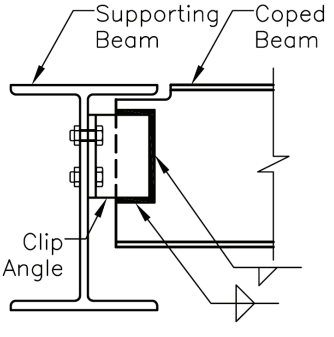

Fig. 8. Schematic of coped beam with a welded clip-angle connection.

Table 7. Summary of Reliability Parameters: Coped Beams with Welded Clip Angles						
Parameter	**Including Web Buckling Tests**			**Excluding Web Buckling Tests**		
U_t	0.3	0.7	0.9	0.3	0.7	0.9
ρ_M		1.05			1.05	
ρ_G		1.00			1.00	
ρ_P	1.38	1.08	0.98	1.40	1.12	1.02
V_M		0.063			0.063	
V_G		0.050			0.050	
V_P	0.09	0.09	0.09	0.07	0.06	0.07
ϕ		0.75			0.75	
β	6.0	4.4	3.7	6.5	4.9	4.2

coped beams using a U_t value of 0.9 for one row of bolts and 0.3 for two rows of bolts (consequently, these values have been adopted into CSA-S16-09). Wei et al. (2010) also calculate the predicted capacity of the specimens using the unified equation with these values of U_t, although they do not perform a reliability study to quantify the level of safety achieved, nor do they include specimens where web buckling occurs after significant block shear deformation. Considering the geometry of typical welded clip-angle connections, it is expected that a value between these limits would be appropriate to account for stress concentrations and to provide accurate capacity predictions for these connections. It was found that for the tests of Yam et al. (2006a) and Wei et al. (2010), a test-to-predicted ratio of unity can be achieved using the unified equation (Equation 3) with a value of $U_t = 0.86$ for all tests, or $U_t = 0.93$ excluding tests showing web buckling at failure; both of these results are similar to the value proposed previously for single-row bolted connections (0.9). It should be noted, however, that connection geometries with greater eccentricities than those accounted for in the limited available test data may require a reduction of the U_t value. The available test data include tension face lengths between 60 mm (2.4 in.) and 110 mm (4.3 in.). As expected, the two lowest test-to-predicted ratios from all 18 tests correspond to two of the specimens with the largest weld eccentricities.

Reliability Study

A reliability study was completed to examine the performance of the unified equation for predicting the capacity of coped beams with welded clip angle connections. Material and geometric parameters are taken from the reliability study on lap plate connections, due to the similarity in relevant design parameters, and are shown in Table 7.

The extreme values of U_t found appropriate in the unified equation for bolted coped beam connections, 0.9 and 0.3, were examined for applicability to welded connections. The reliability study is completed both including and excluding the tests in which web buckling took place, because significant block shear deformations were observed even when web buckling occurred. As reported in Table 6, for $U_t = 0.9$, the coefficient of variation for all the tests is 0.09. This coefficient of variation is significantly higher than those observed for the other types of connections considered in this study, resulting in a lower reliability index, β. While neglecting the tests where web buckling was present improves this value, the mean test-to-predicted ratios for the two cases are similar for all values of U_t considered, which suggests that the block shear capacity of these specimens was effectively reached prior to buckling. For $U_t = 0.3$, the professional factor for both groups is 1.4; this is clearly a gross underprediction of capacity. In order to achieve an acceptable value of β with a resistance factor, ϕ, of 0.75 (the value used for bolted connections and the welded connections discussed above), an intermediate value of $U_t = 0.7$ was also considered.

A summary of all reliability parameters is shown in Table 7 for both groups of test specimens. For a resistance factor of 0.75, and considering all of the test results, reliability indices of 6.0, 4.4 and 3.7 are obtained using U_t values of 0.3, 0.7 and 0.9, respectively, with the unified equation. The reliability index obtained for $U_t = 0.9$ is well below the target value—even though it is associated with a professional factor near unity—due to the relatively large scatter in the experimental results. An acceptable reliability index is achieved for $U_t = 0.7$, which generally provides conservative capacity estimates. Based on the limited test data available, a U_t value of 0.7 is currently recommended for use with the unified equation for predicting the block shear capacity of coped beams with welded clip-angle connections, with a resistance factor of 0.75. However, given that the only available test results where web buckling was not observed are from connections with small eccentricities, and because considering

only these tests leads to a conclusion that $U_t = 0.9$ provides an adequate level of safety, further testing may reveal that a value of $U_t = 0.9$ for very small eccentricities that decreases with increasing eccentricity is most appropriate—an approach that is currently used with the unified equation for bolted coped beam connections.

SUMMARY AND CONCLUSIONS

The results of an experimental study on the block shear behavior of welded lap plate connections are presented and discussed. When compared to experimental results, the block shear equations in AISC 2005 are found to be excessively conservative when applied to welded connections. The unified equation (Equation 3), with an equivalent stress factor $U_t = 1.25$, is recommended for the prediction of the block shear capacity of concentrically loaded welded lap plate connections. A resistance factor of 0.75 is shown to be appropriate.

The application of the unified equation to welded slotted HSS connections is also examined. Based on results from experimental programs by Zhao and Hancock (1995), Zhao et al. (1999), Wilkinson et al. (2002) and Martinez-Saucedo et al. (2006), the unified equation (Equation 3) with an equivalent stress factor of $U_t = 1.25$ and a resistance factor of 0.75 is again shown to be appropriate for the prediction of the block shear capacity. As a slightly more conservative alternative, a value of $U_t = 1.0$ [proposed by Martinez-Saucedo and Packer (2009)] provides similar results due to the relatively small influence of the tension surface on the overall block shear capacity for typical geometries. It is recommended that the area of steel removed from the tension plane by the slot be excluded in the determination of the net area in tension for both type A and B connections.

The performance of the unified equation for the case of coped beams with a welded clip-angle connected to the beam web is also considered, using experimental data reported by Yam et al. (2006a) and Wei et al. (2010). Although the use of the unified equation with an equivalent stress factor of $U_t = 0.9$ gives test-to-predicted ratios close to unity, a reliability study has revealed that due to the large scatter in the test data, this value provides an inadequate level of safety over the range of connection eccentricities studied. Consequently, until further test results are available, an equivalent stress factor of $U_t = 0.7$ is considered appropriate for design, with a resistance factor of 0.75.

ACKNOWLEDGMENTS

The specimens tested as part of this research program were donated by Waiward Steel Fabricators Ltd., Edmonton, Alberta, Canada. Assistance by Qing Cai, Andrew Neilson and Sean Watt in carrying out the tests is appreciated. Funding by the Natural Sciences and Engineering Research Council of Canada and the Faculty of Engineering at the University of Alberta is gratefully acknowledged.

REFERENCES

AISC (2005), *Specification for Structural Steel Buildings*, ANSI/AISC 360-05, American Institute for Steel Construction, Inc., Chicago, IL.

Callele, L.J., Driver, R.G. and Grondin, G.Y. (2009), "Design and Behavior of Multi-orientation Fillet Weld Connections," *Engineering Journal*, American Institute of Steel Construction, Vol. 46, Fourth Quarter, pp. 257–272.

CSA (2009), *Limit States Design of Steel Structures*, CAN/CSA-S16-09, Canadian Standards Association, Toronto, ON, Canada.

Driver, R.G., Grondin, G.Y. and Kulak, G.L. (2006), "Unified Block Shear Equation for Achieving Consistent Reliability," *Journal of Constructional Steel Research*, Vol. 62, No. 3, pp. 210–222.

Franchuk, C.R., Driver, R.G. and Grondin, G.Y. (2003), "Experimental Investigation of Block Shear Failure in Coped Steel Beams," *Canadian Journal of Civil Engineering*, Vol. 30, No. 5, pp. 871–881.

Franchuk, C.R., Driver, R.G. and Grondin, G.Y. (2004), "Reliability Analysis of Block Shear Capacity of Coped Steel Beams," *Journal of Structural Engineering*, Vol. 130, No. 12, pp. 1904–1913.

Hardash, S.G. and Bjorhovde, R. (1984), "Gusset Plate Design Utilizing Block-Shear Concepts," Department of Civil Engineering and Engineering Mechanics, University of Arizona, Tuscon, AZ.

Korol, R.M. (1996), "Shear Lag in Slotted HSS Tension Members," *Canadian Journal of Civil Engineering*, Vol. 23, pp. 1350–1354.

Kulak, G.L. and Grondin, G.Y. (2001), "Block Shear Failure in Steel Members—A Review of Design Practice," *Engineering Journal*, American Institute of Steel Construction, Vol. 38, No. 4, pp. 199–203.

Ling, T.W., Zhao, X.L., Al-Mahaidi, R. and Packer, J.A. (2007), "Investigation of Block Shear Tear-out Failure in Gusset-plate Welded Connections in Structural Steel Hollow Sections and Very High Strength Tubes," *Engineering Structures*, Vol. 24, No. 4, pp. 469–482.

Martinez-Saucedo, G., Packer, J.A. and Willibald, S. (2006), "Parametric Finite Element Study of Slotted End Connections to Circular Hollow Sections," *Engineering Structures*, Vol. 28, pp. 1957–1971.

Martinez-Saucedo, G. and Packer, J.A. (2009), "Static Design Recommendations for Slotted End HSS Connections in Tension," *Journal of Structural Engineering*, Vol. 135, No. 7, pp. 797–805.

Oosterhof, S.A. and Driver, R.G. (2008), "Block Shear Behaviour of Concentrically Loaded Welded Steel Lap Plate Connections," *Proc. Annual Conference, Canadian Society for Civil Engineering*, Vol. 3, pp. 2014–2023.

Ravindra, M.K. and Galambos, T.V. (1978), "Load and Resistance Factor Design for Steel," *Journal of the Structural Division*, Vol. 104, ST9, pp. 1337–1353.

Schmidt, B.J. and Bartlett, F.M. (2002), "Review of Resistance Factor for Steel: Data Collection," *Canadian Journal of Civil Engineering*, Vol. 29, pp. 98–108.

Topkaya, C. (2007), "Block Shear Failure of Gusset Plates with Welded Connections," *Engineering Structures*, Vol. 29, No. 1, pp. 11–20.

Wei, F., Yam, M.C., Chung, K.F. and Grondin, G.Y. (2010), "Tests on Block Shear of Coped Beams with a Welded End Connection," *Journal of Constructional Steel Research*, Vol. 66, pp. 1398–1410.

Wilkinson, T., Petrovski, T., Bechara, E. and Rubal, M. (2002), "Experimental Investigation of Slot Lengths in RHS Bracing Members," *Advances in Steel Structures*, Vol. 1, pp. 205–212.

Yam, M.C., Zhong, Y.C., Lam, A.C.C. and Iu, V.P. (2006a), "An Investigation of the Block Shear Strength of Coped Beams with a Welded Clip Angle Connection—Part I: Experimental Study," *Journal of Constructional Steel Research*, Vol. 63, pp. 96–115.

Yam, M.C., Zhong, Y.C., Lam, A.C.C. and Iu, V.P. (2006b), "An Investigation of the Block Shear Strength of Coped Beams with a Welded Clip Angle Connection—Part II: Numerical Study," *Journal of Constructional Steel Research*, Vol. 63, pp. 116–134.

Zhao, X.L. and Hancock, G.J. (1995), "Longitudinal Fillet Welds in Thin Cold-Formed RHS Members," *Journal of Structural Engineering*, Vol. 121, No. 11, pp. 1683–1690.

Zhao, X.L., Al-Mahaidi, R. and Kiew, K.P. (1999), "Longitudinal Fillet Welds in Thin-Walled C450 RHS Members," *Journal of Structural Engineering*, Vol. 125, No. 8, pp. 821–828.

A Yield Line Component Method for Bolted Flange Connections

BO DOWSWELL

ABSTRACT

Bolted connections are often used in steel structures to transfer of tension loads into wide flange members. The strength of these connections is determined with a prying action design procedure (outlined in the 13th edition AISC *Steel Construction Manual*) that checks the limit states of bolt tension rupture and bending of the flange. This procedure is valid only for fittings with limited bolt spacing and limited edge distance. This paper discusses a method to determine the local flange bending strength of a wide flange member using the yield line method. The proposed design method includes the effect of prying action on the bolts, and can be applied to many different connection configurations, including connections with large bolt spacing and edge distances and connections with web stiffeners. Comparisons with test data from 10 independent research projects will be used to verify the accuracy of the proposed method.

Keywords: bolted tension connections, hangers, prying action.

Many bolted connections in steel structures rely on the transfer of tension loads into wide flange members as shown in Figure 1. The strength of these connections is determined with the prying action design procedure in the *Steel Construction Manual* (AISC, 2005a), hereafter referred to as the *Manual*, which checks the limit states of bolt tension rupture and bending of the flange. The procedure in the *Manual* is valid only for fittings with limited bolt spacing and edge distance such as clip angles at the end of a beam.

The *Manual* does not provide guidance on how to determine the equivalent length of fittings with large edge distances and bolt spacings. In practice, conservative assumptions are often made. It is commonly assumed that the tributary length per bolt is twice the distance from the center of the bolt to the face of the supporting web. This method is slightly conservative for calculating the elastic stress for wide cantilever beams loaded at the free end (Young, 1989); however, it is extremely conservative for calculating the strength of flanges in bending.

In other cases, unconservative assumptions are sometimes made, where web stiffeners are provided to prevent flange bending, and the stiffened flange is assumed adequate to carry the applied loads with no further calculations. However, tests have shown that flange bending is a common failure mode for connections with web stiffeners (Packer and Morris, 1977; Garrett, 1977; Ghassemieh et al., 1983; Moore and Sims, 1986; Zoetemeijer, 1981).

This paper will discuss a method to determine the local flange bending strength of a wide flange member using the yield line method. The proposed design method includes the effect of prying action on the bolts and can be applied to many different connection configurations, including connections with large spacings and edge distances and connections with web stiffeners. Comparisons with test data from 10 independent research projects will be used to verify the accuracy of the proposed method.

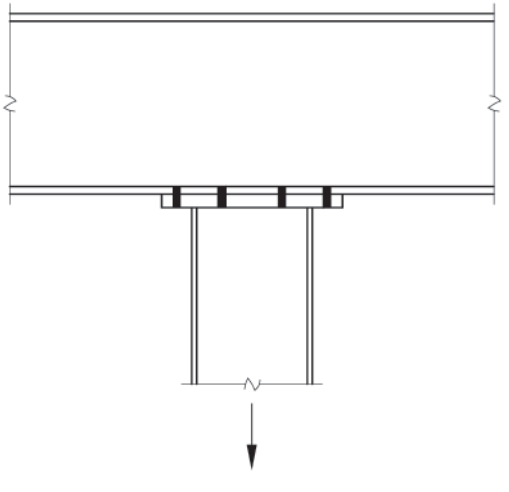

Fig. 1. Bolted hanger connection.

Bo Dowswell, P.E., Ph.D., Principal, SDS Resources, Birmingham, AL. E-mail: bo@sdsresources.com

BACKGROUND

Prying Action

When bolts are loaded in tension, deformation of the connected parts will cause an increase in bolt tension. This additional bolt tension is the prying force, q, shown in Figure 2. Designing for prying action involves checking the limit states of bending of the fitting and tension rupture of the bolts. The two limit states are interdependent—for a given load, an increase in flange thickness leads to a lower prying force on the bolt.

The moment diagram of half of the flange is shown in Figure 2. The moment at the face of the web is always equal to the plastic capacity of the fitting, but the moment at the bolt line can be reduced if required to limit the prying force on the bolt. This behavior is accounted for in the design method in the *Manual*. The background for the design method is provided by Astaneh (1985), Thornton (1985) and Kulak et al. (1987). To calculate the available tensile strength when the connection geometry is known, Equation 1 is applicable:

$$T_a = B\left(\frac{t}{t_c}\right)^2 \left(1+\delta\alpha'\right) \le B \tag{1}$$

where

LRFD	ASD
$t_c = \sqrt{\frac{4.44Bb'}{pF_u}}$	$t_c = \sqrt{\frac{6.66Bb'}{pF_u}}$

$$\alpha' = \frac{1}{\delta(1+\rho)}\left[\left(\frac{t_c}{t}\right)^2 - 1\right] \le 1.00$$

$$\delta = 1-\frac{d'}{p}$$

$$\rho = \frac{b'}{a'}$$

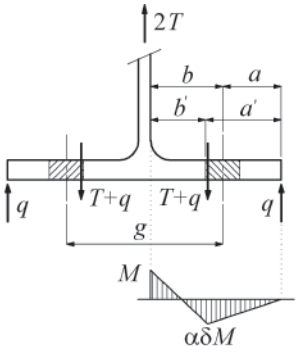

Fig. 2. Model for prying action design method.

$$b' = b-\frac{d_b}{2}$$

$$a' = \left(a+\frac{d_b}{2}\right) \le \left(1.25b+\frac{d_b}{2}\right)$$

B = available tensile strength per bolt, kips
a = distance from the bolt centerline to the edge of the fitting, in.
b = distance from bolt centerline to the face of the web, in.
d_b = bolt diameter, in.
d' = width of the hole along the length of the fitting, in.
F_u = specified minimum tensile strength of connecting element, ksi
p = tributary length of fitting per bolt, in.
t = thickness of the fitting, in.

The Yield Line Method

The yield line method was developed by Hognestad (1953) and Johansen (1962) to determine the ultimate strength of concrete slabs. It is an upper-bound solution based on the principle of virtual work. One form of the upper-bound theorem of limit analysis states that a load calculated based on an assumed mechanism will be greater than or equal to the true limit load.

The yield line method requires the failure pattern to be known prior to calculation of the collapse load. Many patterns may be valid for a particular joint configuration. Because the collapse load is upper bound, the pattern that gives the lowest load will provide results closest to the true failure load. Therefore, selection of the proper yield line pattern is important because an incorrect failure pattern will produce unsafe results.

The collapse load is calculated assuming that a plastic mechanism forms along each line of the chosen failure pattern. To maintain equilibrium, the external work done by the load moving through the virtual displacement, δ, must equal the strain energy due to the plastic moment rotating through virtual rotations, θ_i. The virtual rotations are assumed small, so $\theta_i \approx \tan(\theta_i) \approx \sin(\theta_i)$. The influence of strain hardening and membrane effects are not accounted for in yield line analysis; therefore, there is potentially a large reserve capacity beyond the calculated collapse load.

Some yield line patterns will produce an equation for the load in terms of known geometry, but most cases will require any unknown dimensions to be determined by minimizing the load with respect to the unknown dimension. To do this, the load is differentiated with respect to the unknown dimension and set equal to zero. From this, an equation for the unknown dimension can be determined and substituted into the equation for the load.

The general procedure for deriving an equation based on yield line analysis is as follows:

- Select a valid yield line pattern.
- Determine the equation that describes the external work done by the load moving through the virtual displacement.

$$W_E = P\delta \tag{2}$$

where
P = applied load
δ = virtual displacement

- Determine the equation that describes the internal work done by the rotations along the yield lines,

$$W_I = \sum M_{pi}\theta_i \tag{3}$$

where
M_{pi} = plastic moment capacity of yield line i
= $m_p L_i$
θ_i = virtual rotation of yield line i
m_p = plastic moment capacity per unit length of the fitting
= $F_y t^2/4$
L_i = length of yield line i

- Set the external work equal to the internal work and solve for the load. If required, minimize the load with respect to unknown dimensions.

Traditionally, the prying action equations have been derived using equilibrium methods (Kulak et al., 1987), but the equations can also be derived using energy methods. To show the similarity between the design method for prying action and the yield line equations for flange bending, the *Manual* equation for the required fitting thickness will be derived for the case of an infinitely strong bolt. This exercise will also show the validity of the yield line method for this simple case.

Considering only one side of the connection in Figure 3, the external work is

$$W_E = T\delta \tag{4}$$

The internal work is

$$W_I = \theta m_p(L_1 + L_2) \tag{5}$$

where
L_1 = length of yield line 1
= tributary length per bolt, p
L_2 = length of yield line 2
= net tributary length per bolt, $p-d'$

Substitute $L_1 = p$ and $L_2 = p - d'$ into Equation 5 to get

$$W_I = \theta m_p(2p - d') \tag{6}$$

For small angles, $\theta = \delta/b'$

$$W_I = \frac{\delta}{b'} m_p (2p - d') \tag{7}$$

Substitute $m_p = F_y t^2/4$

$$W_I = \frac{\delta F_y t^2}{4b'}(2p - d') \tag{8}$$

Set internal work equal to external work and solve for T_n

$$T_n = \frac{F_y t^2}{4b'}(2p - d') \tag{9}$$

The available LRFD strength is

$$\phi T_n = \frac{\phi F_y t^2}{4b'}(2p - d') \tag{10}$$

Rearrange Equation 10 and solve for the thickness of the fitting

$$t_{min} = \sqrt{\frac{4Tb'}{\phi F_y (2p - d')}} \tag{11}$$

Substitute $\phi = 0.90$ into Equation 11

$$t_{min} = \sqrt{\frac{4.44Tb'}{F_y (2p - d')}} \tag{12}$$

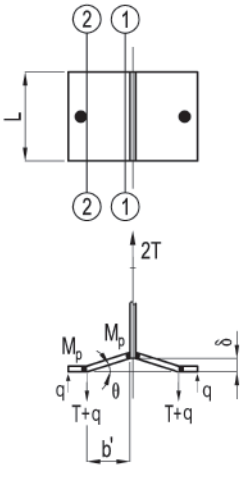

Fig. 3. Yield line model for prying equation.

The LRFD version of the prying equation (on page 9-11 of the *Manual*) is

$$t_{\min} = \sqrt{\frac{4.44Tb'}{pF_u\left(1+\delta\alpha'\right)}} \tag{13}$$

Although the *Manual* procedure uses the ultimate tensile strength, F_u, for prying calculations, which was first suggested by Douty and McGuire (1965) and more recently by Thornton (1992), yield line analysis has traditionally utilized the yield strength, F_y. For comparison with the yield line derivation, F_y will be used here. Replacing F_u with F_y in Equation 13, substituting $\alpha' = 1.0$ for infinitely strong bolts and substituting $\delta = 1 - d'/p$, Equation 12 is obtained.

EXISTING SOLUTIONS

Yield line theory has been presented as a design method for bolted connections in several publications, and many different yield line patterns have been proposed. A component method, similar to the design method proposed in this paper, is currently used in Europe (SCI, 1995; CEN, 2005) to determine the column flange bending strength and the plate bending strength in moment end plate connections.

Zoetemeijer (1974)

The equivalent length concept was first discussed by Zoetemeijer (1974), who used a simplified solution to the yield line pattern in Figure 4 to get an equivalent tributary length per bolt of

$$p_e = 2b + \frac{5a}{8} + \frac{p}{2} \tag{14}$$

where

p = spacing between bolts

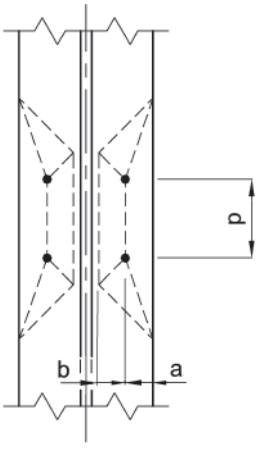

Fig. 4. Yield line pattern from Zoetemeijer (1974).

Dranger (1977)

The yield line pattern in Figure 5 was solved by Dranger (1977), who determined the strength as a function of the unknown dimension x:

$$P_n = F_y t^2 \left(\frac{x}{b} + \frac{c}{x}\right) \tag{15}$$

Dimension x was then determined by minimizing the load:

$$x = \sqrt{bc} \tag{16}$$

If x from Equation 16 is substituted into Equation 15, the nominal strength is

$$P_n = 2F_y t^2 \sqrt{\frac{c}{b}} \tag{17}$$

where

$c = a + b$

Mann and Morris (1979)

Mann and Morris (1979) presented a yield line pattern with circular corners as shown in Figure 6. The nominal strength is

$$P_n = F_y t^2 \left(\pi + \frac{2a + p - d'}{b}\right) \tag{18}$$

Equation 18 defines the total connection strength, which is twice the strength of each independent yield line pattern forming on both sides of the column web. Mann and Morris also suggested an equation similar to Dranger's (1977) for stiffened connections; however, no guidance was given on how close the stiffener has to be to the bolt for that equation to apply.

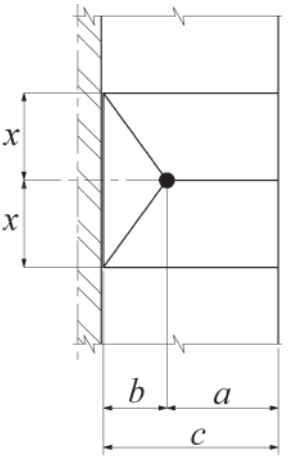

Fig. 5. Yield line pattern from Dranger (1977).

Zoetemeijer (1981)

Zoetemeijer (1981) presented a circular yield line pattern as shown in Figure 7, which he described as a punching failure. For this pull-through mechanism, the prying force is theoretically zero. The yield line solution predicts a nominal strength of

$$P_n = \pi F_y t^2 \tag{19}$$

Thornton and Kane (1999) and Muir and Thornton (2006)

Thornton and Kane (1999) and Muir and Thornton (2006) published the following equation, which provides the average equivalent length per bolt:

$$p_e = \frac{p(n-1) + \pi b + 2a}{n} \tag{20}$$

where

n = number of bolt rows

The equation can be derived by dividing the total equivalent length of the bolt group, based on the yield line pattern of Mann and Morris (1979), by the total number of bolts in the joint. The equivalent length is then used with the prying action procedure in the *Manual*. This equation accounts for the prying effect on the bolts; however, the fact that the outermost bolts take significantly more of the load than the inner bolts is neglected.

EXPERIMENTAL RESEARCH

Ten independent research projects were located with experimental results on bolted tension connections. From these tests, four connection types were identified, based on the edge distance and stiffener configuration. These are presented in Table 1. The specimen details are shown in Table A1 of Appendix A.

The generalized experimental load-deflection curve is bilinear with a nonlinear transition point as shown in Figure 8. There are four points of interest on the curve:

1. The proportional limit, where the curve transitions from linear to nonlinear. The load at this deformation may be of interest as a serviceability limit for connections that can allow only very small deformations. The deformation at this point is δ_p, and the load is P_p.
2. The point where the curve transitions from nonlinear to linear at the second linear part of the curve. Loads increased beyond this point are accompanied by large deformations. The deformation at this point is δ_s, and the load is P_s.
3. The point of ¼-in. deformation. This is proposed here as the serviceability limit. The deformation at this point, $\delta_{1/4}$ is ¼ in., and the load is $P_{1/4}$.

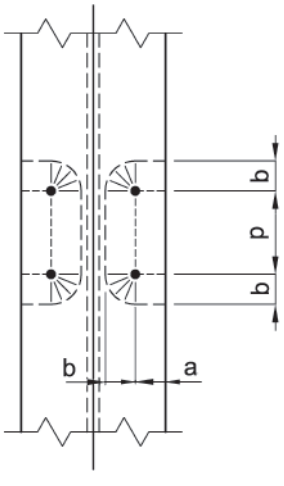

Fig. 6. Yield line pattern from Mann and Morris (1979).

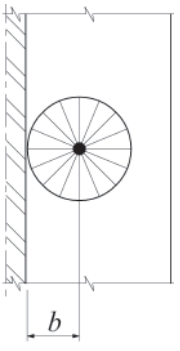

Fig. 7. Circular yield line pattern from Zoetemeijer (1981).

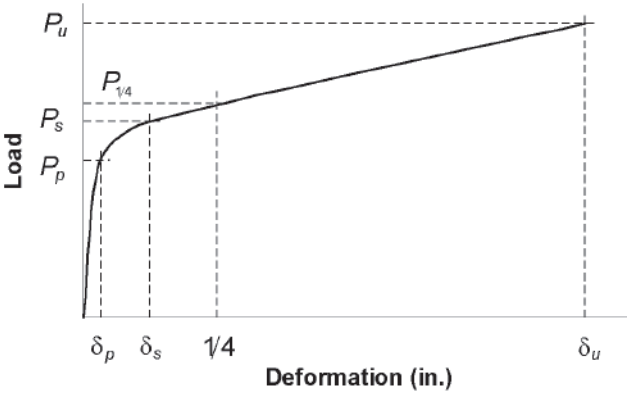

Fig. 8. General load versus deformation curve.

Table 1. Geometry of Experimental Specimens	
Specimen Geometry	**References**
Type 1	
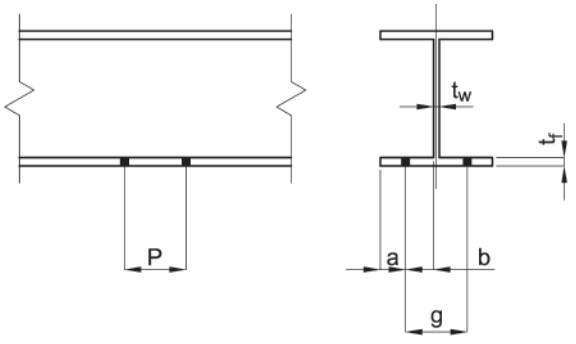	Garrett (1977) Grogan and Surtees (1999) Hendrick and Murray (1983) Moore and Sims (1986) Packer and Morris (1977) Pynnonen and Granstrom (1986) Tawaga and Gurel (2005) Zoetemeijer (1974)
Type 2	
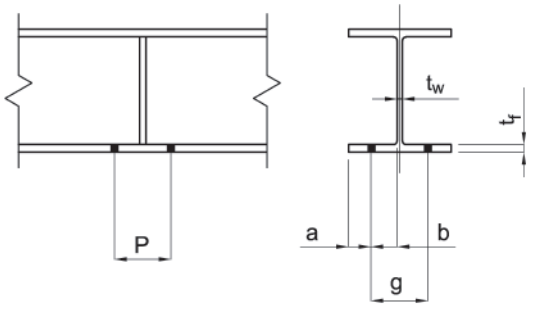	Packer and Morris (1977) Garrett (1977) Moore and Sims (1986) Zoetemeijer (1981)
Type 3	
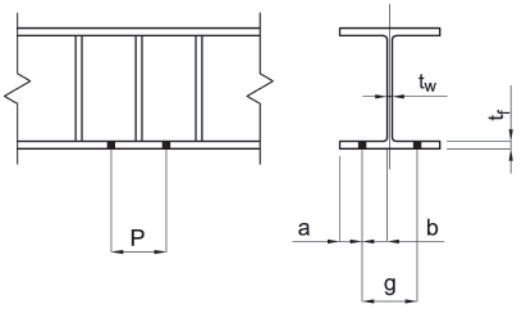	Garrett (1977)
Type 4	
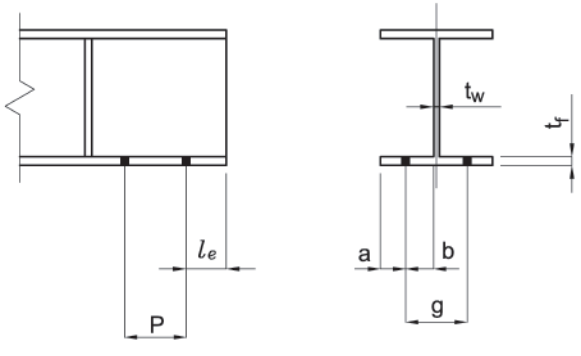	Ghassemieh et al. (1983)

4. The ultimate strength. This is a point of interest for structural integrity and ultimate strength calculations. The deformation at this point is δ_u and the load is P_u.

Table A2 in Appendix A contains all of the loads described for each specimen, where they were reported in the referenced document. Many of the listed values are approximate because they were read from graphs of the test data. The experimental failure modes are also listed in Table A2. Most of the specimens with two failure modes listed had the ultimate strength limited by bolt rupture, but only after a large deformation due to flange bending.

For the specimens with thick flanges, the bolts failed before the nonlinear part of the load-deformation curve was reached. For these specimens, the bolt elongation contributed significantly to the total deformation.

For the specimens with thin flanges, the deformation at ultimate strength was as much as 2 in. Under large deformations, the load-transfer mechanism changes from bending to tension, which results in a tension load with a component perpendicular to the axis of the bolt. This component is resisted by the bolts in shear. Many of these tests resulted in bolt fracture due to the applied tension combined with shear, which was caused by large-deformation membrane action of the fitting.

DEVELOPMENT OF PROPOSED DESIGN METHOD

The purpose of this paper is to formulate a simple, accurate and versatile method to design bolted flange connections. To do this, the theoretical and experimental information presented by previous researchers will be analyzed.

The yield line solutions of Zoetemeijer (1974), Dranger (1977), and Mann and Morris (1979) provide accurate results for thin fittings where the limit state of bolt rupture is not applicable. However, where thick flanges dictate that bolt rupture is the controlling limit state, the yield line solutions do not provide a method to calculate the prying force on the bolt.

The method proposed by Thornton and Kane (1999) and Muir and Thornton (2006) explicitly accounts for the prying forces on the bolts; however, an equal amount of axial load is assigned to each bolt. In reality, the outermost bolts will be more highly stressed than the inner bolts, which could lead to an unzipping action.

In this paper, a more refined solution has been developed, where the forces are distributed according to the equivalent length tributary to each bolt and the strength of each bolt is evaluated independently. The equivalent tributary length is calculated using existing yield line solutions.

The Component Method

Many different bolted flange configurations can be analyzed by the yield line method; however, it would be cumbersome for engineers to deal with a separate yield line pattern for each different configuration. To simplify the design process, the component method can be used, where single-bolt (local) yield line patterns are assembled into a larger (global) pattern for the entire bolt group. To do this, the engineer simply selects a local pattern that is identical to each part of the global pattern. The strength of each local pattern is calculated and summed to get the total strength of the global pattern.

In many cases, the local pattern will not be symmetrical about the center of the bolt, and half-patterns can be used. The strength of a half-pattern is simply half of the strength of the whole pattern.

Stiffened Connections

If a flange is not adequate to carry the applied load, stiffeners can be used to reinforce the joint as shown in Figure 9. For stiffeners to be effective, they must be close enough to the bolt to alter the yield line pattern. Using Dranger's (1977) yield line pattern, the stiffeners are effective if

$$x_s < x \tag{21}$$

where

x_s = distance from the center of the bolt to the edge of the stiffener

$x = \sqrt{bc}$

Then, the strength can be determined by substituting x_s for x in Equation 15:

$$P_n = F_y t^2 \left(\frac{x_s}{b} + \frac{c}{x_s} \right) \tag{22}$$

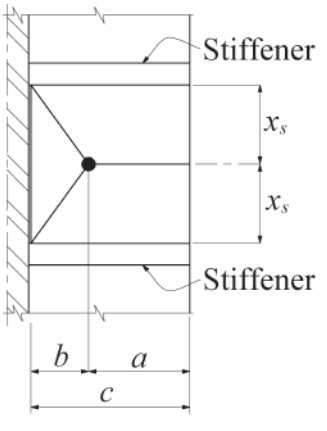

Fig. 9. Yield line pattern for a stiffened flange in bending.

Equivalent Tributary Length Concept

The nominal strength from a given yield line pattern will be equal to that of a straight yield line of length, p. Using Equation 9 with $d' = 0$ and $b' = b$, the nominal strength for a straight yield line is

$$P_n = \frac{F_y t^2 p}{2b} \tag{23}$$

To determine the equivalent tributary length of fitting, the nominal strength of a given yield line solution will be set equal to Equation 23 and solved for p. For the Dranger (1977) pattern in Figure 5, the equivalent length is

$$p_d = 4\sqrt{bc} \tag{24}$$

For single-bolt connections, the equivalent tributary length for the yield line solution of Mann and Morris (1979), shown in Figure 6, is

$$p_m = \pi b + 2a \tag{25}$$

The equivalent tributary length For Zoetemeijer's (1981) circular pattern in Figure 7 is

$$p_c = 2\pi b \tag{26}$$

For the stiffened pattern in Figure 9, the equivalent tributary length is

$$p_s = 2\left(x_s + \frac{cb}{x_s}\right) \tag{27}$$

For single-bolt connections, the yield line solution of Zoetemeijer (1974), given by Equation 14, reduces to

$$p_z = 4b + 1.25a \tag{28}$$

Selection of Proper Yield Line Solution

Because the yield line method is an upper-bound approach, the pattern that gives the lowest load will provide results closest to the true failure load. The normalized equivalent lengths, p_e/c, from the yield line solutions of Zoetemeijer (1974, 1981), Dranger (1977), and Mann and Morris (1979) are plotted against b/a in Figure 10. It can be seen that the Mann and Morris (1979) solution results in the minimum equivalent length for connections with high values of b/a, and the Zoetemeijer (1981) solution produces the minimum equivalent length only for connections with very low values of b/a.

To simplify the design process, it is advantageous to use only one of the available yield line patterns. Analysis of the experimental deformations indicate that the yield line pattern developed by Zoetemeijer (1974), shown in Figure 4, is closest to the actual failure pattern. However, the skewed yield lines are awkward to deal with if stiffeners are present, and for most practical b/a ratios, the difference in strength of the various yield line patterns is small.

The circular yield line pattern presented by Zoetemeijer (1981) will control the design of fittings with large edge distances, a. However, if a limit is placed on the b/a ratio, this yield line pattern will never control the design. The Zoetemeijer solution is equal to the Dranger (1977) solution at $b/a = 0.68$; therefore, if a is limited to $1.47b$ for design purposes, Zoetemeijer's solution will never control. As a slightly conservative (about 5%) limit, the prying action design procedure in the *Manual* (AISC, 2005a) can be used, which limits a to a maximum of $1.25b$.

When comparing the Dranger (1977) pattern to the Mann and Morris (1979) pattern for stiffened flanges, the Dranger pattern more accurately predicts the increase in strength based on the distance from the bolt to the stiffener. This can be verified by reviewing the projects that tested specimens that were identical except for the addition of a stiffener: Packer and Morris's (1977) specimens T6, T7 and T8; Moore and Sims's (1986) specimen T7. For these four specimens, the Mann and Morris model predicted no increase in strength due to the stiffeners; however, the average experimental load increased by 32% compared to identical specimens with no stiffeners. The Dranger model predicted a 37% increase due to the stiffeners.

Due to the simplicity and the more accurate prediction of the strength when stiffeners are present, the Dranger (1977) yield line pattern is proposed here. A plot of p_{min}/p_d versus b/a is shown in Figure 11, where p_d is the tributary length

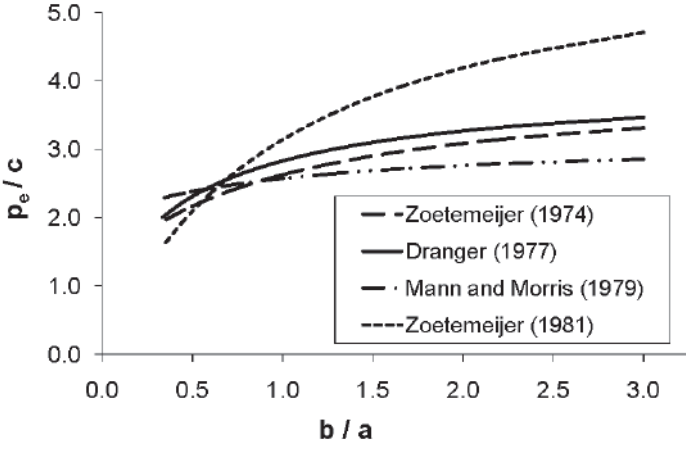

Fig. 10. Comparison of different yield line patterns.

for the Dranger yield line pattern and p_{min} is the minimum tributary length for the yield line patterns of Zoetemeijer (1974), Dranger (1977), and Mann and Morris (1979). It is seen that the Dranger solution is unconservative. However, for most practical *b*/*a* ratios, the difference can be neglected because the beneficial effects of strain hardening and membrane action are not accounted for. Figure 11 also shows the curve-fit equation, which can be used as a reduction factor in design if the engineer wants to explicitly account for the difference among the three different solutions. The curve fit for the reduction factor is

$$C_r = 1.0 - 0.11(b/a) + 0.019(b/a)^2 \quad (29)$$

The coefficient of determination, R^2, is 0.99, indicating a very good fit. If the equivalent tributary length has been calculated using Dranger's solution, the minimum of the three solutions can be approximated as

$$p'_{min} = p_d\, C_r \quad (30)$$

where

p'_{min} = approximate minimum equivalent tributary length per bolt

p_d = equivalent tributary length per bolt calculated according to the yield line pattern, developed by Dranger (1977)

Joints with Bolt Rupture as the Controlling Limit State

In joints where the equivalent tributary length at one bolt is larger than the remaining bolts in the joint, the bolt forces will not be distributed equally. When bolt rupture is the controlling limit state, the design procedure must account for this. The component method accounts for the nonequal distribution of bolt forces by assigning the loads in proportion to the tributary length at each bolt.

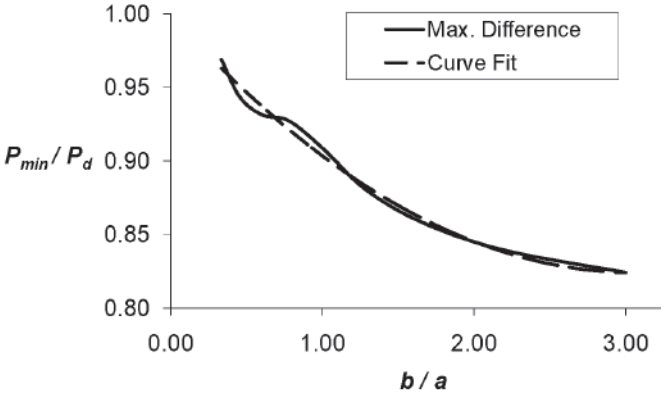

Fig. 11. Comparison of Dranger (1977) yield line solution to the minimum of the Zoetemeijer (1974) and Mann and Morris (1979) solutions.

When bolt rupture controls the design, an additional complication arises because deformation compatibility must be maintained for all bolts in the joint. Under normal conditions, when one of the bolts within the joint ruptures, it is unlikely that the full yield line pattern has formed due to the limited deformation. The local yield line pattern tributary to the adjacent bolt will also be limited to the deformation at bolt rupture. Because the internal energy at the yield lines is proportional to the displacement, deformation compatibility of the adjacent yield lines can be upheld by reducing the strength in proportion to the deformation ratio, δ_r/δ.

$$\frac{\delta_r}{\delta} = \frac{T_a}{T_{\alpha'=1}} \quad (31)$$

where

δ_r = deformation at bolt rupture

δ = deformation at full yield line strength assuming infinitely strong bolts

T_a = strength of the fitting at bolt rupture (calculated using Equation 1)

$T_{\alpha'=1}$ = strength of the fitting assuming a full yield line pattern forms without bolt rupture (calculated using Equation 1 with $\alpha' = 1$)

Using δ_r as the deformation limit for the entire joint, the total strength of the joint as controlled by the critical bolt is

$$P_n = T_{cr}\left[1 + \left(\frac{T_{cr}}{T_{cr(\alpha'=1)}}\right)\left(\frac{\Sigma P_{ei}}{P_{e(max)}} - 1\right)\right] \quad (32)$$

where

T_{cr} = strength of the fitting at the critical bolt (the bolt with the largest equivalent tributary length within the joint) (calculated using Equation 1)

$T_{cr(\alpha'=1)}$ = strength of the fitting at the critical bolt assuming a full yield line pattern forms without bolt rupture (calculated using Equation 1 with $\alpha' = 1$)

ΣP_{ei} = summation of the equivalent tributary lengths for all local yield line patterns within the joint

$P_{e(max)}$ = largest equivalent tributary length for all bolts within the joint

Equation 32 provides a convenient way to deal with the deformation compatibility of the joint; however, when compared to the test results of Ghassemieh et al. (1983), the calculated strengths are very conservative. The conservatism is due to the fact that the equation only accounts for the flexural deformation of the fitting and neglects other deformations within the joint, such as bolt elongation and shear deformation of the fitting. As discussed in the section on experimental research, bolt elongation can be a large portion of the total joint deformation.

Due to the conservatism associated with Equation 32, it is proposed that the strength of each bolt be evaluated independently. Then, the total strength of the joint can be calculated by summing the local capacities for the entire bolt group. To account for the prying force on the bolt, the equivalent tributary length, p_e, is used in the prying action procedure in the *Manual* in lieu of the tributary length, p. This procedure provides nominal strengths that compare well with the experimental loads, as discussed in the Experimental Validation section.

Large Bolt Spacings

If the distance between bolts, p, is greater than the equivalent tributary length from Equation 24, two independent yield lines will form for each bolt as shown in Figure 12a. Figure 12b shows the same bolt pattern with a small bolt spacing, where half-patterns form at each end and a straight pattern forms between the bolts. Figure 13 shows a plot of the equivalent length per bolt versus spacing between bolts. The transition point between the two yield line patterns is at a bolt spacing of $4\sqrt{bc}$.

A similar problem occurs when a bolt is near the end of a member. If the edge distance from the bolt to the end of the member, l_e, is less than $2\sqrt{bc}$, a straight yield line will form between the bolt and the end of the member.

PROPOSED DESIGN METHOD

The proposed design method consists of the following steps:

1. Select a valid yield line pattern local to each bolt in the group. If the yield line pattern is not symmetrical, two half-patterns should be selected.
2. Calculate the strength of each bolt and fitting using the prying action procedure in the *Manual* (AISC, 2005a), replacing p with p_e; F_y should be used in lieu of F_u unless large deformations are acceptable.
3. Repeat for all bolts in the bolt group.
4. Sum the individual strengths to get the total strength of the bolt group.

The equivalent tributary length for the yield line pattern in Figure 5 is

$$p_e = 4\sqrt{bc} \tag{33}$$

Where stiffeners are present, the equivalent length for the pattern in Figure 9 is

$$p_e = 2\left(x_s + \frac{cb}{x_s}\right) \text{ if } x_s < \sqrt{bc} \tag{34a}$$

$$p_e = 4\sqrt{bc} \text{ if } x_s \geq \sqrt{bc} \tag{34b}$$

Straight yield lines will be part of the yield line pattern when the bolt spacing is less than $4\sqrt{bc}$ or the edge distance is less than $2\sqrt{bc}$. The equivalent tributary length per bolt is half the distance between two bolts, $p/2$, or the distance from the bolt to the end of the member, l_e.

In the calculations for the equivalent tributary length, the limit $a \leq 1.25b$ should be used. For connections subjected to combined tension and shear, the bolt tension strength should be reduced to account for the presence of shear.

As shown in the next section, serviceability design of

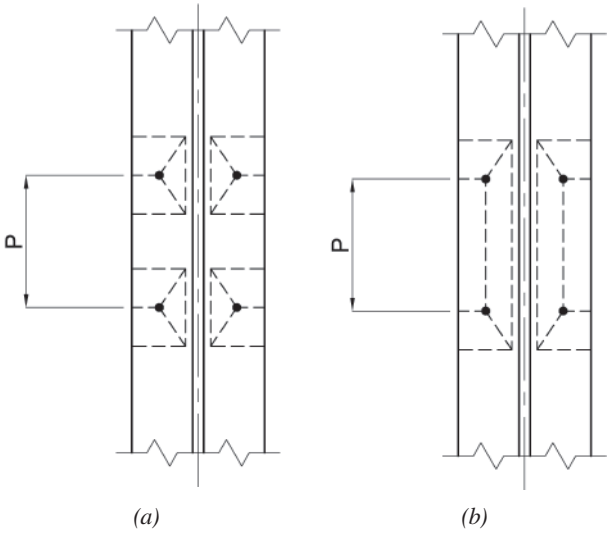

Fig. 12. Effect of bolt spacing on the yield line pattern: (a) large bolt spacing; (b) small bolt spacing.

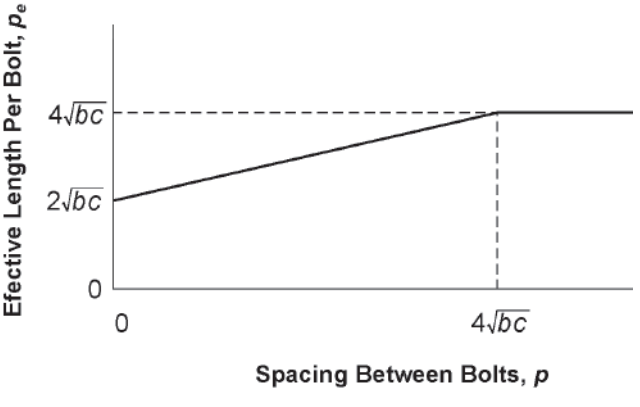

Fig. 13. Equivalent length per bolt versus spacing between bolts.

Table 2. Summary of Calculation Results								
	Using F_y				Using F_u			
[1]	$\frac{P_p}{P_{ny}}$ [2]	$\frac{P_s}{P_{ny}}$ [3]	$\frac{P_{¼}}{P_{ny}}$ [4]	$\frac{P_u}{P_{ny}}$ [5]	$\frac{P_p}{P_{nu}}$ [6]	$\frac{P_s}{P_{nu}}$ [7]	$\frac{P_{¼}}{P_{nu}}$ [8]	$\frac{P_u}{P_{nu}}$ [9]
Number of specimens	43	30	23	52	14	11	8	12
Average	0.675	0.932	1.12	1.61	0.490	0.685	0.763	1.13
Standard deviation	0.173	0.184	0.262	0.378	0.157	0.148	0.170	0.269
95% confidence interval (low value)	0.623	0.866	1.01	1.51	0.407	0.597	0.646	0.976
99% confidence interval (low value)	0.607	0.845	0.976	1.48	0.381	0.570	0.609	0.929

connections that can allow only very small deformations should be based on 60% of the nominal load calculated using F_y with the proposed design method. However, for most standard connections, a reduction for stiffness is not required because a ¼-in. deformation allowance is not uncommon in determining the nominal strength of connections for various limit states. For example, in the AISC *Specification for Structural Steel Buildings* (AISC, 2005b), the nominal strength for bearing strength at bolt holes is based on a deformation limit of ¼ in., with an increase in the nominal strength available if more deformation is allowed.

EXPERIMENTAL VALIDATION

The proposed design method was compared to the results of 59 tests from 10 independent research projects. The experimental results are shown in Table A2 of Appendix A. Table A3 in Appendix A shows the calculated nominal strengths and predicted failure modes for all of the specimens. Table A3 also shows the test-to-calculated ratios for each available data point on the experimental curves.

The procedure outlined in the proposed design method was used to calculate the nominal strength of each specimen using the actual yield strengths and the ultimate strengths reported in the referenced documents. Several of the referenced documents reported the yield strength of the tested material, but omitted the ultimate strength; therefore, there were fewer experimental data points to compare with the ultimate strength calculations.

For each specimen, the nominal strength at each local yield line pattern was calculated using Equation 35, with the nominal value of t_c calculated without the resistance factor, as expressed in Equations 36a and 36b for the yield and ultimate strength solutions, respectively.

$$T_e = r_t \left(\frac{t}{t_c} \right)^2 \left(1 + \delta\alpha' \right) \le r_t \tag{35}$$

$$t_c = \sqrt{\frac{4 r_t b'}{p_e F_y}} \tag{36a}$$

$$t_c = \sqrt{\frac{4 r_t b'}{p_e F_u}} \tag{36b}$$

where

r_t = strength of tested bolt in tension

Then, the individual strengths of all local yield line patterns within the joint were summed to get the total strength of the joint.

The statistical results are summarized in Table 2, which provides the number of specimens with adequate data to be included in the results, the average, the standard deviation and the low values for the 95% and 99% confidence intervals. Note that P_p, P_s, $P_{¼}$ and P_u are defined in the section on Experimental Research, and P_{ny} and P_{nu} are the nominal loads calculated with the yield strength and ultimate strength of the fitting, respectively.

The results show that the load at ¼-in. deformation, $P_{¼}$, can be accurately predicted using F_y with the proposed design method. From column 4 in Table 2, the average test-to-predicted ratio for the 23 specimens is 1.12, and the standard deviation is 0.262. The low values for the 95% and 99% confidence intervals are 1.01 and 0.976, respectively.

The ultimate loads can be accurately predicted using F_u with the proposed design method. However, the deformations at ultimate strength can be very large—Table A2 in Appendix 2 shows experimental deformations greater than 1 in. for several specimens at the maximum test load. From

column 9 in Table 2, the average test-to-predicted ratio for the 12 specimens is 1.13, and the standard deviation is 0.269. The low values for the 95% and 99% confidence intervals are 0.976 and 0.929, respectively.

A comparison of columns 4 and 2 of Table 2 indicates that the load at the proportional limit is about 60% of the load at ¼-in. deformation. Based on this, serviceability design of connections that can allow only very small deformations may be based on 60% of the nominal load calculated using F_y with the proposed design method.

EXAMPLES

Example 1

Determine the equivalent tributary length for each bolt in Figure 14.

For bolt 1: The equivalent length is half of the equivalent length from Equation 33 plus half of the distance between bolts 1 and 2.

$$p_e = 2\sqrt{bc} + \frac{p_{12}}{2}$$

For bolt 2: The equivalent length is half of the distance between bolts 1 and 2 plus half of the distance between bolts 2 and 3.

$$p_e = \frac{p_{12}}{2} + \frac{p_{23}}{2}$$

For bolt 3: The equivalent length is half of the equivalent length from Equation 33 plus half of the distance between bolts 2 and 3.

$$p_e = 2\sqrt{bc} + \frac{p_{23}}{2}$$

Example 2

Determine the equivalent tributary length for each bolt in Figure 15.

For bolt 1: Assume $l_e < 2\sqrt{bc}$. The equivalent length is the distance from bolt 1 to the end of the member plus half of the distance between bolts 1 and 2.

$$p_e = l_e + \frac{p}{2}$$

For bolt 2: The equivalent length is half of the equivalent length from Equation 33 plus half of the distance between bolts 1 and 2.

$$p_e = 2\sqrt{bc} + \frac{p}{2}$$

Example 3

Determine the equivalent tributary length for each bolt in Figure 16.

For bolt 1: Assume $l_e < 2\sqrt{bc}$ and $x_s < x$. The equivalent length is the distance from bolt 1 to the end of the member plus half of the equivalent length from Equation 34a.

$$p_e = l_e + x_{s1} + \frac{bc}{x_{s1}}$$

For bolt 2: Assume $x_s < x$. The equivalent length is half of the equivalent length from Equation 34a plus half of the distance between bolts 2 and 3.

$$p_e = \frac{p_{23}}{2} + x_{s2} + \frac{bc}{x_{s2}}$$

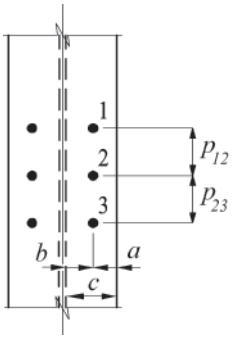

Fig. 14. Example 1.

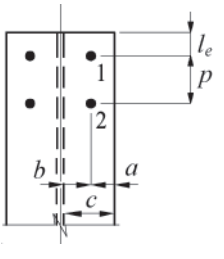

Fig. 15. Example 2.

For bolt 3: The equivalent length is half of the equivalent length from Equation 33 plus half of the distance between bolts 2 and 3.

$$p_e = 2\sqrt{bc} + \frac{p_{23}}{2}$$

Example 4

Determine the equivalent tributary length for each bolt in Figure 17.

For bolts 1 and 2: Assume $x_s < x$. The equivalent length is half of the equivalent length from Equation 33 plus half of the equivalent length from Equation 34a.

$$p_e = 2\sqrt{bc} + x_s + \frac{bc}{x_s}$$

Example 5

Determine the available LRFD strength of the connection in Figure 18 for the limit states of bolt rupture and beam flange bending. The beam is a W21×55 of A992 material. Bolts are ¾-in.-diameter A325 with 13⁄16-in.-diameter holes. The beam gage, *g,* is 5½ in.

$B = \phi r_n = 29.8$ kips
$t_f = 0.522$ in.
$t_w = 0.375$ in.
$b_f = 8.22$ in.

$$b = \frac{5.5 \text{ in.} - 0.375 \text{ in.}}{2} = 2.56 \text{ in.}$$

$$a = \frac{8.22 \text{ in.} - 5.5 \text{ in.}}{2} = 1.36 \text{ in.}$$

For design purposes, a must not be greater than $1.25b$.

$a < 1.25b$
1.36 in. < (1.25)(2.56 in.)

Use $a = 1.36$ in.

$$b' = 2.56 \text{ in.} - \frac{0.75 \text{ in.}}{2}$$
$$= 2.18 \text{ in.}$$

$$a' = 1.36 \text{ in.} + \frac{0.75 \text{ in.}}{2}$$
$$= 1.74 \text{ in.}$$

$$\rho = \frac{b'}{a'}$$
$$= \frac{2.18 \text{ in.}}{1.74 \text{ in.}}$$
$$= 1.25$$

$c = b + a = 2.56$ in. + 1.36 in. = 3.92 in.

For bolts at row 1,

$P_{eff} = 3.00$ in.

$$t_c = \sqrt{\frac{4.44Bb'}{p_{eff}F_y}}$$
$$= \sqrt{\frac{(4.44)(29.8 \text{ kips})(2.18 \text{ in.})}{(3 \text{ in.})(50 \text{ ksi})}}$$
$$= 1.39 \text{ in.}$$

$$\delta = 1 - \frac{d'}{p_{eff}}$$
$$= 1 - \frac{0.8125 \text{ in.}}{3 \text{ in.}}$$
$$= 0.729$$

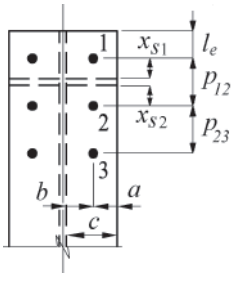

Fig. 16. Example 3.

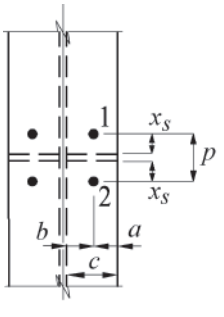

Fig. 17. Example 4.

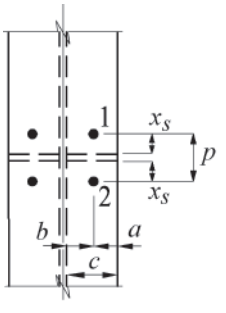

Fig. 18. Example 5—hanger connection without stiffeners.

$$\alpha' = \frac{1}{\delta(1+\rho)}\left[\left(\frac{t_c}{t}\right)^2 - 1\right]$$
$$= \frac{1}{(0.729)(1+1.25)}\left[\left(\frac{1.39 \text{ in.}}{0.522 \text{ in.}}\right)^2 - 1\right]$$
$$= 3.71 > 1.00$$

Use $\alpha' = 1.00$.

$$\phi T_n = B\left(\frac{t}{t_c}\right)^2 (1+\delta\alpha')$$
$$= (29.8 \text{ kips})\left(\frac{0.522 \text{ in.}}{1.39 \text{ in.}}\right)^2 \left[1+(0.729)(1.00)\right]$$
$$= 7.27 \text{ kips}$$

For bolts at row 2,

$$p_{eff} = \frac{3 \text{ in.}}{2} + \frac{6.5 \text{ in.}}{2}$$
$$= 4.75 \text{ in.}$$

$$t_c = \sqrt{\frac{4.44Bb'}{p_{eff}F_y}}$$
$$= \sqrt{\frac{(4.44)(29.8 \text{ kips})(2.18 \text{ in.})}{(4.75 \text{ in.})(50 \text{ ksi})}}$$
$$= 1.10 \text{ in.}$$

$$\delta = 1 - \frac{d'}{p_{eff}}$$
$$= 1 - \frac{0.8125 \text{ in.}}{4.75 \text{ in.}}$$
$$= 0.829$$

$$\alpha' = \frac{1}{\delta(1+\rho)}\left[\left(\frac{t_c}{t}\right)^2 - 1\right]$$
$$= \frac{1}{(0.829)(1+1.25)}\left[\left(\frac{1.10 \text{ in.}}{0.522 \text{ in.}}\right)^2 - 1\right]$$
$$= 1.84$$

Use $\alpha' = 1.00$.

$$\phi T_n = B\left(\frac{t}{t_c}\right)^2 (1+\delta\alpha')$$
$$= (29.8 \text{ kips})\left(\frac{0.522 \text{ in.}}{1.10 \text{ in.}}\right)^2 \left[1+(0.829)(1.00)\right]$$
$$= 12.3 \text{ kips}$$

For bolts at row 3,

$$p_{eff} = 2x + \frac{p}{2}$$
$$= (2)(3.17 \text{ in.}) + \frac{6.5 \text{ in.}}{2}$$
$$= 9.59 \text{ in.}$$

$$t_c = \sqrt{\frac{4.44Bb'}{p_{eff}F_y}}$$
$$= \sqrt{\frac{(4.44)(29.8 \text{ kips})(2.18 \text{ in.})}{(9.59 \text{ in.})(50 \text{ ksi})}}$$
$$= 0.776 \text{ in.}$$

$$\delta = 1 - \frac{d'}{p_{eff}}$$
$$= 1 - \frac{0.8125 \text{ in.}}{9.59 \text{ in.}}$$
$$= 0.915$$

$$\alpha' = \frac{1}{\delta(1+\rho)}\left[\left(\frac{t_c}{t}\right)^2 - 1\right]$$
$$= \frac{1}{(0.915)(1+1.25)}\left[\left(\frac{0.776 \text{ in.}}{0.522 \text{ in.}}\right)^2 - 1\right]$$
$$= 0.588$$

$$\phi T_n = B\left(\frac{t}{t_c}\right)^2 (1+\delta\alpha')$$
$$= (29.8 \text{ kips})\left(\frac{0.522 \text{ in.}}{0.776 \text{ in.}}\right)^2 \left[1+(0.915)(0.588)\right]$$
$$= 20.7 \text{ kips}$$

The available load for the serviceability limit state is

ϕP_n = (2)(7.27 kips) + (4)(12.3 kips + 20.7 kips) = 146 kips

If the ultimate strength, F_u = 65 ksi, is used in the design procedure, the available load for the strength limit state is

ϕP_n = (2)(9.43 kips) + (4)(15.9 kips + 23.0 kips) = 174 kips

Example 6

If more strength is required for the connection in Example 5, stiffeners can be added as shown in Figure 19. Determine the strength of the bolts and beam flange.

For bolts at row 1,

$P_{eff} = 3.00$ in.

$\phi T_n = 7.27$ kips (from Example 5)

For bolts at row 2,

$x_s = 2.50$ in.

$$x = \sqrt{bc} = \sqrt{(2.56 \text{ in.})(3.92 \text{ in.})} = 3.17 \text{ in.}$$

Thus, $x_s < x$; therefore,

$$p_{eff} = \frac{p}{2} + x_s + \frac{bc}{x_s} = \frac{3 \text{ in.}}{2} + 2.50 \text{ in.} + \frac{(2.56 \text{ in.})(3.92 \text{ in.})}{2.50 \text{ in.}} = 8.01 \text{ in.}$$

$$t_c = \sqrt{\frac{4.44Bb'}{p_{eff}F_y}} = \sqrt{\frac{(4.44)(29.8 \text{ kips})(2.18 \text{ in.})}{(8.01 \text{ in.})(50 \text{ ksi})}} = 0.849 \text{ in.}$$

$$\delta = 1 - \frac{d'}{p_{eff}} = 1 - \frac{0.8125}{8.01 \text{ in}} = 0.899$$

$$\alpha' = \frac{1}{\delta(1+\rho)}\left[\left(\frac{t_c}{t}\right)^2 - 1\right] = \frac{1}{(0.899)(1+1.25)}\left[\left(\frac{0.849 \text{ in.}}{0.522 \text{ in.}}\right)^2 - 1\right] = 0.813$$

$$\phi T_n = B\left(\frac{t}{t_c}\right)^2(1+\delta\alpha') = (29.8 \text{ kips})\left(\frac{0.522 \text{ in.}}{0.849 \text{ in.}}\right)^2\left[1+(0.899)(0.813)\right] = 19.5 \text{ kips}$$

For bolts at row 3,

$x_s = 3.50$ in.

$x_s = 3.17$ in.

Thus, $x_s > x$; therefore,

$$p_{eff} = 4x = (4)(3.17 \text{ in.}) = 12.7 \text{ in.}$$

$$t_c = \sqrt{\frac{4.44Bb'}{p_{eff}F_y}} = \sqrt{\frac{(4.44)(29.8 \text{ kips})(2.18 \text{ in.})}{(12.7 \text{ in.})(50 \text{ ksi})}} = 0.674 \text{ in.}$$

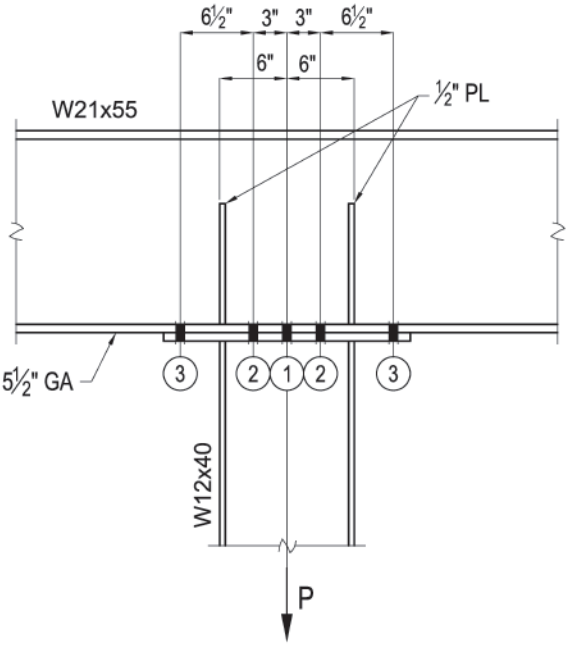

Fig. 19. Example 6—hanger connection with stiffeners.

$$\delta = 1 - \frac{d'}{p_{eff}}$$
$$= 1 - \frac{0.8125 \text{ in.}}{12.7 \text{ in.}}$$
$$= 0.936$$

$$\alpha' = \frac{1}{\delta(1+\rho)}\left[\left(\frac{t_c}{t}\right)^2 - 1\right]$$
$$= \frac{1}{(0.936)(1+1.25)}\left[\left(\frac{0.674 \text{ in.}}{0.522 \text{ in.}}\right)^2 - 1\right]$$
$$= 0.317$$

$$\phi T_n = B\left(\frac{t}{t_c}\right)^2(1+\delta\alpha')$$
$$= (29.8 \text{ kips})\left(\frac{0.522 \text{ in.}}{0.674 \text{ in.}}\right)^2\left[1+(0.936)(0.317)\right]$$
$$= 23.2 \text{ kips}$$

The available load for the serviceability limit state is

$\phi P_n = (2)(7.27 \text{ kips}) + (4)(19.5 \text{ kips} + 23.2 \text{ kips}) = 185 \text{ kips}$

If the ultimate strength, F_u = 65 ksi, is used in the design procedure, the available load for the strength limit state is

$\phi P_n = (2)(9.43 \text{ kips}) + (4)(21.4 \text{ kips} + 26.2 \text{ kips}) = 209 \text{ kips}$

CONCLUSIONS

A method has been proposed to calculate the tension strength of bolted flange connections, which includes the effects of prying action. The proposed design procedure, based on yield line theory, is simple, accurate and versatile. It can be used to calculate the strength of many different connection configurations, including stiffened connections, connections with large bolt spacing and connections close to the end of the member.

The bolt forces within a group are distributed according to the equivalent length tributary to each bolt, and the strength of each bolt is evaluated independently. The total strength of the joint is then calculated by summing the nominal strength at each bolt for the entire bolt group.

The calculated strengths were compared to the results of 59 tests from 10 independent research projects, and the proposed design method, which uses the yield strength of the fitting, was shown to be accurate for a deformation limit of approximately ¼ in. The ultimate strength of the fitting can be determined by using the proposed design procedure with the ultimate strength, F_u, of the fitting. However, the deformations at the ultimate strength can be large.

SYMBOLS

B	Available tension per bolt
C_r	Curve fit for the reduction factor is
F_y	Specified minimum yield strength of the fitting
F_u	Specified minimum tensile strength of the fitting
L_i	Length of yield line i
M_{pi}	Plastic moment capacity of yield line i
P	Applied load
P_{ny}	Nominal load calculated with the yield strength of the fitting
P_{nu}	Nominal load calculated with the ultimate strength of the fitting
P_p	Experimental load at the proportional limit
P_s	Experimental load at the nonlinear transition point on the load-deformation curve
P_u	Experimental load at ultimate failure
$P_{¼}$	Experimental load at ¼-in. deformation
T_a	Available tensile strength of fitting
T_{cr}	Strength of the fitting at the critical bolt (the bolt with the largest equivalent tributary length within the joint) (calculated using Equation 1)
$T_{cr(\alpha'=1)}$	Strength of the fitting at the critical bolt assuming a full yield line pattern forms without bolt rupture (calculated using Equation 1 with $\alpha' = 1$)
$T_{\alpha'=1}$	Strength of the fitting assuming a full yield line pattern forms without bolt rupture (calculated using Equation 1 with $\alpha' = 1$)
a	Distance from the bolt centerline to the edge of the fitting, but ≤ 1.25b for calculations using the proposed design method
b	Distance from bolt centerline to the face of the web
d_b	Bolt diameter
d'	Width of the hole along the length of the fitting
l_e	Edge distance from the bolt to the end of the member
m_p	Plastic moment capacity per unit length of the fitting
n	Number of bolt rows
p	Spacing between bolts

p_c Equivalent tributary length per bolt calculated according to the circular yield line pattern developed by Zoetemeijer (1981)

p_d Equivalent tributary length per bolt calculated according to the yield line pattern developed by Dranger (1977)

p_e Equivalent length of fitting tributary to the bolt in question for connection type 4, the equivalent length of fitting tributary to the bolt farthest from the end

p_{el} For connection type 4, the equivalent length of fitting tributary to the bolt closest to the end

p_m Equivalent tributary length per bolt calculated according to the yield line pattern developed by Mann and Morris (1979)

p_{min} Minimum equivalent tributary length per bolt; minimum of p_d, p_z and p_m

p'_{min} Approximate minimum equivalent tributary length per bolt calculated with Equation 30

p_s Equivalent tributary length per bolt calculated according to the stiffened yield line pattern in Figure 9

p_z Equivalent tributary length per bolt calculated according to the yield line pattern developed by Zoetemeijer (1974)

r_t Strength of tested bolt in tension

r_n Nominal strength of bolt in tension

t Thickness of the fitting, in.

x $\sqrt{bc}$

x_s Distance from the center of the bolt to the edge of the stiffener

Δ Virtual displacement

θ_i Virtual rotation of yield line i

δ_p Experimental deformation at the proportional limit

δ_s Experimental deformation at the nonlinear transition point on the load-deformation curve

δ_u Experimental deformation at ultimate failure

APPENDIX A

Table A1. Specimen Properties

Specimen	F_y (ksi)	F_u (ksi)	t (in.)	b (in.)	a (in.)	p_e (in.)	p_{el} (in.)	d_b (in.)	d' (in.)	r_t (kips)	Notes
Garrett (1977)											
1	41.2	66.5	0.465	1.62	1.51	7.00	—	0.875	0.938	54.1	
2	41.2	66.5	0.465	1.62	1.51	9.00	—	0.875	0.938	54.1	
3	41.2	66.5	0.465	1.62	1.51	9.00	—	0.875	0.938	54.1	
Ghassemieh et al. (1983)											
TH-1	43.5	65.9	0.5	1.5	2.92	5.62	2.08	0.625	0.688	27.1	
TH-2	38.7	70.1	0.5	2.5	2.92	8.23	2.08	0.625	0.688	27.1	
TH-3	45.4	66.5	1	1.5	2.92	5.00	2.08	0.625	0.688	27.1	
TH-4	43.1	73.9	1	2.5	2.92	10.3	2.08	0.625	0.688	27.1	
TH-5	44.9	72.5	0.75	1.5	2.92	5.62	2.08	0.625	0.688	27.1	
TH-6	37.7	65.2	0.75	2.5	2.92	8.23	2.08	0.625	0.688	27.1	
Grogan and Surtees (1999)											
E1	42.8	—	0.559	2.59	2.24	10.0	—	1.18	1.30	64.4	
E15	42.2	—	0.559	2.59	2.24	14.4	—	1.18	1.30	64.4	
Hendrick and Murray (1983)											
1	38.3	—	0.778	2.52	3.26	9.95	—	1.38	1.44	133	
2	34.6	—	0.813	2.50	4.54	10.7	—	1.38	1.44	133	
3	39.7	—	0.718	2.54	3.25	9.57	—	1.13	1.19	89.5	
4	39.7	—	0.718	2.54	3.25	10.14	—	1.50	1.56	159	
Moore and Sims (1986)											
T1	44.8	—	0.268	1.57	1.30	6.22	—	0.630	0.709	25.2	
T8	44.8	—	0.268	1.57	1.30	8.54	—	0.630	0.709	25.2	
Packer and Morris (1977)											
T1	42.9	—	0.268	1.58	1.12	6.04	—	0.630	0.811	36.7	
T2	43.0	—	0.268	1.58	1.12	6.04	—	0.630	0.811	36.7	
T3	42.5	—	0.354	1.56	1.12	6.01	—	0.630	0.811	36.7	
T4	44.7	—	0.268	1.73	0.96	7.26	—	0.630	0.811	36.7	
T5	43.6	—	0.528	1.49	1.12	5.86	—	0.630	0.811	36.7	
T6	43.2	—	0.268	1.58	1.12	8.30	—	0.630	0.811	36.7	
T7	43.9	—	0.268	1.58	1.12	8.30	—	0.630	0.811	36.7	
T8	44.8	—	0.268	1.58	1.12	8.30	—	0.630	0.811	36.7	
Pynnonen and Granstrom (1986)											
1	46.1	68.4	0.366	1.38	1.65	6.07	—	0.630	0.709	31.1	
5	46.1	68.4	0.366	1.74	1.30	6.57	—	0.630	0.709	31.1	
11	46.1	68.4	0.366	1.74	1.30	6.57	—	0.945	1.02	71.6	
15	44.8	64.4	0.551	2.19	3.54	9.07	—	0.945	1.02	71.6	
21	44.8	64.4	0.551	3.42	2.32	10.8	—	0.945	1.02	71.6	

Table A1. Specimen Properties (continued)											
Specimen	F_y (ksi)	F_u (ksi)	t (in.)	b (in.)	a (in.)	p_e (in.)	p_{el} (in.)	d_b (in.)	d' (in.)	r_t (kips)	**Notes**
Tawaga and Gurel (2005)											
T-N	41.8	61.9	0.394	1.44	1.38	6.03	—	0.787	0.866	50.9	
Zoetemeijer (1981)											
1	36.4	—	0.457	2.21	2.36	13.9	—	0.787	0.866	50.9	
2	36.4	—	0.457	3.18	1.38	18.2	—	0.787	0.866	50.9	
4	36.4	—	0.457	2.21	2.36	12.8	—	0.787	0.866	50.9	
5	36.4	—	0.457	3.18	1.38	9.54	—	0.787	0.866	50.9	
6	36.4	—	0.457	3.18	1.38	15.3	—	0.630	0.709	32.9	
7	36.4	—	0.457	3.18	1.38	15.8	—	0.787	0.866	50.9	
8	40.6	—	0.492	4.39	1.36	20.7	—	0.945	1.02	67.5	
9	40.6	—	0.492	2.19	3.56	13.7	—	0.945	1.02	67.5	
10	40.6	—	0.492	4.39	1.36	20.7	—	0.945	1.02	67.5	
11	40.6	—	0.492	2.19	3.56	14.2	—	0.945	1.02	67.5	1
12	40.6	—	0.492	4.39	1.36	27.6	—	0.945	1.02	67.5	
13	40.6	—	0.492	2.19	3.56	13.7	—	0.945	1.02	67.5	
14	40.6	—	0.492	2.19	3.56	17.5	—	0.945	1.02	67.5	1
15	40.6	—	0.492	4.39	1.36	27.6	—	0.945	1.02	67.5	
Zoetemeijer (1974)											
5	37.7	—	0.315	1.68	0.965	5.78	—	0.787	0.866	39.4	
6	37.7	—	0.315	1.28	1.13	5.09	—	0.787	0.866	39.4	
7	38.8	—	0.335	1.77	1.26	6.21	—	0.787	0.866	39.4	
8	41.8	—	0.492	1.77	1.22	6.17	—	0.787	0.866	41.1	
9	41.8	—	0.492	1.38	1.13	5.29	—	0.787	0.866	41.1	
10	39.2	—	0.906	1.61	1.26	5.88	—	0.787	0.866	38.9	
11	43.5	—	0.591	1.87	1.12	6.29	—	0.787	0.866	41.1	
12	43.5	—	0.669	1.69	1.26	6.03	—	0.787	0.866	38.3	
13	37.7	—	0.315	1.68	0.97	5.78	—	0.787	0.866	39.4	
14	37.7	—	0.315	1.68	0.97	5.78	—	0.787	0.866	39.4	
20	30.5	—	0.571	2.48	1.12	7.54	—	0.787	0.866	40.7	
21	30.5	—	0.571	2.48	1.12	7.54	—	0.787	0.866	40.7	
22	30.5	—	0.571	2.48	1.12	7.54	—	0.787	0.866	37.2	
23	30.5	—	0.571	2.48	1.12	7.54	—	0.787	0.866	37.2	
1. Four bolts per bolt row.											

Table A2. Experimental Results									
Specimen	**P_p (kips)**	**P_s (kips)**	**$P_{¼}$ (kips)**	**P_u (kips)**	**δ_p (in.)**	**δ_n (in.)**	**δ_u (in.)**	**Failure Mode**	**Notes**
Garrett (1977)									
1	56	82	92	164	0.08	0.18	1.39	F	
2	72	102	106	174	0.12	0.23	0.74	F	
3	85	97	117	239	0.13	0.17	1.29	F	
Ghassemieh et al. (1983)									
TH-1	80	—	—	105	0.002	—	0.006	B	
TH-2	40	110	—	140	0.001	0.016	> 0.1	F B	
TH-3	165	—	—	200	0.006	—	—	N	1
TH-4	150	175	—	195	0.007	0.014	0.03	B	
TH-5	130	150	—	170	0.006	0.012	> 0.02	F B	
TH-6	70	—	—	140	0.001	—	0.011	N	2
Grogan and Surtees (1999)									
E1	90	124	—	248	—	—	—	F	
E15	112	169	—	292	—	—	—	F	
Hendrick and Murray (1983)									
1	110	160	—	200	0.003	0.021	0.065	N	1
2	120	160	—	200	0.012	0.033	0.088	N	1
3	60	—	—	200	0.023	—	0.22	N	1
4	110	170	—	200	0.012	0.056	0.14	N	1
Moore and Sims (1986)									
T1	22	27	31	60	0.10	0.18	> 0.7	O	
T8	34	40	43	74	0.16	0.22	> 0.6	O	
Packer and Morris (1977)									
T1	22.5	—	—	63.0	—	—	—	F B	
T2	22.1	—	—	62.8	—	—	—	F B	
T3	36.0	—	—	69.3	—	—	—	F B	
T4	27.0	—	—	45.5	—	—	—	F O	
T5	63.0	—	—	103	—	—	—	O B	
T6	31.5	—	—	73.6	—	—	—	F O	
T7	31.5	—	—	73.6	—	—	—	F O	
T8	29.3	—	—	67.7	—	—	—	F O	
Pynnonen and Granstrom (1986)									
1	51	68	83	97.7	0.03	0.08	> 0.6	F B	
5	22	50	61	90.0	0.05	0.08	> 0.6	F B	
11	30	57	94	151	< 0.01	0.05	> 0.9	F	
15	72	110	130	212	< 0.01	0.03	> 0.9	F B	
21	—	—	—	191	—	—	—	F B	

Table A2. Experimental Results (continued)									
Specimen	**P_p (kips)**	**P_s (kips)**	**$P_{¼}$ (kips)**	**P_u (kips)**	**δ_p (in.)**	**δ_n (in.)**	**δ_u (in.)**	**Failure Mode**	**Notes**
Tawaga and Gurel (2005)									
T-N	61	74	94	97	0.024	0.063	0.32	N	3
Zoetemeijer (1981)									
1	—	—	—	167	—	—	—	F	
2	56	76	79	144	0.08	0.24	1.2	F	
4	—	—	—	161	—	—	—	F	
5	—	—	—	135	—	—	—	F	
6	—	—	—	117	—	—	—	B	
7	—	—	—	133	—	—	—	F	
8	50	80	79	183	0.09	0.18	2.4	B	
9	90	150	140	244	0.04	0.35	2.0	B	
10	40	65	68	183	0.08	0.20	2.2	O	
11	97	150	140	266	0.06	0.35	1.4	B	
12	—	—	—	150	—	—	—	O	
13	130	—	190	221	0.08	—	—	B	
14	250	290	280	300	0.12	0.43	0.59	O	
15	—	—	—	159	—	—	—	O	
Zoetemeijer (1974)									
5	22	32	45	49.5	0.004	0.02	> 0.2	F	4
6	32	45	63	67.4	0.01	0.03	> 0.2	F	4
7	26	40	48	67.4	0.01	0.03	> 0.2	F	4
8	—	—	—	135	—	—	—	F B	
9	—	—	—	135	—	—	—	F B	
10	—	—	—	148	—	—	—	F B	
11	—	—	—	126	—	—	—	F B	
12	—	—	—	153	—	—	—	F B	
13	22	29	36	49.5	0.02	0.04	> 0.2	F	4
14	25	30	36	40.5	0.04	0.05	> 0.2	F	4
20	—	—	—	120	—	—	—	F B	
21	43	63	84	103	0.02	0.04	> 0.2	F B	4
22	—	—	—	111	—	—	—	F B	
23	—	—	—	128	—	—	—	F B	

Failure modes
N: No failure
F: Flange bending
B: Bolt rupture
O: Other

Notes
1. Maximum test load was 200 kips, which was the machine capacity.
2. Test result for ultimate load was not available; 140-kip load was taken from finite element model.
3. Test was stopped at a load of 97 kips.
4. Loads at ¼-in. deformation were conservatively read from the highest graphed deformations, which were between 0.12 and 0.16 in.

Table A3. Calculation Results													
Specimen	Nominal Strength (kips)		Predicted Failure Mode		$\frac{P_p}{P_{ny}}$	$\frac{P_s}{P_{ny}}$	$\frac{P_{¼}}{P_{ny}}$	$\frac{P_u}{P_{ny}}$	$\frac{P_p}{P_{nu}}$	$\frac{P_s}{P_{nu}}$	$\frac{P_{¼}}{P_{nu}}$	$\frac{P_u}{P_{nu}}$	Notes
	Using F_y	Using F_u	Using F_y	Using F_u									
Garrett (1977)													
1	98.6	159	F	F	0.57	0.83	0.93	1.66	0.35	0.52	0.58	1.03	
2	129	176	F	F B	0.56	0.79	0.82	1.35	0.41	0.58	0.60	0.99	2
3	129	176	F	F B	0.66	0.75	0.91	1.85	0.48	0.55	0.66	1.36	2
Ghassemieh et al. (1983)													
TH-1	116	144	F B	F B	0.69	—	—	0.91	0.56	—	—	0.73	1
TH-2	81.8	111	F B	F B	0.49	1.34	—	1.71	0.36	0.99	—	1.26	1
TH-3	204	217	B	B	0.81	—	—	—	0.76	—	—	—	1
TH-4	177	195	B	B	0.85	0.99	—	1.10	0.77	0.90	—	1.00	1
TH-5	182	201	B	B	0.71	0.82	—	0.93	0.65	0.75	—	0.85	1
TH-6	125	167	F B	B	0.56	—	—	—	0.42	—	—	—	1
Grogan and Surtees (1999)													
E1	126	—	F	—	0.71	0.98	—	1.97	—	—	—	—	
E15	181	—	F	—	0.62	0.93	—	1.61	—	—	—	—	
Hendrick and Murray (1983)													
1	233	—	F	—	0.47	0.69	—	—	—	—	—	—	
2	252	—	F	—	0.48	0.63	—	—	—	—	—	—	
3	186	—	F	—	0.32	—	—	—	—	—	—	—	
4	215	—	F	—	0.51	0.79	—	—	—	—	—	—	
Moore and Sims (1986)													
T1	30.0	—	F	—	0.73	0.90	1.03	2.00	—	—	—	—	
T8	41.8	—	F	—	0.81	0.96	1.03	1.77	—	—	—	—	1
Packer and Morris (1977)													
T1	27.4	—	F	—	0.82	—	—	2.30	—	—	—	—	
T2	27.5	—	F	—	0.80	—	—	2.28	—	—	—	—	
T3	47.9	—	F	—	0.75	—	—	1.45	—	—	—	—	
T4	31.1	—	F	—	0.87	—	—	1.46	—	—	—	—	
T5	108	—	F B	—	0.58	—	—	0.95	—	—	—	—	
T6	38.7	—	F	—	0.81	—	—	1.90	—	—	—	—	1
T7	39.3	—	F	—	0.80	—	—	1.87	—	—	—	—	1
T8	40.1	—	F	—	0.73	—	—	1.69	—	—	—	—	1
Pynnonen and Granstrom (1986)													
1	66.1	98.1	F	F	0.77	1.03	1.26	1.48	0.52	0.69	0.85	1.00	
5	54.0	80.1	F	F	0.41	0.93	1.13	1.67	0.27	0.62	0.76	1.12	
11	59.1	87.8	F	F	0.51	0.96	1.59	2.55	0.34	0.65	1.07	1.72	
15	135	194	F	F	0.53	0.81	0.96	1.57	0.37	0.57	0.67	1.09	
21	95.4	137	F	F	—	—	—	2.00	—	—	—	1.39	

Table A3. Calculation Results (continued)													
Specimen	Nominal Strength (kips)		Predicted Failure Mode		$\frac{P_p}{P_{ny}}$	$\frac{P_s}{P_{ny}}$	$\frac{P_{¼}}{P_{ny}}$	$\frac{P_u}{P_{ny}}$	$\frac{P_p}{P_{nu}}$	$\frac{P_s}{P_{nu}}$	$\frac{P_{¼}}{P_{nu}}$	$\frac{P_u}{P_{nu}}$	Notes
	Using F_y	Using F_u	Using F_y	Using F_u									
Tawaga and Gurel (2005)													
T-N	69.5	103	F	F	0.88	1.06	1.35	—	0.59	0.72	0.91	—	
Zoetemeijer (1981)													
1	112	—	F	—	—	—	—	1.49	—	—	—	—	1, 3
2	96.8	—	F	—	0.58	0.79	0.82	1.49	—	—	—	—	1
4	103	—	F	—	—	—	—	1.56	—	—	—	—	1
5	49.5	—	F	—	—	—	—	2.73	—	—	—	—	1
6	74.2	—	B	—	—	—	—	1.58	—	—	—	—	
7	83.5	—	F	—	—	—	—	1.59	—	—	—	—	
8	101	—	F	—	0.50	0.79	0.78	1.81	—	—	—	—	1
9	152	—	F	—	0.59	0.99	0.92	1.61	—	—	—	—	3
10	101	—	F	—	0.40	0.64	0.67	1.81	—	—	—	—	1
11	157	—	F	—	0.62	0.96	0.89	1.69	—	—	—	—	
12	133	—	B	—	—	—	—	1.13	—	—	—	—	1, 3
13	152	—	F	—	0.86	—	1.25	1.45	—	—	—	—	1, 3
14	195	—	F	—	1.28	1.49	1.44	1.54	—	—	—	—	1
15	133	—	B	—	—	—	—	1.20	—	—	—	—	1, 3
Zoetemeijer (1974)													
5	31.2	—	F	—	0.71	1.03	1.44	1.59	—	—	—	—	
6	39.2	—	F	—	0.82	1.15	1.61	1.72	—	—	—	—	
7	36.5	—	F	—	0.71	1.10	1.32	1.85	—	—	—	—	
8	84.3	—	F	—	—	—	—	1.60	—	—	—	—	
9	99.8	—	F	—	—	—	—	1.35	—	—	—	—	
10	155	—	B	—	—	—	—	0.95	—	—	—	—	
11	115	—	F B	—	—	—	—	1.10	—	—	—	—	
12	126	—	F B	—	—	—	—	1.21	—	—	—	—	
13	31.2	—	F	—	0.71	0.93	1.15	1.59	—	—	—	—	
14	31.2	—	F	—	0.80	0.96	1.15	1.30	—	—	—	—	
20	67.9	—	F	—	—	—	—	1.77	—	—	—	—	
21	67.9	—	F	—	0.63	0.93	1.24	1.52	—	—	—	—	
22	67.9	—	F	—	—	—	—	1.63	—	—	—	—	
23	67.9	—	F	—	—	—	—	1.89	—	—	—	—	

Notes
1. $x_s < x$
2. $x_s > x$
3. Theory indicates circular yield line controls the design. This was accounted for in the listed values.

REFERENCES

AISC (2005a), *Steel Construction Manual*, 13th ed., American Institute of Steel Construction, Chicago, IL.

AISC (2005b), *Specification for Structural Steel Buildings*, American Institute of Steel Construction, Chicago, IL.

Astaneh, A. (1985), "Procedure for Design and Analysis of Hanger-Type Connections," *Engineering Journal*, AISC, Vol. 22, No. 2, pp. 63–66.

CEN (2005), *Eurocode 3: Design of Steel Structures-Part 1–8: Design of Joints*, European Committee for Standardization.

Douty, R.T. and McGuire W. (1965), "High Strength Bolted Moment Connections," *Journal of the Structural Division*, ASCE, Vol. 91, No. ST2, pp. 101–128.

Dranger, T.S. (1977), "Yield Line Analysis of Bolted Hanging Connections," *Engineering Journal*. AISC, Vol. 14, No. 3.

Garrett, J.L. (1977), "An Investigation of High Strength Bolted Tension Connections," Master's Thesis, Iowa State University.

Ghassemieh, M., Kukreti, A. and Murray, T.M. (1983), "Inelastic Finite Element Analysis of Stiffened End Plate Moment Connections," Report FSEL/AISC 83-02, School of Civil Engineering and Environmental Science, University of Oklahoma, June.

Grogan, W. and Surtees, J.O. (1999), "Experimental Behavior of End Plate Connections Reinforced with Bolted Backing Angles," *Journal of Constructional Steel Research*, Vol. 50, pp. 71–96.

Hendrick, A. and Murray, T.M. (1983), "Column Web and Flange Strength at End-Plate Connections," Report FSEL/AISC 83-01, School of Civil Engineering and Environmental Science, University of Oklahoma, February.

Hognestad, E. (1953), "Yield Line Theory for the Ultimate Flexural Strength of Reinforced Concrete Slabs," *Journal of the American Concrete Institute*, Vol. 24, No. 7.

Johansen, K.W. (1962), *Yield Line Theory*, Cement and Concrete Association, London, England.

Kulak, G.L., Fisher, J.W. and Struik, J.H.A. (1987), *Guide to Design Criteria for Bolted and Rivited Joints*, John Wiley and Sons, New York.

Mann, A.P. and Morris, L.J. (1979), "Limit Design of Extended End-Plate Connections," *Journal of the Structural Division*, ASCE, March, pp. 511–526.

Moore, D.B. and Sims, P.A.C. (1986), "Preliminary Investigations into the Behavior of Extended End-Plate Steel Connections with Backing Plates," *Journal of Constructional Steel Research*, pp. 95–122.

Muir, L.S. and Thornton, W.A. (2006), "Connections," Ch. 3, *Structural Steel Designer's Handbook*, R.L. Brockenbrough and F.S. Merritt, Eds., McGraw-Hill, New York.

Packer, J.A. and Morris, L.J. (1977), "A Limit State Method for the Tension Region of Bolted Beam-Column Connections," *The Structural Engineer*, Vol. 5, No. 10.

Pynnonen, J. and Granstrom, A. (1986), "Beam-to-Column Connections with Backing Plates," Swedish Institute of Steel Construction Report 86:6, April.

SCI (1995), *Joints in Steel Construction-Moment Connections*, The Steel Construction Institute, Ascot, Berkshire, UK.

Tawaga, H. and Gurel, S. (2005), "Strength Evaluation of Bolted Moment Connections Stiffened with Channels," Handout for poster session at the North American Steel Construction Conference.

Thornton, W.A. (1985), "Prying Action—A General Treatment," *Engineering Journal*, AISC, Vol. 22, No. 2, pp. 67–75.

Thornton, W.A. (1992), "Strength and Serviceability of Hanger Connections," *Engineering Journal*, Vol. 29, No. 4, pp. 145–149.

Thornton, W.A. and Kane, T. (1999), "Design of Connections for Axial, Moment and Shear Forces," Ch. 2, *Handbook of Structural Steel Connection Design and Details*, A.R. Tamboli, Ed., McGraw-Hill, New York.

Young, W.C. (1989), *Roark's Formulas for Stress and Strain*, 6th ed., McGraw-Hill, p. 207.

Zoetemeijer, P. (1974), "A Design Method for the Tension Side of Statically Loaded, Bolted Beam-to-Column Connections," *Heron*, Vol. 20, No. 1.

Zoetemeijer, P. (1981), "Semi-Rigid Bolted Beam-to-Beam Column Connections with Stiffened Column Flanges and Flush End Plates," *Joints in Structural Steelwork, Proc. International Conference,* Teesside Polytechnic, April 6–9, John Wiley and Sons.

On the Need for Stiffeners for and the Effect of Lap Eccentricity on Extended Single-Plate Connections

WILLIAM A. THORNTON and PATRICK J. FORTNEY

ABSTRACT

The design procedure for extended single-plate connections presented in the 13th edition of the *Steel Construction Manual* contains many design checks to ensure satisfactory performance but does not include a check of lateral-torsional stability of the extended single plate, which resembles a double-coped beam. Research has shown that coping of beams can reduce the lateral-torsional buckling strength of beams. This paper presents a proposal to use the double-coped-beam concept to ensure the lateral-torsional stability of the extended plate. The question of stiffeners and the effect of the small eccentricity due to the lapping of the plate with the beam web will also be addressed.

Keywords: extended single-plate connections, lap eccentricity, shear tabs, stiffeners.

The design procedure for extended single-plate connections (also known as extended shear tabs) presented in the 13th edition of the AISC *Steel Construction Manual* (AISC, 2005, pp. 10-102–10-104), hereafter referred to as the *Manual,* contains many design checks to ensure satisfactory performance, but it does not include a check on the effect of the extended tab on lateral-torsional stability. An extended single-plate connection to a beam end resembles a beam with a double-coped end. Research (Cheng et al., 1984) has shown that coping of beams can reduce the lateral torsional buckling strength of beams below what can be achieved with the same beam without coped ends. Because of the similarity between the extended shear tab and the double-coped beam end, this paper presents a proposal to use the latter to ensure the lateral-torsional stability of the former. The question of optional stiffeners and the effect of the small eccentricity due to the lapping of the shear tab with the beam web will also be addressed.

A research study on extended tabs (Sherman and Ghorbanpoor, 2002) recommended that unstiffened tabs not be used because of excessive lateral twist. The study considered eight unstiffened extended tabs, and the beams were essentially laterally unsupported for their full span. Table 1 contains the data from these tests necessary to understand that, using the design procedure for extended tabs presented in the *Manual*, the shear tabs will not twist excessively.

The excessive twists reported by Sherman and Ghorbanpoor occurred at the ultimate capacity of the beam connection system at a load far in excess of the capacity that would be calculated using the recommended AISC design procedure. This can be seen in Table 1. For instance, for test 1-U, the reported ultimate capacity is 58.7 kips, and the AISC Allowable Strength Design (ASD) capacity of the system is 11.3 kips. The elastic twist at 11.3 kips is 0.02 radian, which is negligible considering that the calculated elastic twist corresponds to a lateral translation of the tab equal to $\theta l/2 = (0.02)(9 \text{ in.})/2 = 0.09$ in. The tab thickness for test 1-U was 0.371 in., giving a lateral translation of only 24% of the thickness of the tab. Similar observations can be made for the other seven tests presented in Table 1.

The beam strength information (uniform design load, or UDL) reported in Table 1 is given to show that the connection strengths in these eight tests were not matched to the beam strengths. These connection strengths are very low compared to the beams they are supporting and do not represent practical connections. The physical tests were effectively unbraced so the "UDL Unbraced" column of Table 1 gives the beam strength of the actual tests. These are seen to be much larger than the connection strength. Connection 1-U, for example, can only carry (11.3/68.2)(100) = 16.5% of the total load the beam can carry. Practically, one would consider this percentage to be on the order of about 50%.

THE QUESTION OF OPTIONAL STIFFENERS

Figure 10-12 of the *Manual* shows "optional" stiffeners. The purpose of this discussion is to provide some guidance as to when stiffeners may be required. Considering that a

William A. Thornton, Corporate Consultant, Cives Steel Company, Roswell, GA (corresponding). E-mail: bthornton@cives.com

Patrick J. Fortney, Chief Engineer and Manager, Cives Steel Company, Roswell, GA. E-mail: pfortney@cives.com

Table 1. Evaluation of Data Reported by Sherman and Ghorbanpoor (2002)									
Test Case	Reported Ultimate Load (kips)	Lap Eccentricity (in.)	Loads		Strength	M_t*** (kip-in.)	Calculated Angle of Twist, ϕ (rads)	Calculated Lateral Translation (in.)	Percentage of Lateral Translation** (%)
			ASD UDL (CLB)* (kips)	ASD UDL (unbraced) (kips)	AISC Conn. Strength R_a(ASD) (kips)				
1-U	58.7	0.443	43.9	34.1	11.3	5.0	0.020	0.090	24.3
2-U	82.9	0.433	72.8	42.8	33.1	14.7	0.032	0.243	65.4
3-U	54.8	0.443	43.9	34.1	11.3	4.5	0.018	0.081	22.0
3-UM	58.6	0.443	43.9	34.1	11.3	4.5	0.018	0.081	22.0
4-U	98.7	0.501	72.8	42.8	22.0	10.6	0.015	0.110	21.7
6-U	138	0.578	126	80.0	31.2	17.4	0.020	0.181	35.8
6-UB	136	0.578	126	80.0	31.2	17.4	0.020	0.181	35.8
8-U	174	0.578	152	68.4	52.9	29.6	0.026	0.307	60.7

*CLB = continuously laterally braced
**Percentage of lateral translation of the tab relative to the tab thickness
*** $M_t = (R_a)$(lap eccentricity)

double-coped beam and a beam with an extended shear tab are similar in geometry, we can use research on double-coped beam lateral-torsional stability to estimate the lateral-torsional stability of beams with extended tabs. Cheng et al. (1984) show that the lateral-torsional buckling (LTB) mode of double-coped beams occurs primarily in the double-coped sections (the extended tab), and the uncoped beam acts essentially as a rigid body. In their research, this is apparent for beams that are laterally unbraced or braced only at the midspan load point. For a beam laterally supported for its full span—that is, $L_b \le L_p$—the authors postulate that the uncoped portion of the beam can be treated as a rigid body and that lateral-torsional buckling is dependent solely on the coped section or extended tab.

Theory

With the previous assumption, the LTB capacity of the tab (coped section) under pure moment is (see Figure 1):

$$M_{rec} = \frac{\pi}{2a}\sqrt{EGI_yJ} \tag{1}$$

where M_{rec} is the pure moment buckling strength of the rectangular section of the coped beam with a cope length, or shear tab length, of a.

As stated by Cheng et al., the pure moment case is a conservative approximation to the actual case where the moment in the tab varies from zero at the support to a maximum at the junction with the uncoped section of the beam.

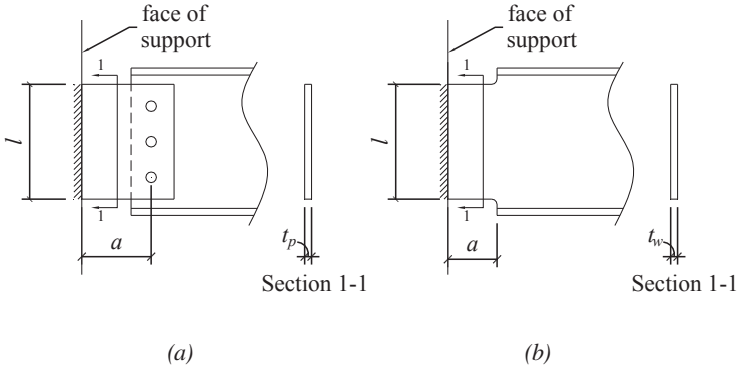

Fig. 1. (a) Shear tab and (b) coped beam.

Substituting

$I_y = \frac{1}{12} lt^3$ and $J = \frac{1}{3} lt^3$, and taking the product of EG as 324,800 ksi^2, Equation 1 becomes:

$$M_{rec} = 1500\pi \frac{lt^3}{a} \tag{2}$$

where

l = depth of shear tab
t = thickness of shear tab, t_p, or thickness of beam web, t_w
a = length of shear tab from support to first line of bolts

Equation 2 controls the lateral-torsional buckling of the shear tab.

To ensure that the tab does not buckle, the required moment strength, $M_{req'd}$ (the load or demand) needs to be less than the LTB strength of the tab, M_{rec}.

$$M_{req'd} \le M_{rec} \tag{3}$$

It is more convenient to deal with a reaction than a moment. Assuming a case of constant shear over length a and moment varying from zero at the support to maximum at the end of the cope or tab, $M_{req,d}$ (an approximation of the common case with uniform loading along the length of the beam), the required reaction strength, $R_{req'd}$, at the support is

$$R_{req'd} = \frac{M_{req'd}}{a} \tag{4}$$

and

$$R_{req'd} \le \frac{M_{rec}}{a} = 1500\pi \frac{lt^3}{a^2} \tag{5}$$

In specification notation, stiffeners are not required when Equation 6, as follows, is satisfied.

$$R_{req'd} \le \phi R_n \text{ (LRFD)}$$

$$R_{req'd} \le \frac{R_n}{\Omega} \text{ (ASD)}$$

where

$\phi = 0.9$
$\Omega = 1.67$

$$R_n = 1500\pi \frac{lt^3}{a^2} \tag{6}$$

It may be convenient to check the need for stiffeners by evaluating the ratio of available shear to required shear as shown in Equation 7, as follows.

When $\eta \ge 1.0$, stiffeners are not required, calculate η as follows:

$$\eta = \frac{\phi R_n}{R_u} \text{ (LRFD)} \tag{7a}$$

$$\eta = \frac{R_n/\Omega}{R_a} \text{ (ASD)} \tag{7b}$$

The following are examples of implementation of the proposed limit state as given in Equation 6. In the first example, an artificial problem is presented, and the need for stiffening a shear tab is determined using the proposed procedure. The second example problem compares the strength predicted using the proposed procedure to the measured strength of a test specimen as reported by Cheng et al. (1984). In the third example problem, the measured strength of one of Cheng et al.'s coped beams is compared to the strength of the same beam converted from a coped beam to an extended tab of similar proportions, and then its strength predicted using the proposed theory given in Equation 6. Finally, the procedure proposed in this paper is compared to the results of a design example reported by Brockenbrough and Merritt (2006).

EXAMPLES

Example 1: A shear tab connection at the end of a W30×90 beam is used with the following properties (see Figure 2); L = 28 ft = 336 in., l = 24 in., t_p = 0.5 in., a = 9 in., and shear stud spacing is 12 in. o.c. over the length of the beam. Check both the ASD and LRFD methods. The Load and Resistance Factor Design (LRFD) required shear, R_u, is 115 kips, and assume that the ASD required shear, R_a, equals R_u/1.5.

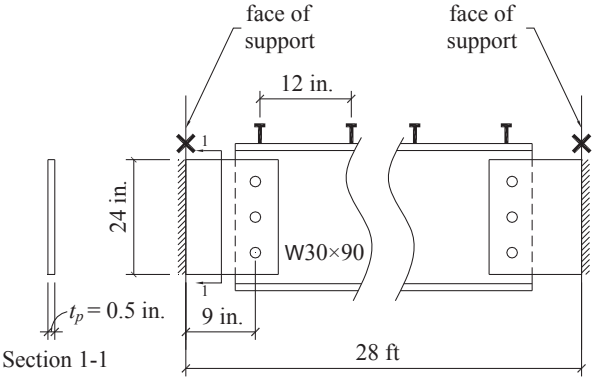

Fig. 2. Single-plate connection for Example 1.

Solution

L_b = 12 in. (stud spacing) < L_p = 7.38 ft
= 88.6 in. **o.k.**

$$R_n = \left(1500 \text{ kip/in.}^2\right)(\pi)\left(\frac{24 \text{ in.}}{(9 \text{ in.})^2}\right)(0.5 \text{ in.})^3$$
$$= 175 \text{ kips}$$

$$R_a = R_u/1.5$$
$$= 115 \text{ kips}/1.5$$
$$= 76.7 \text{ kips}$$

$$\phi R_n = 0.9(175 \text{ kips})$$
$$= 157 \text{ kips} > R_u = 115 \text{ kips (LRFD)} \quad \textbf{o.k.}$$

$$\frac{R_n}{\Omega} = \frac{175 \text{ kips}}{1.67}$$
$$= 105 \text{ kips} > R_a = 76.7 \text{ kips (ASD)} \quad \textbf{o.k.}$$

Thus, for this example, the tab does not need the optional stiffeners.

From the test of Equation 7,

$$\eta = \frac{157}{115} = 1.4 \text{ (LRFD)}$$

$$\eta = \frac{105}{76.7} = 1.4 \text{ (ASD)}$$

Because $\eta = 1.4 \geq 1.0$, the shear tab does not affect the beam strength and the optional stiffeners noted in Figure 10-12 are not required. If the extended tab affects beam strength, $\eta < 1.0$, the term a can be reduced by adding the optional stiffeners, or a thicker tab plate can be used, and then again checking if η is ≥ 1.0.

For this example, η is greater than 1.0, so stiffeners are not required.

Example 2: This example is from Cheng et al. (1984), Illustrative Example 2, page 127. The beam is a W12×14 beam, the span L = 223.2 in., loaded at the center, and laterally supported at the ends and at the point of loading, which is approximately at the beam center. The cope length is a = 12 in., the depth is d_c = 1.19 in.

From the measured properties of the test beam (beam LTB3), l = 9.504 in., and the web thickness t_w = 0.212 in. The test beam had flange and web yield stresses, F_y, of 57.4 and 55.3 ksi, respectively. Considering that the flanges are dominant in flexure, use F_y = 57.4 ksi. Also, Cheng et al. used G = 11,600 ksi rather than the AISC-recommended nominal value of 11,200 ksi and reported a shear strength of R_n = 2.75 kips. See Figure 3 for details of the problem.

Solution

Applying the proposed Equation 6,

$$R_n = 1500\pi\left(\frac{(9.504)(0.212)^3}{12^2}\right)\sqrt{\frac{11{,}600}{11{,}200}} = 3.02 \text{ kips}$$

(cope or tab LTB strength)

Assuming the more accurate value is that obtained by Cheng et al., the proposed theory given by Equation 6 is unconservative by 9.82% as shown in the following calculation. However, continuous lateral support of the beam is assumed in the derivation of Equation 6 (i.e., $L_b \leq L_p$ = 31.92 in. for a W12×14 beam), whereas Cheng et al. provided lateral support only at midspan and the ends of the beam (L_b = 119.3 in.).

$$\frac{3.02 - 2.75}{2.75}(100) = 9.82\%$$

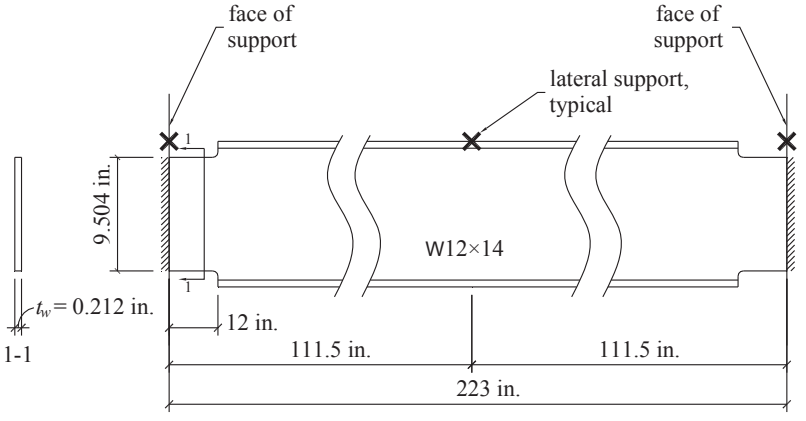

Fig. 3. Coped beam end for Example 2.

If Cheng et al.'s proposed equation (Equation 4.3 of their report) is used with $L_b = L_p = 31.92$ in., $R_n = 2.87$ kips and the difference is 4.97%.

$$\frac{3.02 - 2.87}{3.02}(100) = 4.97\%$$

The two theories thus give approximately the same answer to the same problem. Note that neither theory is an exact solution. However, the theory proposed in this paper provides a much simpler approach in that the only assumption required is that the uncoped portion of the beam acts like a rigid body. This assumption is validated by the results presented by Cheng et al. Cheng et al. use an interaction equation that is also an approximation to the exact differential equation formulations.

Continuing with Example 2, suppose the required shear strength is $R_u = 14$ kips. The uncoped beam has sufficient strength to produce an end reaction of 14 kips when the beam is uniformly loaded. The η test gives $\eta = (0.9)(3.02)/14 = 0.194 < 1.0$. Because this is less than 1.0, the strength of the beam is reduced by the copes and, hence, for an extended tab connection of similar geometry. If the beam must carry a load greater than $\phi(2R_n) = 2(0.9)(3.02) = 5.44$ kips, the optional stiffeners are required, or perhaps a thicker shear tab will suffice. If the optional stiffeners are used, the *a* dimension will be reduced from the outer edge of the stiffeners to the first line of bolts. Note that the original *a* is still used in the design of the extended tab. Regardless, if the parameters remain unchanged, stiffeners would be required, or the available strength of the beam would have to be taken as 5.44 kips.

Example 3: Assume the coped beam presented in Example 2 of Cheng et al. is converted to a shear tab configuration with similar proportioning. The beam is W12×14 with a span of 223 in. = 18.6 ft. The length of the tab plate, from the face of the support to the first column of bolts, is taken as the same as the cope length of Example 2 (i.e., a = 12 in.). The depth of the tab is l = 9 in., the reaction is Ru = 14 kips (assuming maximum total uniform load), and Zx = 17.4 in.3 (from the AISC Manual). Using the procedure for extended shear tabs from the Manual (p. 10-103), a plate thickness of $tp = 0.375$ in. will suffice.

Solution

From Equation 6:

$$\phi R_n = (0.9)\left(\frac{(1500)(\pi)(9)(0.375)^3}{(12)^2}\right)$$
$$= 14.0 \text{ kips} \geq 14 \text{ kips} \qquad \textbf{o.k.}$$

From Equation 7:

$$\eta = \frac{14}{14} = 1.0$$

The connection is perfectly proportioned so as not to reduce the LTB strength of the beam, and therefore, stiffeners are not required. In the event η was less than 1.0, the designer would need to make a decision to provide stiffeners, or increase the plate thickness while considering the maximum thickness prescribed by the *Manual* procedure.

Example 4: Consider a beam with a shear tab connection discussed by Brockenbrough and Merritt (2006), Section 3.4.3. The beam is W16×45 with $R_u = 51$ kips (as given by Brockenbrough and Merritt), $L = 24$ ft, $a = 10.5$ in., $t_p = 0.625$ in., $l = 12$ in., and all material has a yield strength of $F_y = 50$ ksi. See Figure 4 for a similar connection.

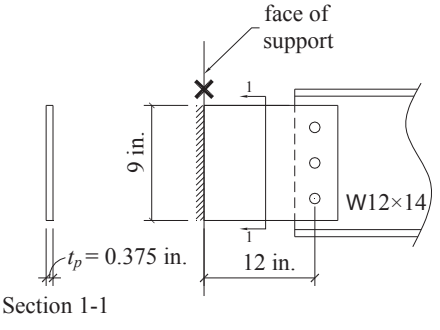

Fig. 4. Example 3; beam used in Example 2, but with a shear tab connection.

Solution

From Equation 6:

$$\phi R_n = (0.9)\frac{(1500)(\pi)(12)(0.625)^3}{(10.5)^2} = 113 \text{ kips}$$

Because ϕR_n = 113 kips > R_u = 51.0 kips, this design is satisfactory for lateral-torsional buckling.

Also, $\eta = \frac{113}{51} = 2.22 > 1.0$ **o.k.**

THE EFFECT OF LAP SPLICE ECCENTRICITY

Because of the lap joint between the shear tab and the beam web, there is a small eccentricity equal to $(t_p + t_w)/2$, which produces a torsional moment $M_t = R(t_p + t_w)/2$. This torsional moment also exists for the standard shear tab, but has been found to have no effect on connection strength in research (Astaneh et al., 1998; Creech, 2005) studies and in actual practice for at least 30 years. Extended tabs are a relatively new connection, with the design procedure first introduced in the AISC *Manual* (2005). Because of a lack of experience with this connection, the purpose of this discussion is to provide some guidance in its treatment.

Theory

The moment M_t defined earlier is resisted by two parts of the connection system: (1) the torsional strength of the tab itself and (2) the local torsional strength of the beam due to the floor slab or roof deck (see Figure 5). Also, recall that only laterally supported beams with $L_b \le L_p$ are considered in this paper.

The torsional resistance of the connection assembly is the sum of the torsional resistances of the tab plate and the beam. Let these be denoted by $M_{t,tab}$ and $M_{t,beam}$, respectively. Each of the two resistance components needs to be evaluated separately. As long as the total resistance exceeds the required torsional moment, M_t, the connection is satisfactory.

Torsional Resistance of the Tab

The tab shear stress is the sum of the torsional shear stress and the vertical shear stress due directly to the load R. Thus, using the plastic strength of the tab:

$$\frac{2}{lt_p^2}M_t + \frac{R}{lt_p} \le 0.6F_{yp} \quad (8)$$

Solving for M_t and setting M_t equal to the nominal strength of the tab, $M_{t,tab}$,

$$M_{t,tab} = \left[0.6F_{yp} - \frac{R}{lt_p}\right]\frac{lt_p^2}{2} \ge 0 \quad (9)$$

Note that when $M_{t,tab} < 0$, the tab can carry no torsion and $M_{t,tab}$ should be taken as zero. However, $M_{t,tab}$ must be greater than zero in order to proceed.

Torsion of the Beam Local to the Connection

In addition to the torsional resistance of the tab, the beam will also provide some torsional resistance due to the floor or roof slab. Because the beam tends to rotate, the slab on the "high" side will resist the rotation simply due to its weight and the imposed live load. Note that because no consideration here is given to studs, puddle welds or TEK screws, this is a conservative approach. Only the total dead and live loads local to the connection are used. It is assumed that the dead and live floor load imparts a contact load that is uniformly distributed across the flange of the beam, regardless of the direction of the span of the decking. Note that these dead plus live loads give rise to the beam reaction R.

The length of the beam, l_w, effective in resisting the moment, M_t, is controlled by the beam web thickness, t_w, as

$$M_t = R\left(\frac{t_w + t_p}{2}\right) = \frac{1}{4}\left(F_{yb}\right)t_w^2 l_w \quad (10)$$

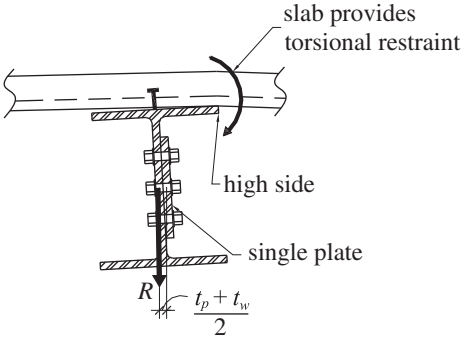

Fig. 5. Composite slab and metal roof or floor deck provides torsional resistance.

and solving for lw,

$$l_w = \frac{2R\left(t_w + t_p\right)}{\left(F_{yb}\right)t_w{}^2} \tag{11}$$

The maximum force, *F,* that can be exerted at the tip of the high-side beam flange (see Figure 5) is controlled by the beam loading. The beam loading per unit length is 2*R/L*, and for a length, l_w:

$$F = \frac{2Rl_w}{L} = \frac{4R^2\left(t_w + t_p\right)}{\left(F_{yb}\right)Lt_w{}^2} \tag{12}$$

The nominal strength of the beam is thus

$$M_{t,beam} = \frac{Fb_f}{2} = \frac{2R^2\left(t_w + t_p\right)b_f}{\left(F_{yb}\right)Lt_w^2} \tag{13}$$

A design is satisfactory based on beam strength if

$$M_t \le M_{t,beam} \tag{14}$$

As mentioned earlier, the total strength is the sum of the strength of the tab and the strength of the beam. So, a satisfactory design is one for which

$$M_t \le M_{t,tab} + M_{t,beam} \tag{15}$$

In *Specification* notation,

$$M_{t,u} \le \left[\phi_v\left(0.6F_{yp}\right) - \frac{R_u}{lt_p}\right]\frac{lt_p^2}{2} + \frac{2R_u^2\left(t_w + t_p\right)b_f}{\left(\phi_b F_{yb}\right)Lt_w{}^2} \quad \text{(LRFD)} \tag{16a}$$

$$M_{t,a} \le \left[\frac{0.6F_{yp}}{\Omega_v} - \frac{R_a}{lt_p}\right]\frac{lt_p^2}{2} + \frac{\Omega_b 2R_a^2\left(t_w + t_p\right)b_f}{F_{yb}Lt_w{}^2} \quad \text{(ASD)} \tag{16b}$$

where

$\phi_v = 1.0$
$\phi_b = 0.9$
$\Omega_v = 1.5$
$\Omega_b = 1.67$

ADDITIONAL EXAMPLES

Example 5: This is the same example as Example 1. The given data are $R_u = 115$ kips, $L = 336$ in., $t_w = 0.470$ in., $t_p = 0.5$ in., b_f =10.4 in. and $l = 24$ in., From Equation 16,

$$\phi M_t = \left[(1.0)(0.6)(50) - \frac{115}{(24)(0.5)}\right]\left(\frac{(24)(0.5)^2}{2}\right) + \frac{(2)(115)^2\left(0.470 + 0.5\right)(10.4)}{(0.9)(50)(336)(0.470)^2}$$

$$\phi M_t = 61.25 \text{ kips} + 79.88 \text{ kips} = 141 \text{ kip-in.}$$

$$M_{t,u} = (115)\left(\frac{0.470 + 0.500}{2}\right)$$

$$= 55.8 \text{ kip-in.} < 141 \text{ kip-in.} \qquad \textbf{o.k.}$$

From Examples 1 and 5, the W30×90 beam with an extended tab connection is o.k. for lateral-torsional buckling and lap eccentricity.

Example 6: This is the problem shown in Example 3. From the data of Example 3, R = 14 kips, l = 9 in., a = 12 in., $t_p = 0.375$ in., $t_w = 0.20$ in., $L = 233$ in., and $b_f = 3.97$ in., assuming Grade 50 plate material.

Solution

From Equation 16:

$$\phi M_t = \left[(1.0)(0.6)(50) - \frac{14}{(9)(0.375)}\right]\left(\frac{(9)(0.375)^2}{2}\right) + \frac{(2)(14)^2\left(0.200 + 0.375\right)(3.97)}{(0.9)(50)(223)(0.2)^2}$$

$$\phi M_t = 16.35 + 2.23$$

$$= 18.6 \text{ kip-in.}$$

The required torsional moment $M_{t,u}$ is:

$$M_{t,u} = 14\left(\frac{0.200 + 0.375}{2}\right)$$

$$= 4.02 \text{ kip-in.} < 18.6 \text{ kip-in.} \qquad \textbf{o.k.}$$

From Examples 3 and 6, the extended shear tab is satisfactory for lateral-torsional buckling and lap eccentricity.

Example 7: This is the extended shear tab of Example 4. Using the data of Example 4, and $b_f = 7.04$ in., Equation 16 gives the following:

Solution

$$\phi M_t = \left[(1.0)(0.6)(50) - \frac{51}{(12)(0.625)}\right]\left(\frac{(12)(0.625)^2}{2}\right) + \frac{(2)(51)^2\left(0.345+0.625\right)(7.04)}{(0.9)(50)(288)\left(0.345\right)^2}$$

$$\phi M_t = 54.4 + 23.0$$

$$= 77.4 \text{ kip-in.}$$

The required moment, $M_{t,u}$, is:

$$M_{t,u} = 51\left(\frac{0.345+0.625}{2}\right)$$

$$= 24.7 \text{ kip-in.} < 77.4 \text{ kip-in.} \quad \textbf{o.k.}$$

From Examples 4 and 7, the extended tab is satisfactory for lateral-torsional stability and lap eccentricity.

CONCLUSIONS AND RECOMMENDATIONS

The lateral displacement of beams with coped ends or extended plate connections is primarily due to the torsional strength of the connection or connection region. It is assumed that the main beam section, or uncoped length, displaces laterally as a rigid body, and as discussed, this provides a reasonable prediction of the lateral-torsional buckling capacity of the connected beam. The authors recommend that the need for stiffeners be evaluated using Equations 6 and 7 (repeated here for convenience). When η is less than 1.0, the "optional" stiffeners as noted in Figure 10-12 of the AISC *Manual* (2005) should be provided, or in the case of a shear tab, perhaps a thicker shear plate will suffice. When η is greater than or equal to 1.0, stiffeners need not be used.

Recommended Check for Stiffening of Extended Single-Plate Connections or Coped Ends

The following checks will be included in the revised design procedure for extended single-plate connections in the 14th edition of the *Steel Construction Manual*:

$R_{req'd} \le \phi R_n$ (LRFD)

$R_{req'd} \le \dfrac{R_n}{\Omega}$ (ASD)

where

$\phi = 0.9$

$\Omega = 1.67$

$$R_n = 1500\pi\frac{lt^3}{a^2} \tag{6}$$

Stiffeners are not required when $\eta \ge 1.0$, where:

$$\eta = \frac{\phi R_n}{R_u} \text{ (LRFD)} \tag{7a}$$

$$\eta = \frac{R_n/\Omega}{R_a} \text{ (ASD)} \tag{7b}$$

The torsional resistance of lap splice shear connections is the sum of two components; the lateral resistance of the tab and the lateral resistance of the beam in the connected region. The example problems presented in this paper suggest that the effect of the eccentricity inherent in the connection is negligible relative to the total torsional capacity of the connection. However, the following is a recommended check.

$$M_{t,u} \le \left[\phi_v\left(0.6F_{yp}\right) - \frac{R_u}{lt_p}\right]\frac{lt_p^2}{2} + \frac{2R_u^2\left(t_w + t_p\right)b_f}{\left(\phi_b F_{yb}\right)Lt_w{}^2} \quad \text{(LRFD)} \tag{16a}$$

$$M_{t,a} \le \left[\frac{0.6F_{yp}}{\Omega_v} - \frac{R_a}{lt_p}\right]\frac{lt_p^2}{2} + \frac{\Omega_b 2R_a^2\left(t_w + t_p\right)b_f}{F_{yb}Lt_w{}^2} \quad \text{(ASD)} \tag{16b}$$

where

$\phi_v = 1.0$

$\phi_b = 0.9$

$\Omega_v = 1.5$

$\Omega_b = 1.67$

SYMBOLS

E	Young's modulus
F	Force at beam flange tip resisting beam rotation
F_{yb}	Yield stress of beam web
F_{yp}	Yield stress of tab plate (or coped beam web)
G	Shear modulus
J	Torsional constant
L	Length of beam
L_b	Unbraced length of beam
L_p	Limiting laterally unbraced length for the limit state of yielding
M_a	Design required moment strength (ASD)
M_{rec}	Elastic lateral-torsional buckling moment of a rectangular beam section
M_{rec}	Critical lateral-torsional moment of the shear tab or double coped portion of beam
$M_{req'd}$	Required moment strength
M_t	Torsional moment due to lap eccentricity
$M_{t,a}$	Design required torsional moment strength (ASD)
$M_{t,u}$	Design required torsional moment strength (LRFD)
M_u	Design required moment strength (LRFD)
R_a	Design required reaction strength (ASD)
R, R_{req}	Required reaction strength
R_u	Design required reaction strength (LRFD)
W	Total load on beam
a	Length of cope or length of shear tab to first column of bolts
b_f	Width of beam flange
l	Depth of tab plate or cope
l_w	Effective length of beam to resist rotation
t	See t_p or t_w
t_p	Thickness of tab plate
t_w	Thickness of beam web
w	Uniform load on beams

REFERENCES

AISC (2005), *Steel Construction Manual*, 13th ed., American Institute of Steel Construction, Chicago, IL.

Astaneh-Asl, H., Call, S.M. and McMullin, K.M. (1989), "Design of Single-Plate Shear Conections," *Engineering Journal*, American Institute of Steel Construction, Vol. 26, No. 1, pp. 21–32.

Brockenbrough, R.L. and Merritt, F.S. (2006), *Structural Steel Designer's Handbook*, 4th ed., Ch. 3, L.S. Muir and W.A. Thornton, Eds., McGraw-Hill, New York.

Cheng, J.J., Yura, J.A. and Johnson, C.F. (1984), "Design and Behavior of Coped Beams," Phil M. Ferguson Structural Engineering Laboratory, University of Texas at Austin, Austin, TX.

Creech, D.D. (2005), "Behavior of Single-Plate Shear Connections with Rigid and Flexible Supports," Masters Thesis, North Carolina State University, Department of Civil and Environmental Engineering, Raleigh, NC.

Sherman, D.R. and Ghorbanpoor, A. (2002), "Design of Extended Shear Tabs," Final report for the American Institute of Steel Construction, October, University of Wisconsin, Milwaukee, WI.

Strength Design Criteria for Steel Beam-Columns with Fire-Induced Thermal Gradients

MAHMUD M.S. DWAIKAT and VENKATESH K.R. KODUR

ABSTRACT

When exposed to fire, restrained steel members develop significant internal forces, and these forces transform their behavior from beams or columns to that of beam-columns. The current provisions for fire-resistance assessment of such beam-columns through *P-M* interaction equations are an extension to the ambient interaction equations. These fire design equations take into consideration the reduction in the capacity arising from temperature-induced degradation of strength and stiffness properties but do not take into account the effect of other critical factors, such as thermal gradient, end restraints and realistic fire scenarios (with cooling phase). In this study, the different fire design equations for steel beam-columns are compared against results from nonlinear finite element simulations. Results from the analysis show that fire-induced thermal gradient leads to not only a reduction in the *P-M* diagrams, but also a noticeable distortion in the shape of the *P-M* diagrams. Therefore, modifications are proposed to the current design interaction equations for steel beam-columns at elevated temperatures. The modified *P-M* design equations are validated against results from fire tests and from finite element analysis and then illustrated through a design example. The proposed approach requires minimum computational effort and provides better assessment of beam-columns under fire when compared to current provisions.

Keywords: beam-columns, elevated temperatures, fire, interaction equations.

INTRODUCTION

The current approach of computing *P-M* curves and related fire resistance of steel structural members is based on the assumption that a uniform temperature prevails across the depth of the section (AISC, 2005; EC3, 2005). However, in practice a steel beam or column might be exposed to fire from one, two or three sides, such as in beams supporting slabs or columns in the perimeter of a framed building. In such scenarios, the beams and columns are likely to develop nonuniform thermal gradients across the depth of the section, and this will significantly alter the shape of the *P-M* capacity curves (Dwaikat and Kodur, 2009).

The effect of thermal gradients on the load-carrying capacity of beam-columns has received little attention in the literature. The plastic *P-M* interaction curves for steel sections under fire conditions were studied by Ma and Liew (2004) by simulating inelastic response of beam-columns in steel frames. However, the authors used average steel temperature and did not account for the effect of thermal gradients. The influence of thermal gradients on the plastic moment capacity was investigated by Burgess et al. (1990) by discretizing the section into strips and then numerically integrating the sectional stresses at full yield. However, the effect of axial force on the plastic moment capacity was not considered in the analysis.

Takagi and Deierlein (2007) assessed the sensibility of extending the room-temperature Eurocode 3 and AISC design equations to fire design through finite element analysis. In their study, they found that the AISC design equations are nonconservative when applied under fire conditions. Takagi and Deierlein proposed adjustments to room-temperature moment and axial capacities (M_{cr} and P_{cr}) of steel members for use at elevated temperature. Further, they recommended the use of the modified M_{cr} and P_{cr} into the AISC *P-M* interaction equations at elevated temperature, and these modified equations are being implemented in the 2010 AISC *Specification for Structural Steel Buildings*. However, the proposed adjustments do not take into consideration the influence of thermal gradients on M_{cr}, P_{cr} or the *P-M* interaction equation.

The underlying mechanics of the distortion of *P-M* diagrams that is induced by thermal gradients was studied by Garlock and Quiel (2007, 2008). These studies showed that a thermal gradient in a steel section causes the center of stiffness, *CS*, of the cross section to migrate toward the cooler (stiffer) regions and away from the heated (softer) regions. This migration of the center of stiffness generates an eccentricity, *e*, between the geometric center, *CG*, and the center of stiffness of the cross section. As a result of

Mahmud M.S. Dwaikat, Ph.D. candidate, Civil and Environmental Engineering Department, Michigan State University, East Lansing, MI. E-mail: dwaikat1@egr.msu.edu

Venkatesh K.R. Kodur, Professor, Civil and Environmental Engineering Department, Michigan State University, East Lansing, MI. E-mail: kodur@egr.msu.edu

this eccentricity, bending moment is generated because the axial force will now act eccentrically with respect to the new center of stiffness of the section. This generated bending moment may counteract the bending moment that results due to thermal bowing. Therefore, this migration of center of stiffness causes a distortion in the plastic *P-M* interactive diagram (Dwaikat and Kodur, 2009; Garlock and Quiel, 2007, 2008).

Based on these studies, Garlock and Quiel (2008) proposed a numerical procedure to compute the resulting distorted *P-M* diagrams for an I-shaped cross section subjected to any thermal gradient of any shape. The proposed method requires intensive use of numerical programs, such as MATLAB, or spreadsheets. For example, lengthy algorithms are required to compute the lumped temperature in each steel plate of the section to numerically integrate the temperature-dependent ultimate stresses along the depth of the cross section. This makes the method laborious and not straightforward.

Further research by Dwaikat and Kodur (2009) on the influence of fire-induced thermal gradient on *P-M* diagrams has led to modifications to the current interaction *P-M* equations in codes and standards. However, the study by Dwaikat and Kodur (2009) was limited to rigid plastic failure modes (plastic *P-M* diagrams). In this study, an improved and simplified approach is presented for estimating the distorted *P-M* diagrams of I-shaped cross section induced by thermal gradients. The proposed approach accounts for plastic as well as second-order inelastic failure modes in steel beam-columns under fire conditions. While the idea of this paper is true for any kind of beam-column subjected to thermal gradient, the proposed equations are only valid for I-shaped cross sections subjected to thermal gradient in their strong direction. The proposed method utilizes simplifying assumptions for predicting the distorted *P-M* curves and does not require complex numerical integration of sectional ultimate stresses.

CURRENT FIRE PROVISIONS FOR BEAM-COLUMNS

AISC Approach

The 2005 AISC *Specification* recommends the use of ambient temperature design equations for fire design, but with temperature-reduced strength and stiffness steel properties (AISC, 2005). The design capacity of steel beam-columns in AISC is given in the form of an interaction relation between bending moment and the axial force:

$$c_1 \frac{P}{\phi P_{cr}} + c_2 \frac{M}{\phi M_{cr}} \le 1.0 \tag{1}$$

where P and M are the applied axial force and bending moment, P_{cr} and M_{cr} are the critical axial force and bending moment capacities; $c_1 = 1$ and $c_2 = 8/9$ when $P/P_{cr} \ge 0.2$, but when $P/P_{cr} < 0.2$, $c_1 = 0.5$ and $c_2 = 1$.

The critical axial capacity (P_{cr}) is given as:

$$P_{cr}^{\text{AISC}} = \begin{cases} \left(0.658^{F_y(T)/F_e(T)}\right) P_y(T), & K\lambda \le 4.71\sqrt{\dfrac{E_s(T)}{F_y(T)}} \\ 0.877 A_s F_e(T), & K\lambda > 4.71\sqrt{\dfrac{E_s(T)}{F_y(T)}} \end{cases} \tag{2}$$

where $\lambda = L/r_y$ is the slenderness ratio, K is the effective length factor, and r_y and A_s are the minimum radius of gyration and the cross sectional area of the column, respectively. $F_y(T)$ and $E_s(T)$ are the temperature-dependent yield strength and elastic modulus of steel, respectively. The plastic axial capacity, $P_y(T)$, is defined as $A_s F_y(T)$, and $F_e(T)$ is the temperature-dependent elastic Euler buckling stress given as:

$$F_e(T) = \frac{E_s(T)\pi^2}{(K\lambda)^2} \tag{3}$$

The critical bending moment capacity M_{cr} in Equation 1 is computed as:

$$M_{cr}^{\text{AISC}} = \begin{cases} M_p(T), & \lambda \le \lambda_p(T) \\ C_b\left(M_p(T) - \left(M_p(T) - S_x F_r(T)\right)\dfrac{\lambda - \lambda_p}{\lambda - \lambda_r}\right), & \lambda_p(T) < \lambda \le \lambda_r(T) \\ C_b M_e(T), & \lambda > \lambda_r(T) \end{cases} \le M_p(T) \tag{4}$$

In Equation 4, $F_r(T) = 0.7F_y(T)$ is the stress required to reach initial yielding when added to the residual stress. Here, Z_x and S_x are the plastic and elastic sectional moduli, respectively; $M_p(T)$ is the temperature-dependent plastic moment defined as $M_p(T) = F_y(T)Z_x$; C_b is a factor that accounts for the shape of the bending moment diagram, where $C_b = 1.14$ for uniformly loaded simply supported beam; and $M_e(T)$ is the temperature-dependent elastic lateral-torsional buckling moment:

$$M_e(T) = \frac{\pi}{L}\sqrt{E_s(T)I_y G_s(T)J + I_y C_w\left(\frac{\pi}{L}E_s(T)\right)^2} \tag{5}$$

The limiting slenderness ratios in Equation 4 are:

$$\lambda_p = 1.76\sqrt{E_s(T)/F_y(T)} \tag{6a}$$

$$\lambda_r(T) = \frac{\pi}{F_r(T)S_x}\sqrt{\frac{E_s(T)G_s(T)JA_s}{2}} \sqrt{1+\sqrt{1+4\frac{C_w}{I_y}\left(\frac{F_{cr}(T)S_x}{G_s(T)J}\right)^2}} \tag{6b}$$

where I_y, C_w and J are the second moment of area around the weak axis, the warping constant, and the torsional constant of the section, respectively, and $G_s(T)$ is the elastic shear modulus. In order to account for the second-order effect, the applied bending moment (M_o) is generally magnified by a factor β such that:

$$M = \beta_{AISC} \times M_o \tag{7}$$

where M is the second-order moment and M_o is the first-order elastic bending moment. The magnification factor β_{AISC} is defined as:

$$\beta_{AISC} = \frac{C_m}{1 - P/P_e} \geq 1 \tag{8}$$

where C_m is a coefficient that accounts for the moment gradient on the beam-column and is given as:

$$C_m = 0.6 - 0.4(M_1/M_2) \tag{9}$$

Here, M_1 and M_2 are the smaller and larger moments, respectively, at the ends of the beam-column; M_1/M_2 is positive when the member is bent in reverse curvature but negative when bent in single curvature, and P_e is the elastic Euler axial buckling load, [$P_e = A_s F_e(T)$, with $K = 1.0$, unless the analysis indicates that a smaller value of K may be used].

The critical bending and axial compressive capacity equations according to the 2005 AISC *Specification* are plotted in Figures 1 and 2, respectively, as a function of slenderness ratio and for different temperatures.

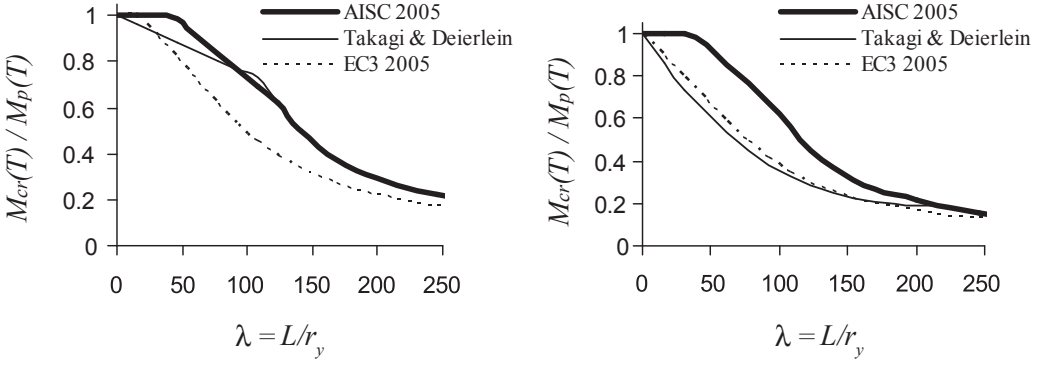

Fig. 1. Critical moment capacity at elevated temperature for W-shapes: (a) T = 20 °C (68 °F); (b) T = 500 °C (932 °F).

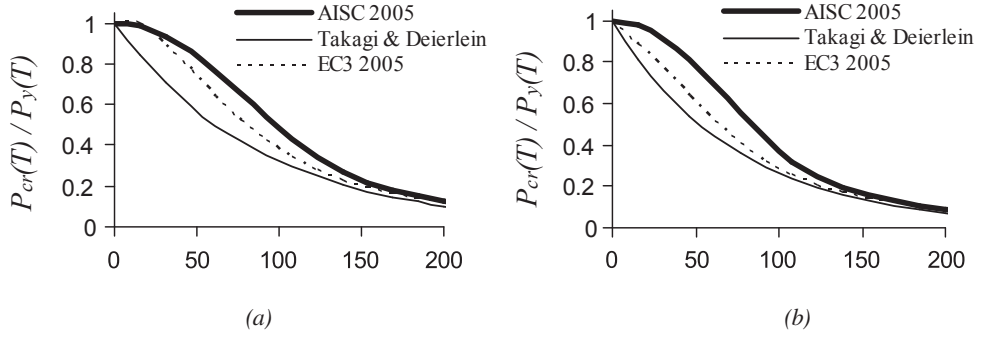

Fig. 2. Critical axial capacity at elevated temperature for W-shapes: (a) T = 20 °C (68 °F); (b) T = 500 °C (932 °F).

Eurocode Approach

In the Eurocode 3 (EC3, 2005) the capacity of steel beam-columns under fire is assessed using an interaction equation similar to AISC (Equation 1), but with $c_1 = c_2 = 1$. The critical moment and axial capacities, M_{cr} and P_{cr} in Equation 1, have different definitions in EC3.

The critical axial capacity is defined in EC3 as:

$$P_{cr}^{\mathrm{EC3}} = \chi_C(T) P_y(T) \tag{10}$$

where

$$\chi_{\mathrm{C}}(\mathrm{T}) = \frac{1}{\phi + \sqrt{\phi^2 - \bar{\lambda}^2}} \le 1 \tag{11a}$$

$$\phi = \frac{1 + \alpha\,\bar{\lambda} + \bar{\lambda}^2}{2} \tag{11b}$$

$$\alpha = 10 / \sqrt{F_y(\text{in MPa})} \tag{11c}$$

$$\bar{\lambda} \quad \bar{\lambda} = \sqrt{F_y(T)/F_e(T)} \tag{11d}$$

The critical bending moment is defined in EC3 as:

$$M_{cr}^{\mathrm{EC3}} = \chi_B(T) M_p(T) \tag{12}$$

where $\chi_B(T)$ accounts for reduction due to lateral torsional buckling and is computed similar to $\chi_C(T)$ but using normalized slenderness of $\bar{\lambda} = \sqrt{M_p(T)/M_e(T)}$.

The second-order effect factor β in Eurocode has a different form:

$$\beta_{\mathrm{EC3}} = 1 - \mu \frac{P}{P_{cr}} \le 1 \tag{13}$$

The factor μ is to account for lateral torsional buckling and is defined for compact sections as:

$$\mu = 0.15\bar{\lambda}\beta_{\mathrm{M}} - 0.15 \le 0.9 \tag{14}$$

where β_{M} is the equivalent uniform moment factor that depends on the shape of bending moment diagram. In case of uniform bending moment, $\beta_{\mathrm{M}} = 0.7$.

The critical bending and axial compressive capacity equations according to Eurocode are plotted in Figures 1 and 2, respectively, as function of slenderness ratio and for different temperatures.

Takagi and Deierlein (T&D) Approach

Based on a comparison between the current design approaches and nonlinear finite element analysis, Takagi and Deierlein (2007) suggested modifications to the 2005 AISC *Specification* strength and stability design equations under fire conditions. The modifications included new expressions for critical moment and axial capacities (M_{cr} and P_{cr}); however, the same AISC *P-M* interaction equation (Equation 1) was maintained. It is worth mentioning that these proposed adjustments are based on uniform temperature distribution across the beam cross section.

According to Takagi and Deierlein, the critical axial capacity is given as:

$$P_{cr}^{\mathrm{T\&D}} = \left[0.42^{\sqrt{F_y(T)/F_e(T)}}\right] P_y(T) \tag{15}$$

The critical moment capacity is given as:

$$M_{cr}^{\mathrm{T\&D}} = \begin{cases} S_x F_{cr}(T) + \left[M_p(T) - S_x F_{cr}(T)\right]\left(1 - \dfrac{\lambda}{\lambda_r(T)}\right)^{C_X}, \\ \dfrac{\pi}{L}\sqrt{E_s(T) I_y G_s(T) J + I_y C_w \left(\dfrac{\pi}{L} E_s(T)\right)^2}, \end{cases} \le M_p(T) \tag{16}$$

$$\lambda \le \lambda_r(T)$$

$$\lambda > \lambda_r(T)$$

The equation for $\lambda_r(T)$ is the same as Equation 6b but using a different value of $F_r(T)$:

$$F_r(T) = k_p(T) F_y - k_y(T) F_{rs} \tag{17}$$

where $k_p(T)$ and $k_y(T)$ are the temperature-dependent reduction factors for proportionality limit and yield strength of steel, respectively, as specified by Eurocode 3 (2005); F_{rs} is the residual stress at ambient temperature and is specified in AISC (2005) as 69 MPa; $C_x = 0.6 - T/250$, where T is steel uniform temperature in degrees Celsius, and C_x must always be less than 3.

Figures 1 and 2 compare AISC, Eurocode 3 and Takagi and Deierlein design curves for bending and axial compressive capacity of steel beams at elevated temperature as a function of slenderness ratio λ. The curves shown in Figures 1 and 2 are adapted from Takagi and Deierlein (2007) and form a basis for provisions in the 2010 AISC *Specification*. The bending and axial capacities as a function of steel temperature [$M_{cr}(T)$ and $P_{cr}(T)$] are normalized with respect to the plastic bending and axial capacities at elevated temperature [$M_p(T)$ and $P_y(T)$].

Based on the trends in Figures 1 and 2, the Eurocode approach is the most conservative under fire conditions [for $M_{cr}(T)$], while the 2005 AISC equations are the least conservative. Further, while the reduction in M_{cr} and P_{cr} according to Eurocode and 2005 AISC equations starts after a certain slenderness ratio, the reduction in M_{cr} and P_{cr} according to the T&D approach starts immediately for

nonzero slenderness (see Figure 1). The results of nonlinear finite element analysis carried out by Takagi and Deierlein showed that the reduction in M_{cr} indeed starts immediately for nonzero slenderness and that plastic bending capacity is only achieved for fully braced members under fire conditions. Based on these conclusions, Takagi and Deierlein proposed modified equations such that reduction in M_{cr} occurs immediately for nonzero slenderness beams.

INFLUENCE OF THERMAL GRADIENT

In all of the previously mentioned approaches, effect of fire-induced thermal gradient is accounted for by applying temperature-dependent reduction factors to room-temperature steel strength properties. The Eurocode (EC3, 2005) accounts for thermal gradient through applying numerical integrals for the axial and moment plastic capacities of the section only; that is:

$$P_y(T) = F_y \int k_y(T_i)dA = F_y \sum A_i k_y(T_i) \tag{18}$$

$$M_p(T) = F_y \int k_y(T_i) z_i dA = F_y \sum z_i A_i k_y(T_i) \tag{19}$$

The Eurocode procedure accounts for strength variation due to thermal gradient across the steel section; however, the stiffness variation due to thermal gradient across the section is not captured by this approach. In the AISC and T&D proposed equations, the influence of thermal gradient is not treated at all.

Thermal gradient can have a major influence on the shape of the interaction *P-M* Equation 1. Due to uneven heat distribution in the section, the center of stiffness of the section shifts from its original position. Because of the gradient-induced shift in the center of stiffness, the axial force will act eccentrically on the section and thus generate bending moment. This issue of shifting center of stiffness, which can have a major influence on beam-column response, is not treated in most design standards.

Also, thermal gradient has a direct influence on the second-order bending moments acting on the beam-column. This is due to the fact that thermal gradient leads to thermal bowing of the beam-column, and this increases the bending moment induced due to the *P*-Δ effect. Therefore, if the beam-column is not fully braced, the moment due to the *P*-Δ effect, which results from the thermal bowing, can be quite significant and thus causes premature strength failure of the beam-column. In all codes and standards, this critical influence of thermal gradient on the *P*-Δ effect is not treated explicitly and is left to the designer to quantify. The quantification of the *P*-Δ effect resulting from the thermal gradient often requires intensive use of complex finite element modeling.

PROPOSED MODIFICATIONS

Modifications to the design equations specified in codes and standards are proposed in order to account for the influence of thermal gradient on the capacity of steel beam-columns. The first modification is at the sectional level and is related to the distortion of the *P-M* diagram, which occurs as a result of the gradient-induced shift between center of stiffness and center of geometry of the cross section. The second modification is at the global (member) level and is related to the increased second-order effect (*P*-Δ effect) that results from thermal bowing caused by fire-induced thermal gradients. Both modifications will lead to change in the applied bending moment on the beam-column.

In a previous study by the authors (Dwaikat and Kodur, 2009), it was shown that the distortion of the *P-M* diagrams for beam-columns subjected to thermal gradient in the weak direction is negligible. Also, because the beam-columns are generally braced in their weak direction, the *P*-Δ effect (that would result from thermal bowing) can be neglected too. Thus, no modifications are required for the *P-M* diagrams in the weak direction of the beam-columns. Herein, modifications are proposed for the *P-M* diagrams for beam-columns subjected to thermal gradient across their strong (generally unbraced) axis.

When a beam-column is exposed to fire from one, two or three sides only, as shown in Figure 3a, thermal gradient (ΔT) develops across the cross section, and this gradient causes a migration of the center of stiffness from the hotter side to the cooler side of the cross section. This migration of center of stiffness leads to a corresponding distortion of the *P-M* diagrams of the beam-column. The basic features of the distorted plastic *P-M* diagrams for a W-section with thermal gradient in the strong direction are compared to the case of a uniform temperature in Figure 3b. The figure shows that the value of moment capacity under peak axial capacity (point A in Figure 3b) moves back and forth (to point A′ in Figure 3b) depending on the eccentricity *e* between center of stiffness, *CS*, and center of geometry, *CG*, that is caused by the thermal gradient in a W-section. The magnitude of the shift M_{TG} in the *P-M* capacity envelope (Figure 3b) is assumed to be numerically equal to the ultimate axial capacity $P_{u,Tave}$ of the section multiplied by the eccentricity *e* between the center of geometry, *CG*, and of the center of stiffness, *CS*, of the section as shown in Figure 3b. The ultimate capacity is computed based on the average temperature of the section:

$$M_{TG} = e \times P_{y,Tave} = e \times k_y(T_{s,Ave}) \times F_y \times A_s \tag{20}$$

To compute the eccentricity *e* between Y_{CS} and Y_{CG}, the reduction in the elastic modulus of steel is assumed to vary linearly across the depth of the section as shown in Figure 4. Each plate of the section is assumed to have a constant rate

of reduction, k_E, in the elastic modulus, depending on its average temperature. The reduction in elastic modulus of the steel in the web is assumed to equal the average of the reductions of both the top (cool) and bottom (hot) flanges. With these assumptions, the eccentricity e between Y_{CG} and Y_{CS} across the strong axis can then be calculated as follows:

$$e = Y_{CS} - Y_{CG} = \frac{\sum A_i \times k_E(T_i) \times y_i}{\sum A_i \times k_E(T_i)} - \frac{d}{2} \tag{21}$$

$$e = \frac{b_F t_F k_E(T_{s,CF}) \times d + \left(\frac{k_E(T_{s,CF}) + k_E(T_{s,HF})}{2}\right) t_w d \times \frac{d}{2}}{b_F t_F k_E(T_{s,CF}) + \left(\frac{k_E(T_{s,CF}) + k_E(T_{s,HF})}{2}\right) t_w d + b_F t_F k_E(T_{s,HF})} - \frac{d}{2} \tag{22}$$

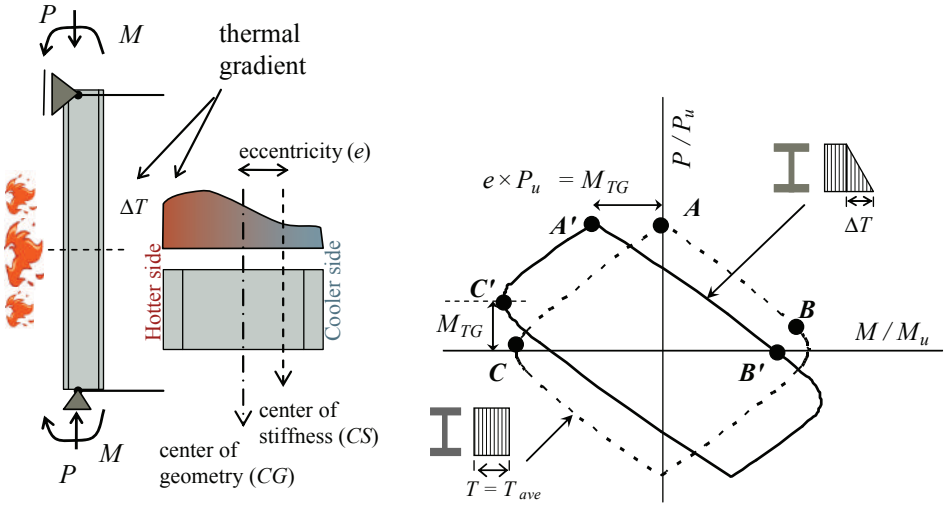

Fig. 3. Characterizing plastic P-M diagram for a W-shape with thermal gradient in the strong direction: (a) development of thermal gradient; (b) effect of thermal gradient on P-M diagrams.

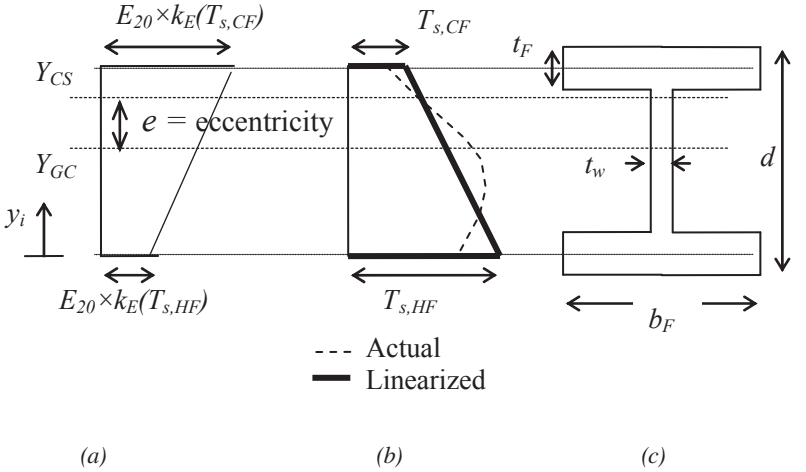

Fig. 4. Eccentricity between center of stiffness and center of geometry of a W-shape with thermal gradient: (a) elastic modulus profile; (b) temperature profile; (c) section dimensions.

$$e = \frac{d}{2}\left(\frac{2b_F t_F k_E(T_{s,CF}) + t_w d k_E(T_{s,Ave})}{k_E(T_{s,Ave})(2b_F t_F + t_w d)} - 1 \right) \quad (23)$$

where b_F, t_F, t_w and d are dimensions of the section as shown in Figure 4, and $k_E(T)$ is the reduction factor for elastic modulus at steel temperature T.

On the global (member) level, thermal gradient leads to the development of thermal curvature in the beam-column, and this leads to thermal bowing. This is illustrated in Figure 5, which shows the influence of thermal gradient on the local P-Δ effect of the beam-column. Thermal curvature and thermal bowing cause lateral deflection of the beam-column, and this lateral deflection will generate additional P-Δ moment. If we assume a uniform thermal gradient along the length of the beam-column, then thermal curvature will be constant along the beam-column. If the applied end moments on the beam-column are equal and opposite, as shown in Figure 5, then the mechanical curvature due to these bending moments will also be constant. The *elastic* lateral deflection in this case (as shown in Figure 5) can be obtained, according to Mohr's theorem, by integrating the moment of the resultant curvature (thermal minus mechanical curvature) as:

$$\Delta_{TB} = \int_{z=0}^{z=L/2} \left(\alpha \frac{\Delta T}{h} - \frac{M}{E_s(T_{ave})I} \right) z dz \quad (24)$$

$$= \left(\alpha \frac{\Delta T}{h} - \frac{M}{E_s(T_{ave})I} \right) \frac{L^2}{8}$$

The increase in bending moment due to thermal bowing can then be evaluated by multiplying the lateral deflection by the axial force in the beam-column:

$$M_{TB} = P \times \Delta_{TB} \quad (25)$$

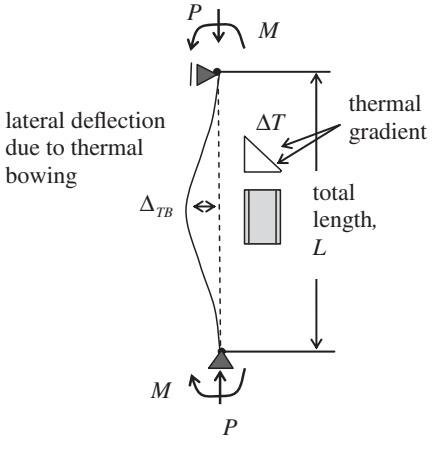

Fig. 5. Influence of thermal gradient on P-Δ effect.

The modification of the P-M interaction curves is based on using the average temperature of steel section with a shift M_{TG} that occurs as a result of thermal gradient in the section, and with second-order effects that arise due to thermal bowing, M_{TB}. The adjustment of P-M diagram is aimed at preserving the room-temperature shape of the P-M diagram and only introducing the shift M_{TG} to account for the thermal gradient effect. The adjusted equations of the plastic P-M diagrams for a wide-flange section with linearized thermal gradient in the strong direction can be written as:

$$\frac{|M + M_{TB} + M_{TG}|}{M_{cr,Tave}} + \frac{P}{P_{cr,Tave}} \le 1.0 \quad (26a)$$

$$\frac{|M + M_{TB} - M_{TG}|}{M_{cr,Tave}} - \frac{P}{P_{cr,Tave}} \le 1.0 \quad (26b)$$

VERIFICATION OF THE PROPOSED APPROACH

The proposed modifications are verified by comparing the predictions against results from nonlinear finite element analysis. In the following section, the nonlinear finite element model for the steel beam-column is introduced, and then the model is validated against data from fire tests. Once the model is validated, it is utilized to verify the proposed modifications as per Equation 26.

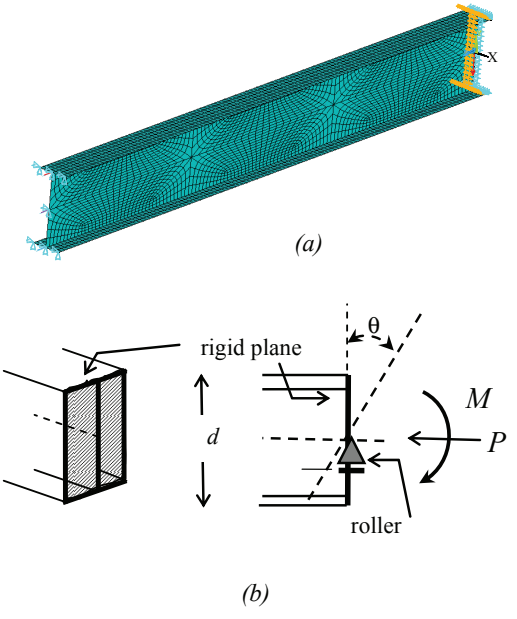

Fig. 6. Structural discretization and modeling of end restraint of beam-column: (a) structural mesh and boundary conditions; (b) model axial and rotational restraints.

Nonlinear Finite Element Analysis

The structural model for the steel beam-column was created using ANSYS (2007). Figure 6a shows the structural mesh and boundary conditions of the beam adopted for the structural analysis. To save on computational expenses, symmetry is utilized, and only half of the beam is modeled. For applying symmetry, in-plane translations and out-of-plane rotations are prevented at the nodes of the midspan section of the beam as shown in Figure 6a. The steel beam is discretized using shell elements (the eight-noded SHELL93 element in ANSYS 2007) that account for material and geometric nonlinearities. Based on sensitivity studies (Dwaikat and Kodur, 2009), the mesh size of the finite elements was chosen to be 30 mm × 30 mm, which means that each plate is modeled with at least three elements of the eight-noded shell element; thus, at least seven nodes were generated across the width of each plate. In the analysis, material nonlinearities include nonlinear temperature-stress-strain curves for steel and temperature-dependent thermal strain. Geometric nonlinearities include large deformations and large rotations. Kinematic constraints are applied on the boundary of the beam-column as shown in Figure 6b. This was to ensure consistent rotation of the end supports conditions according to the applied bending moment.

The high-temperature properties of steel used in the analysis are based on Eurocode properties (EC3, 2005). This is because the temperature-dependent reduction factors for the material properties of structural steel according to AISC specifications are identical to those specified in the Eurocode. Therefore, temperature-stress-strain curves for structural steel according to Eurocode are used for the analysis. The Eurocode coefficient of thermal expansion as a function of steel temperature is also used in the analysis.

Analysis Procedure

Three load steps were applied on the steel beam-column in order to obtain the capacity. In the first step, bending moment M is applied gradually on the meshed finite element model of the beam-column. Temperature and thermal gradient along the cross section and over the entire length of the beam-column is applied gradually in the second load step. Finally, in the third step, the axial force P is increased until failure occurs in the beam-column. In the numerical analysis, failure is said to occur at the last time step at which convergence is achieved. The maximum sustained axial force and the applied bending moment on the beam-column define a single point on the failure surface (P-M diagram) of the beam-column. To obtain another failure point on the P-M diagram, the same analysis is repeated but with a different value of initial applied bending moment on the supports. The analysis is also repeated for different span lengths, for average steel temperature and for the case with thermal gradients.

Model Validation

The finite element model is validated by comparing the predictions from analysis with measured data in fire-resistance tests on beam-columns. For this validation, data from fire-resistance tests on steel beam-columns subjected to fire induced thermal gradient are used. The details of the fire resistance test can be found elsewhere (Dwaikat, 2010; Kodur et al., 2009). The tested beam-column—a W8×48 cross section that is 3.3 m (130 in.) in height—was instrumented with thermocouples to measure steel temperatures, strain gauges to measure bending moment, and linear variable differential transformers (LVDTs) to measure displacement and top end rotations. The base of the

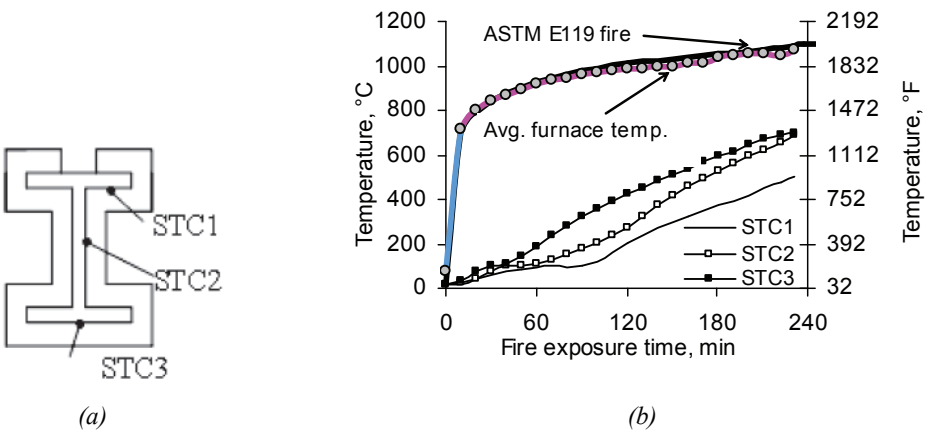

(a) *(b)*

Fig. 7. Recorded steel temperatures in tested beam-column: (a) cross section and thermocouples; (b) fire and steel temperatures.

beam-column was fully fixed using thick steel brackets, while the top end was free to rotate but restrained against lateral translations. The beam-column was subjected to an axial force corresponding to approximately 25% of its room-temperature plastic capacity. The beam-column was exposed to ASTM E119 standard fire (ASTM, 2008) from four sides, and the average insulation thickness was 25 mm (1 in.). In order to generate thermal gradient along the cross section, insulation material was removed from one side, as shown in Figure 7a. The recorded temperatures in the beam-columns in fire-resistance experiments are shown in Figure 7b at the base and at the location of the plastic hinge. The fire-induced axial force and bending moment in the beam-column are plotted in Figure 8 as a function of fire-exposure time.

The base bending moment (shown in Figure 8a) was directly computed using the readings of the strain gauges at the base of the beam-column which remained cool [below 40 °C (104 °F)] during the fire test (Dwaikat, 2010; Kodur et al., 2009). The bending moment at the critical section—where plastic hinge developed at 1930 mm (76 in.) from the base—was interpolated between the moment at the base and zero at the top end. The pressure recorded in the vertical actuators was also used to directly measure the fire-induced axial force. Figure 8 shows that both the axial force and bending moment increase first and then decrease with fire-exposure time. This is because the beam-columns expand nonuniformly under the influence of temperature and thermal gradients until the spread of plasticity in the beam-columns causes a reduction in the axial force.

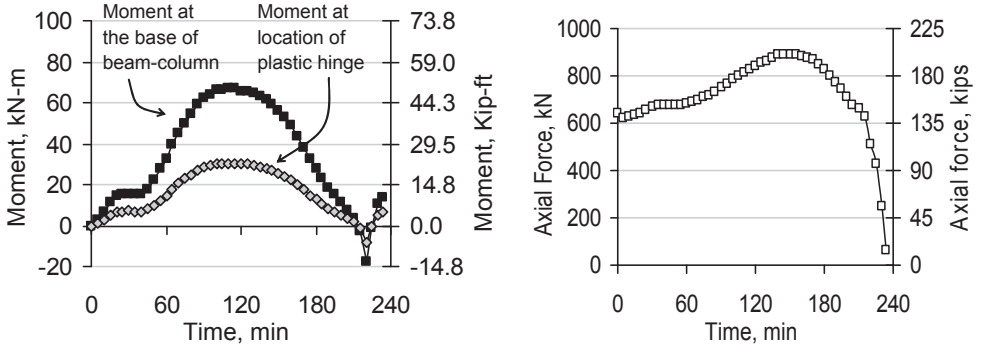

(a) *(b)*

Fig. 8. Measured fire-induced axial force and bending moment in the tested beam-column: (a) bending moment; (b) fire-induced axial force.

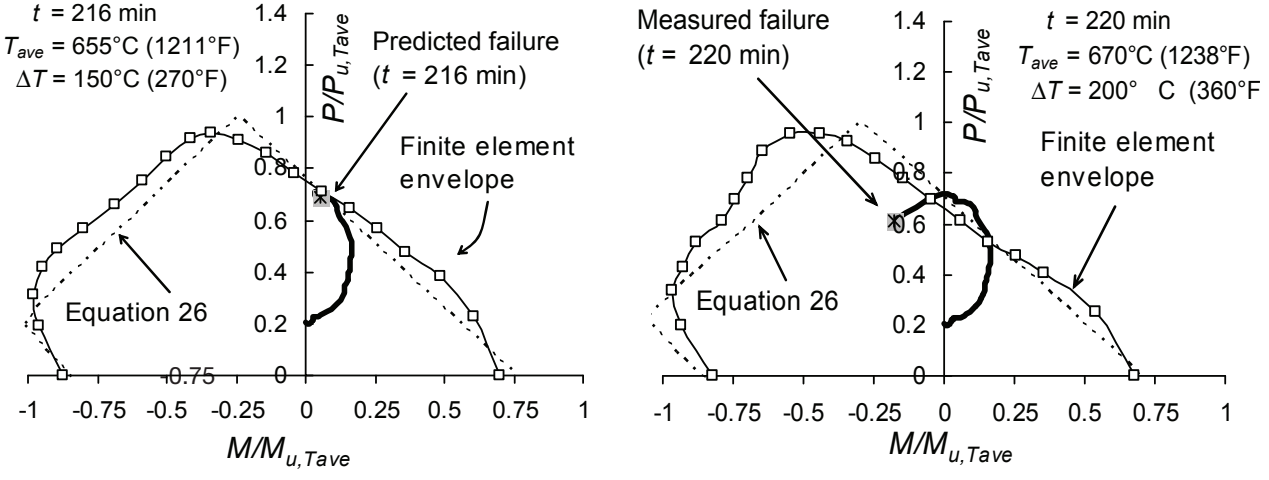

(a) *(b)*

Fig. 9. Measured and predicted P-M response for the tested beam-column: (a) at t = 216 min of fire exposure; (b) at t = 220 min of fire exposure.

Figure 9 plots the development of the fire-induced P and M in the tested beam-column. The P-M envelope as predicted using finite element analysis and the simplified approach (Equation 26) at two fire-exposure times is also plotted in Figure 9. It is seen in the figure that at different time steps, the beam-column experiences different thermal gradients, which cause different shifts in the P-M diagrams.

Based on the results in Figure 9a, the failure time of the beam-column is conservatively predicted by the detailed finite element analysis at t = 216 min, which matches well with predicted failure envelope using Equation 26. The actual failure of the beam-column was observed in the fire test at t = 220 min, as shown in Figure 9b. The actual failure in test is said to occur at the time after which the beam-column is no longer capable of carrying the applied axial load and thus starts to deflect at an accelerated rate. The predicted failure is assumed to be the time at which the fire-induced P and M exceed the capacity envelope given in Equation 26. The measured failure point is inside the capacity envelope mainly due to the experimental parameters. For instance, the fact that the temperature is not exactly uniform along the length of the beam-column can result in shifting the failure point more conservatively toward the inside of the capacity envelope. The comparison presented in Figure 9 shows that the finite element model is capable of predicting the P-M envelop of beam-columns subjected to thermal gradients.

Comparison with Finite Element Analysis

In order to verify the proposed approach in Equation 26 for predicting P-M diagrams, two steel sections with different cases of thermal gradients are analyzed. Figures 10 and 11 show the comparison between the plastic P-M diagrams for these two sections obtained through nonlinear finite element

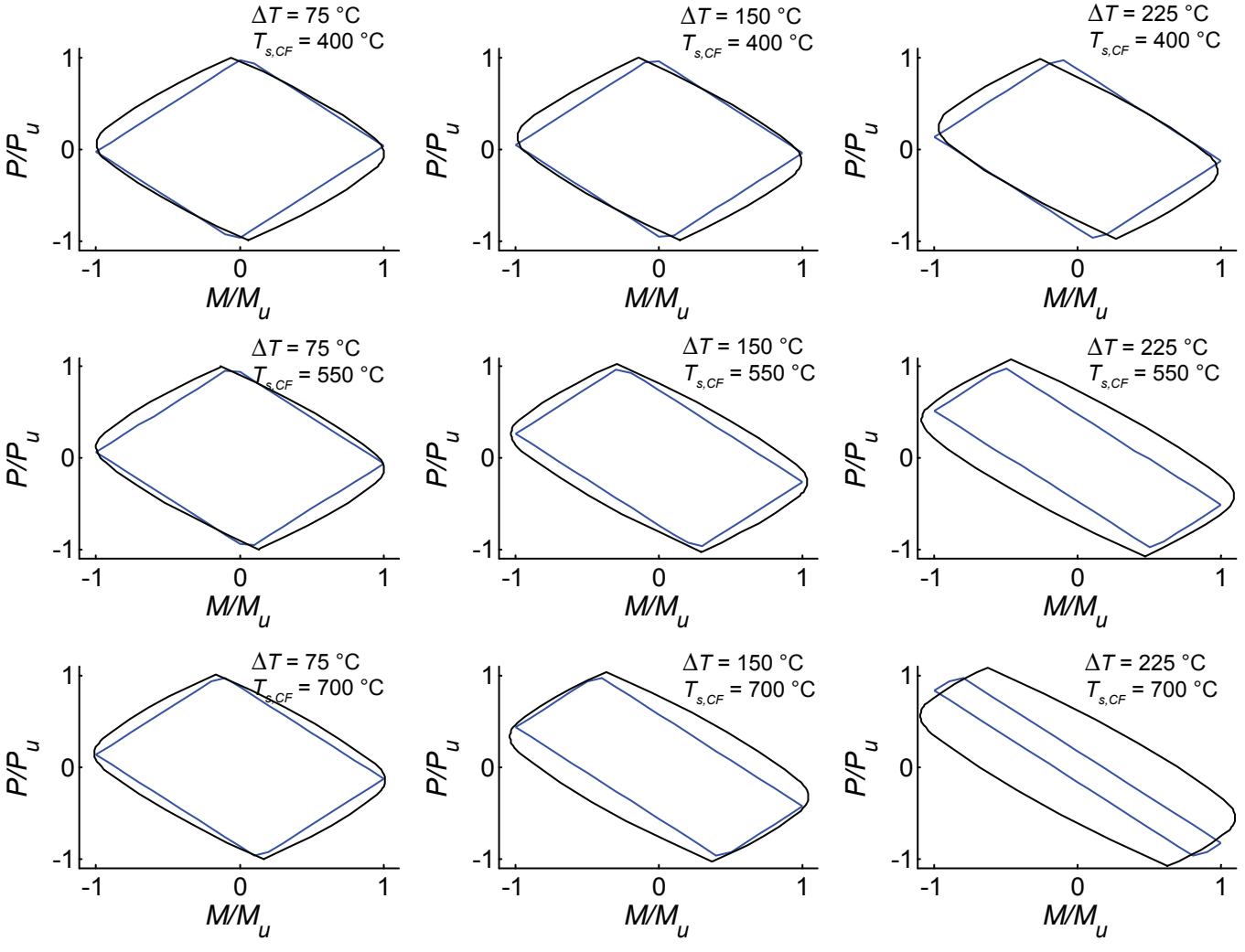

Fig. 10. Plastic P-M diagrams obtained from analysis (solid curves) and as predicted by Equation 26 (dashed curves) for a W24×76 section with different linear thermal gradients along its strong axis ($\Delta T = T_{s,HF} - T_{s,CF}$).

analysis (solid lines) and through the proposed equation (dashed lines). The two sections are W24×76 with relatively thin steel plates and W14×311 with thicker steel plates. These sections were selected to compare the effect of the different steel plate thicknesses on the *P-M* diagrams. The selected sections (W24×76 and W14×311) were subjected to different thermal gradients along their strong axis, and the resulting *P-M* diagrams are normalized to the axial and moment plastic capacities (P_u and M_u) using average temperatures. It can be seen in Figures 10 and 11 that the distortion in the *P-M* diagrams is well predicted using the proposed Equation 26 for both sections. Also, it can be seen in the figures that the distortion is larger for higher temperatures and higher thermal gradients. This is because at higher temperatures [$T_s > 400$ °C (752 °F)], the reduction in steel elastic modulus E_s becomes steeper and thus causes larger eccentricity e between center of stiffness and center of geometry of the nonhomogenous section. Further, the comparisons in Figures 10 and 11 indicate that increasing plate thicknesses has a very small influence on the shape of the *P-M* diagrams under extreme cases of thermal gradients [case ΔT = 225 °C (405 °F)]. It can be seen that Equation 26 conservatively predicts the *P-M* capacity envelopes for realistic cases of thermal gradients.

Figure 12 shows the shape of the *P-M* diagram for beam-columns subjected to thermal gradient and experiencing different types of failure modes. Steel section W18×76 was analyzed for different effective lengths [KL = 0, 5 and 10 m (0, 16.4 and 32.8 ft)]. The first case, whose results are presented in Figure 12a, represents plastic failure ($M_{cr} = M_p$ and $P_{cr} = P_y$), while the other cases, as shown in Figures 12b and c, represent inelastic and elastic buckling failure modes ($M_{cr} \le M_p$ and $P_{cr} \le P_y$), respectively. Results presented in Figure 12 indicate that the shift in *P-M* diagram

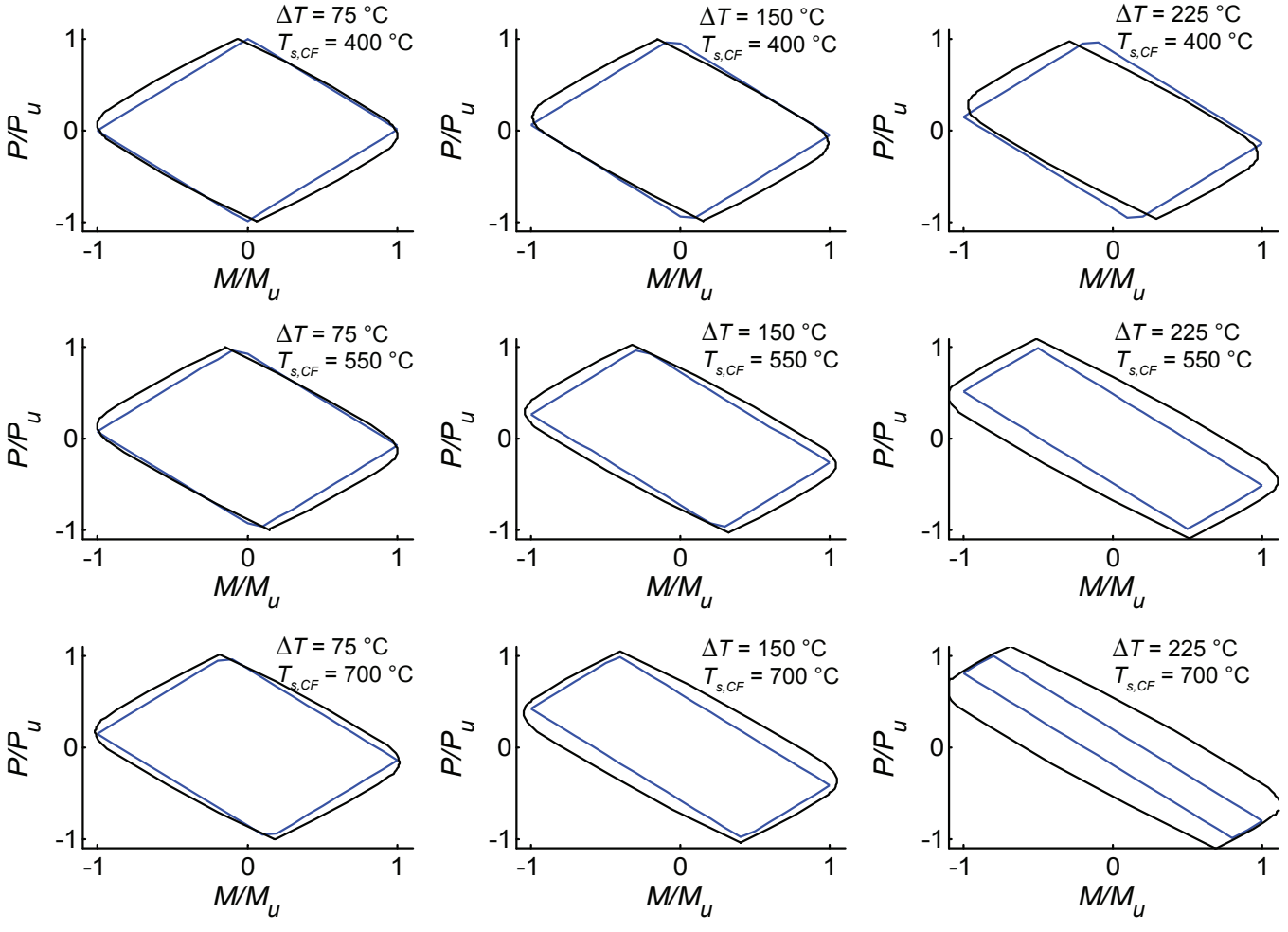

Fig. 11. Plastic P-M diagrams obtained from analysis (solid curves) and as predicted by Equation 26 (dashed curves) for a W14×311 section with different linear thermal gradients along its strong axis ($\Delta T = T_{s,HF} - T_{s,CF}$).

due to thermal bowing (Figures 12b and c) is in the opposite direction as compared to the shift arising due to migration of center of stiffness of the cross section (Figure 12a). This is because the bending moment due to lateral bowing, M_{TB}, and the moment due to thermal gradient, M_{TG}, always occur in an opposite direction to the migration of center of stiffness from the hotter to the cooler side of the cross section. The proposed Equation 26 captures this effect of thermal gradient on the *P-M* capacity envelopes. To date, the *P-M* interaction equations specified in codes and standards do not account for these changes in *P-M* diagrams that arise due to thermal gradient in the beam-column cross section.

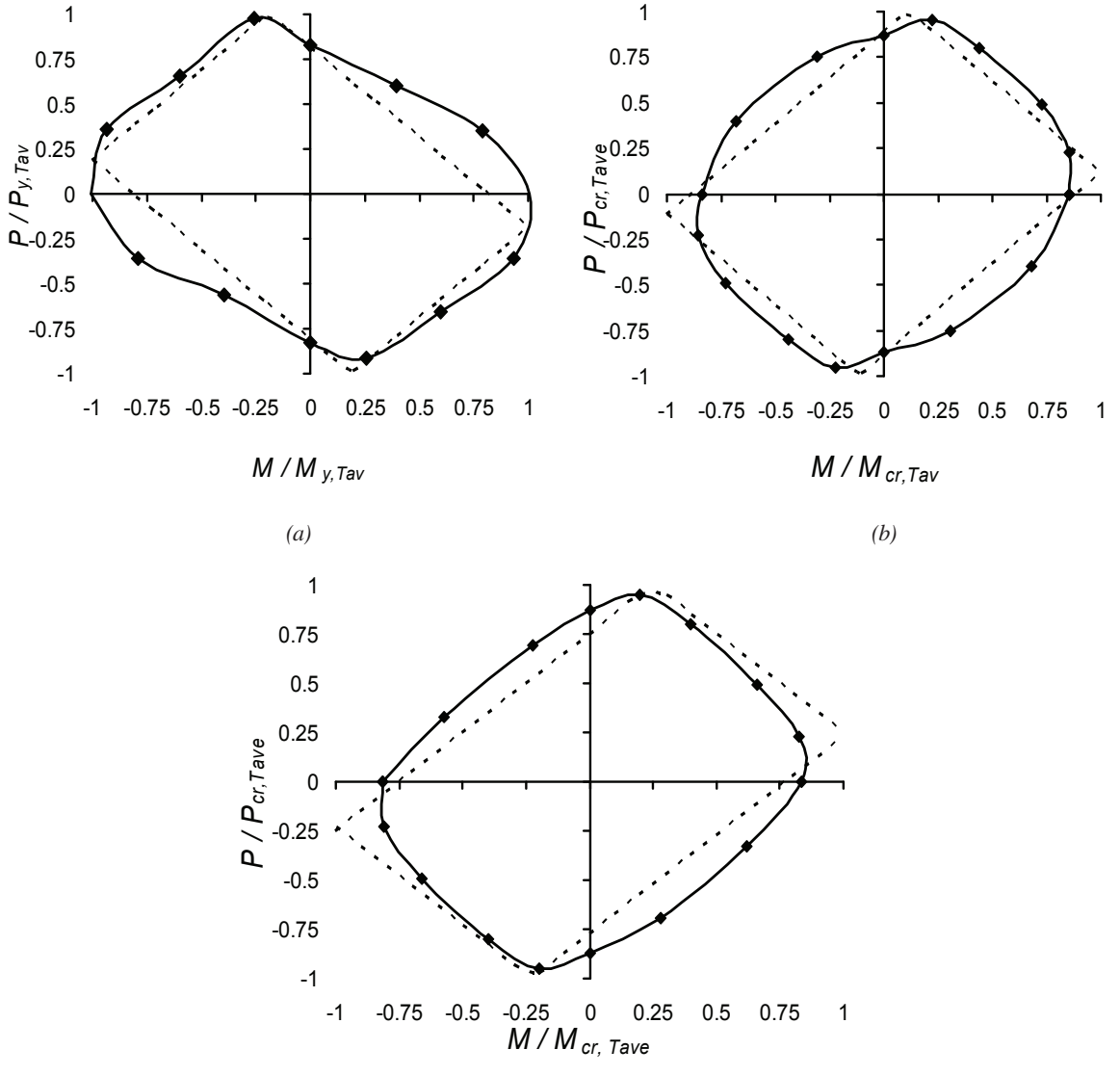

Fig. 12. P-M diagrams obtained from finite element analysis (solid curves) and as predicted by Equation 26 (dashed curves) for a W18×76 section with linear thermal gradient [ΔT = 200 ºC (360 ºF)] and average temperature of 500 ºC (932 ºF), but different effective lengths: (a) KL = 0 (plastic failure); (b) KL = 5000 mm (16.4 ft) (inelastic failure); (c) KL = 10,000 mm (32.8 ft) (elastic failure).

Table 1. Axial and Moment Critical Capacities According to the AISC, Eurocode, and Takagi and Deierlein Approaches			
Critical Capacities	**AISC**	**Eurocode**	**T&D**
M_{cr} [kN-m (kip-ft)]	1330 (981)	985 (727)	1130 (835)
P_{cr} [kN (kips)]	7150 (1610)	5690 (1280)	4810 (1080)
P_{max} [kN (kips)] using current provisions	3710 (834)	1530 (344)	2090 (470)
Relative error in P_{max} with respect to finite element solution	123%	–7.8%	25.9%
P_{max} [kN (kips)] using Equation 26	1940 (436)	1270 (287)	1780 (401)
P_{max} [kN (kips)] from finite element solution	1660 (374)		

DESIGN EXAMPLE

To demonstrate the applicability of the simplified approach in design situations, a numerical example is presented for a beam-column exposed to ASTM E119 standard fire (ASTM, 2008).

Problem

Assuming the beam-column is braced in the weak direction, compute the maximum compressive force P attained in the beam-column with the following characteristics:

- Beam-column section W14×176 with F_y = 345 MPa (50 ksi)
- Effective and unbraced length of the beam-column is $KL = L_b = 4.5$ m (14.7 ft)
- Average temperature T_{ave} = 500 ºC (932 ºF), thermal gradient $\Delta T = 200$ ºC (360º F)
- Initial bending moment $M_o = 320$ kN-m (531 kip-ft)

Bending and Axial Capacities

The M_{cr} and P_{cr} for the beam-column described earlier are computed in the strong direction using the three approaches discussed in this paper. The computations are carried out with strength reduction factor ϕ of unity. The results are tabulated in Table 1.

The results in Table 1 show that the *P-M* interaction equations specified in codes and standards overestimate the maximum axial force that can be sustained by the prescribed beam-column. The most nonconservative predictions are using the current AISC *P-M* equations, where the maximum compressive force of 3707 kN (834 kips) was overestimated by more than 123%. The adjustments made by Takagi and Deierlein to the AISC design equation resulted in an improved prediction of 2090 kN (470 kips); however, the maximum axial force that can be carried by the prescribed beam-column is still overestimated by more than 26%, as seen in Table 1. The reason for these nonconservative predictions using *P-M* equations specified in codes and standards is that these equations do not account for the influence of thermal gradient on both stiffness and second-order effect, which greatly affect the capacity of beam-columns.

The Eurocode *P-M* interaction equation provided a reasonable conservative prediction of the maximum compressive force of 1530 kN (344 kips), which was 8% less than the actual compressive force predicted by nonlinear finite element analysis. The reason for improved predictions using the Eurocode is that it uses numerical integration for computing the plastic axial and bending capacities on the sectional level. The numerical sectional integration captures the variation of strength in the cross section arising from the nonuniform thermal gradient.

Table 1 also shows that the predictions of the axial capacity of the beam-column are greatly improved by adopting the modifications proposed in Equation 26 for AISC and T&D equations. This is because these modifications in Equation 26 account for fire-induced thermal gradients by introducing the bending moments M_{TG} and M_{TB} that arise due to the migration of center of stiffness and the thermal bowing in the beam-column, respectively. Applying these modifications to the current Eurocode *P-M* diagrams resulted in further conservatism in the estimation of the axial capacity, *P*, of the beam-column.

CONCLUSIONS

Based on this study, the following conclusions can be drawn:

1. Current fire design provisions in codes and standards recommend the use of *P-M* based on uniform temperature. These *P-M* diagrams, though adequate for four-sided fire exposure, may not be conservative for beam-columns exposed to fire from one, two or three sides due to fire-induced thermal gradients.
2. A simplified approach is proposed for adjusting the uniform temperature *P-M* curves of an I-shaped cross section to account for the shape distortion, which results due to thermal gradient experienced through one-, two- or three-side fire exposure of beam-columns.
3. The effect of thermal gradient on the *P-M* capacity is twofold. First, thermal gradient causes a migration of center of stiffness of the cross section toward the cooler side. Second, thermal gradient results in a thermal bowing effect, which causes lateral deflection and thus an increase in the *P*-Δ effect on the beam-column.
4. The proposed method of computing plastic *P-M* diagrams, under thermal gradients, requires minimum computational effort and can easily be incorporated into design situations.

ACKNOWLEDGMENTS

The authors wish to acknowledge the support of the National Institute of Standards and Technology (through Building and Fire Research Laboratory Fire Grant 60NANB7D6120) and the National Science Foundation (through award CMMI 0652292). Any opinions, findings, conclusions, or recommendations expressed in this paper are those of the authors and do not necessarily reflect the views of the sponsors.

REFERENCES

AISC (2005), *Steel Construction Manual*, 13th ed., American Institute of Steel Construction, Chicago, IL.

AISC (2010), *Specification for Structural Steel Buildings*, ANSI/AISC 360-10, American Institute of Steel Construction, Chicago, IL.

ANSYS (2007), *ANSYS Multiphysics Version 11.0 SP1*, ANSYS Inc., Canonsburg, PA.

ASTM (2008), *Standard Methods of Fire Test of Building Construction and Materials: Test Method E119-01*. American Society for Testing and Materials, West Conshohocken, PA.

Burgess, I.W., El-Rimawi, J.A. and Plank, R.J. (1990), "Analysis of Beams with Non-Uniform Temperature Profile Due to Fire Exposure," *Journal of Constructional Steel Research*, Vol. 16, pp. 169–192.

Dwaikat, M.M.S. (2010), "Response of Restrained Steel Beam Subjected to Fire Induced Thermal Gradients," Ph.D. Thesis, Michigan State University, East Lansing, MI.

Dwaikat, M.M.S. and Kodur, V.K.R. (2009), "A Simplified Approach for Evaluating Plastic Axial and Moment Capacity Curves for Beam-Columns with Non-uniform Thermal Gradients," *Engineering Structures*, Vol. 32, pp. 1423–1436.

EC3 (2005). *Eurocode 3: Design of Steel Structures. Part 1-2: General Rules—Structural Fire Design*, EN1993-1-2, European Committee for Standardization, Brussels, Belgium.

Garlock, M.E.M. and Quiel, S.E. (2007), "The Behavior of Steel Perimeter Columns in a High-Rise Building under Fire." *Engineering Journal,* AISC, Vol. 44, No. 4, pp. 359–372.

Garlock, M.E.M. and Quiel, S.E. (2008), "Plastic Axial Load and Moment Interaction Curves for Fire-Exposed Steel Sections with Thermal Gradients," *Journal of Structural Engineering*, ASCE, Vol. 134, No. 6, pp. 874–880.

Kodur, V.R., Garlock, M.E, Dwaikat, M.S. and Quiel, S. (2009), "Collaborative Research: Fire Engineering Guidelines for the Design of Steel Beam-Columns," *Proc. 2009 NSF Engineering Research and Innovation Conference,* Honolulu, HI.

Ma, K.Y. and Liew, J.Y.R. (2004), "Nonlinear Plastic Hinge Analysis of Three-Dimensional Steel Frames in Fire," *Journal of Structural Engineering*, ASCE, Vol. 130, No. 7, pp. 981–990.

Takagi, J. and Deierlein, G.G. (2007), "Strength Design Criteria for Steel Members at Elevated Temperatures," *Journal of Constructional Steel Research*, Vol. 63, pp. 1036–1050.

The Development of a New Design Procedure for Conventional Single-Plate Shear Connections

LARRY S. MUIR and WILLIAM A. THORNTON

ABSTRACT

Conventional single-plate shear connections are common and economical connections. The design procedure outlined in the 13th edition AISC *Steel Construction Manual,* relies on the bolt shear values given in the 2005 AISC *Specification for Structural Steel Buildings*. The nominal bolt shear values listed in *Specification* Table J3.2 have historically been 20% lower than the theoretical bolt values. This reduction was provided to account for uneven force distribution among the bolts in end-loaded connections, such as bolted lap splices. The reduction served the secondary function of providing an additional factor of safety for all bolted connections designed in accordance with the *Specification*. The design procedure for conventional single-plate shear connections contained in the 13th edition *Manual* relied on this reduction to justify the practice of neglecting eccentricity in the bolt group for most configurations. The 2010 AISC *Specification* increases the nominal bolt shear values, necessitating a revised design procedure for single-plate shear connections in the 14th edition AISC *Manual*. This paper outlines the revised procedure.

Keywords: single-plate shear connections.

Single-plate shear connections consist of a single plate welded to the supporting beam or column and field bolted to the supported beam. Two different configurations of single-plate shear connections will be recognized in the 14th edition of the AISC *Steel Construction Manual*: the conventional configuration and the extended configuration. The extended configuration is a more general configuration in that it allows greater variation in the distance between the weld and the bolts, the number of bolts, and the plate thicknesses used. The conventional configuration limits the distance between the weld and the bolts to a maximum of 3 in., allows between 2 and 12 bolts in a single vertical line, and limits the ratio of the plate thickness to the bolt diameter.

Conventional single-plate shear connections (Figure 1) are common and economical connections. They provide simple and economical fabrication and erection, and because bolted connections are only used in the connection to the supported member, there is no safety concern over the use of shared bolts through the web of the support during erection.

The design procedure contained in the 14th edition of the *Manual* will be similar to that contained in the 13th edition (AISC, 2005a), but with a few key differences, including revised design eccentricities and further limitation on plate thickness for deeper connections using standard holes.

Larry S. Muir, Structural Steel Consultant, Atlanta, GA (corresponding). E-mail: larrymuir@larrymuir.com

William A. Thornton, Consultant, Cives Steel Company, Roswell, GA. E-mail: bthornton@cives.com

NEED FOR REVISED DESIGN PROCEDURE

The need to reevaluate and revise the design procedure contained in the 13th edition *Manual* arose from an increase in the nominal bolt shear values provided in AISC's 2010 *Specification for Structural Steel Buildings*. The nominal bolt shear values listed in *Specification* Table J3.2 have historically been 20% lower than the theoretical bolt values. This reduction was provided to account for uneven force distribution among the bolts in end-loaded connections, such as bolted lap splices. The reduction served the secondary

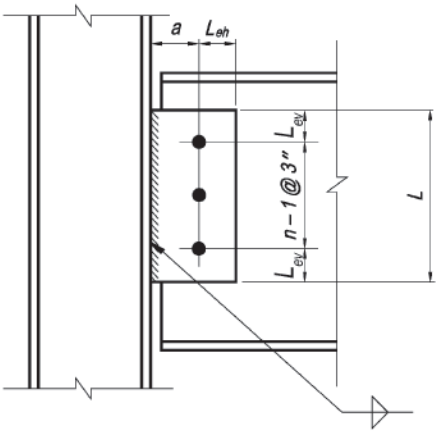

Fig. 1. Single-plate connection. (Fig. 10-11 in the AISC Manual, 13th ed.)

function of providing an additional factor of safety for all bolted connections designed in accordance with the *Specification*.

The design procedure for conventional single-plate shear connections contained in the 13th edition *Manual* relied on this reduction to justify the practice of neglecting eccentricity in the bolt group for most configurations. Reanalysis has shown that neglecting the eccentricity is no longer appropriate, considering the increased 2010 *Specification* bolt strengths.

14TH EDITION *MANUAL* DESIGN PROCEDURE

Because what follows is largely a discussion of the rationale underlying the design procedure for single-plate shear connections contained in the 14th edition *Manual*, it is appropriate to present the procedure and then present the individual considerations is greater detail.

The procedure presented in this paper has been adopted into the 14th edition *Manual* as a method of designing conventional single-plate shear connections that is applicable over the entire range of support rigidities. This procedure can be used to determine the strength of single-plate shear connections, which meet the dimensional limitations set forth in the procedure.

Shared Provisions

The conventional configuration and the extended configuration of the single-plate shear connection share some attributes and requirements. Although this paper specifically addresses the design of the conventional configuration, the requirements that apply to both configurations are presented together to better reflect the organization as contained in the *Manual*. These shared requirements include:

1. The use of either group A (ASTM A325 or F1852) or group B (ASTM A490 or F2280) bolts is acceptable.
2. The use of snug-tightened, pretensioned, or slip-critical bolts is acceptable.
3. The use of material with either $F_y = 36$ ksi or $F_y = 50$ ksi is acceptable.
4. The weld size shall be $\frac{5}{8}t_p$.

Dimensional Limitations

1. Only a single vertical row of bolts is permitted. The number of bolts in the connection, n, is limited to 2 to 12.
2. The distance from the bolt line to the weld line, a, must be equal to or less than 3½ in.
3. Standard or short-slotted holes are permitted to be used as noted in Table 1.

Table 1. Recommended Design Parameters for Conventional Single-Plate Shear Connections

N	Hole Type	e_b	Maximum t_w or t_p
2–5	SSL	$a/2$	None
	STD	$a/2$	$d_b/2 + \frac{1}{16}$ in.
6–12	SSL	$a/2$	$d_b/2 + \frac{1}{16}$ in.
	STD	a	$d_b/2 - \frac{1}{16}$ in.

4. The horizontal distance L_{eh} must be equal to or greater than $2d_b$ for both the plate and the beam web. Note that L_{eh} is measured to the center of the hole or slot.
5. Either the plate or the beam web must satisfy the maximum thickness requirement given in Table 1.

Design Checks

The bolts and plate must be checked for the required shear with an eccentricity equal to e_b, as given in Table 1.

Plate buckling will not govern for the conventional configuration.

PREVIOUS RESEARCH

A number of research programs have investigated the behavior of single-plate shear connections. A brief summary includes:

- White (1965) conducted tests involving single-plate shear connections to HSS columns.
- Lipson (1968) conducted tests of both single angle and single-plate connections.
- Richard et al. (1980) conducted tests on single-plate shear connections using stub beams.
- Hormby et al. (1984) conducted tests on single-plate connections with Grade 50 steel and composite construction.
- Astaneh et al. (1988) conducted tests on single-plate shear connections with standard holes to rigid supports.
- Astaneh and Porter (1990) conducted tests on single-plate shear connections with short-slotted holes to rigid supports.
- Astaneh and Shaw (1992) conducted tests on single-plate shear connections to support girder webs.
- Sarkar and Wallace (1992) conducted tests on single-plate shear connections to rigid supports.

- Creech (2005) conducted tests on single-plate shear connections to rigid and flexible supports.
- Baldwin Metzger (2006) conducted tests on conventional and extended single-plate shear connections to rigid supports.

The analysis reflected in this paper centered on the tests conducted by Astaneh and colleagues, Sarkar and Wallace, Creech, and Baldwin Metzger. Richard et al. did not test their connections to failure. Therefore, while their tests aid in the understanding of the behavior of single-plate shear connections, they do not provide much information regarding the ultimate strength of these connections. The purpose of White's tests was to determine the effect of connections on hollow structural section (HSS) columns, so though his findings were considered they were not integral to the analysis. The Hormby et al. tests were not included because the design procedure was intended to be used for both composite and noncomposite construction.

ESTABLISHING A DESIGN MODEL

The inherent rigidity of single-plate connections has been a concern for designers worried about considerable, unanticipated moments that could be developed in the connections, which could precipitate a sudden rupture of either the weld or the bolts. Further, Section B3.6a of the AISC *Specification,* requires that simple shear connections have sufficient rotational capacity to accommodate the required beam end rotation. The potential of developing moments in the connection beyond those resulting from the eccentricity between the support and the bolts, the need to accommodate simple beam end rotations, and ductility concerns become primary considerations in the development of a design model for the single plate shear connection. Much of the research and resulting design procedures developed over the years has concentrated on predicting and/or controlling this behavior.

The design model used in the 14th edition *Manual* builds on previous work. First, ductility requirements relating the strength of the plate (or beam web) to the bolt and weld strengths are set. These requirements are based on a combination of theoretically derived ratios and empirical results. The goal of the ductility requirements is to accommodate a target end rotation of 0.03 radian without rupture of any of the elements. The mechanisms used to achieve this ductility are discussed in greater detail later.

Having ensured sufficient ductility, the bolts are then designed to resist the required beam end reaction at an empirically derived effective eccentricity. Finally the plate is assumed to be subjected to loads consistent with the other elements, the beam end reaction applied at the effective eccentricity.

Rotational Demand

Before procedures for ensuring ductility can be derived, a target end rotation to be accommodated must first be defined. Among researchers and AISC committees, 0.03 radian has become a de facto standard; 0.03 radian is roughly equal to the end rotation of a beam whose span is 24 times its depth, is loaded with the maximum uniform design load and is commonly accepted to be a reasonable upper bound for beam end rotation. This level of end rotation is unlikely to occur in many instances, but in order to provide a design procedure that can be applied to a wide range of practical conditions, AISC has adopted 0.03 radian as the target rotation.

Beyond establishing a target magnitude for the rotation, a center of rotation must also be established. If 0.03 radian of rotation occurs at the top bolt of the connection, the movement of the bottom bolt relative to the plate that must be accommodated is about twice that required if the rotation occurs about the center of the bolt group. Research has shown that the center of rotation can vary considerably throughout the loading of the connection. However, when the connection is made to a rigid support, the center of rotation will coincide roughly with the center of the bolt group as the load approaches ultimate. It was observed that "during the test, neutral axis remained very close to the mid-height of the single plate." (Astaneh et al., 1988) Even when the mid-depth of the connection and beam are not coincident, the center of rotation remains near the mid-depth of the connection. (Hormby et al., 1984). No comments are provided in the research regarding the center of rotation of single-plate connections supporting composite beams; however, Hormby et al. (1984) noted, with regard to the use of single-plate connections used with composite beams, that "since full-scale beam tests of off-axis bolt groups resulted in essentially the same moment-rotation and center of rotation response as symmetrical connections, it is concluded that the behavior of the single plate is not affected by its location relative to beam's neutral axis."

The preceding findings relative to the location of the center of rotation are based on the observed behavior of single-plate connections to rigid supports. There is a lack of similar data pertaining to flexible supports; however, because the simple beam end rotation can be accommodated through movement of the flexible support, instead of plowing of the bolts, the location of the center of rotation is of less importance for these conditions.

Theoretically, the single-plate shear connection with standard holes can accommodate the requisite beam end rotations through a combination of plate flexural yielding; bolt deformation; bolt plowing; and, in the case of a connection to a flexible support, through support rotation. Bolt plowing is the local yielding of the plate or beam web, which occurs

at the bolt holes causing elongation of the holes. The relatively short distance between the bolts and the welds, which is an integral feature of the conventional single-plate shear connections, allows only a small area over which yielding can occur, so plate yielding is usually discounted as a means of accommodating the simple beam end rotation. Support rotation is not relied on to accommodate simple beam end rotations, because this mechanism cannot be applied to rigid supports and because other effects associated with support rotation can lead to serviceability problems.

Both bolt deformation and bolt plowing are dependent on determining not so much the end rotation, but rather the movement of the bolts relative to the plate that occurs as a result of the end rotation. For a given center of rotation, there is a direct relationship between the beam end rotation and the amount of movement the bolt group must accommodate either through deformation in the bolt itself and/or plowing through the joined materials. Assuming a center of rotation at the center of the bolt group, the relative horizontal movement of the bolts and the connected materials can be approximated as:

$$\delta = (0.03\,\text{radian})\frac{(n-1)b}{2} \tag{1}$$

This results in a maximum relative horizontal movement of 0.495 in. for a 12-row connection. Deformation of this magnitude would essentially exhaust the capacity of the bolt—as can be shown using the load-deformation relationship given on page 7-6 of the AISC 13th edition *Manual* (which can be used to calculate the force on a bolt given a deformation, in this instance a deformation of about 0.5 in.):

$$\begin{aligned} R &= R_{ult}\left(1-e^{-10\Delta}\right)^{0.55} = R_{ult}\left(1-e^{-10(0.5)}\right)^{0.55} \\ &= 0.996R_{ult} \end{aligned} \tag{2}$$

To accommodate even the modest deformational demands of a two-bolt connection, nearly 60% of the bolt capacity would be exhausted. Therefore, deformation in the bolt alone cannot be counted on to accommodate the simple beam end rotation.

Eliminating plate flexural yielding and support rotation as a possible means of accommodating the beam end rotations leaves only the combined effects of bolt deformation and bolt plowing. In order for the bolts to plow, however, there must be an upper limit placed on the stiffness and strength of the plate and/or the beam web relative to that of the bolts. Prior to the 13th edition *Manual*, the plate thickness was limited to one-half the diameter of the bolt plus 1/16 in. In the 13th edition *Manual,* the possibility that deformations could occur in either the plate or the beam web was formally recognized, and the requirement was changed such that the thickness of *either* the plate or the beam web was limited to one-half the diameter of the bolt plus 1/16 in.

Table 2. Results of Bolt Plowing Tests

Bolt	t_p (in.)	Δ (in.)	Plate F_y (ksi)	Plate F_u (ksi)
¾-in. A325-N	¼	0.65	47.5	65.9
¾-in. A325-N	5/16	0.6	47.3	65.5
¾-in. A325-N	⅜	0.3	47.6	67.1
¾-in. A490-N	5/16	0.7	47.3	65.5
¾-in. A490-N	⅜	0.4	47.6	67.1

To evaluate this requirement, it is instructive to look at the results of tests in which a single bolt was essentially plowed through various thicknesses of plates. Sarkar and Wallace (1992) ran a series of such tests. The results are provided in Table 2.

These results indicate that for a plate thickness equal to one-half the bolt diameter, approximately 0.3 in. of bolt plowing, Δ, can occur. Limiting the plate thickness to approximately half the bolt diameter can, therefore, be expected to accommodate end rotations for up to a seven-row connection. Further limiting the plate thickness to half the bolt diameter minus 1/16 in. can accommodate the larger deformations required for deeper connections. Because the tests were run with ¾-in. bolts, it is believed that the results can be safely extrapolated to larger-diameter and -strength bolts. Bolts less than ¾-in. diameter are rarely used in structural connections.

Providing short-slotted holes in the plate can also help to accommodate the simple beam end rotation. The short slots will provide between ¼ in. and 5/16 in. of horizontal movement in typical connections, before any deformation must occur in the bolts, the plate or the beam web. This ¼ in. alone is enough to provide the 0.03 radian of rotation for a five-row connection. In other words, when short slots are provided in a single-plate shear connection of five rows or less, the ratio between plate thickness and bolt diameter is immaterial.

As stated previously, 0.03 radian is considered a conservative upper bound for the end rotation. It might be reasonable to relax the plate thickness to bolt diameter requirements when the end rotation is known to be less than 0.03 radian, such as when the beam span is short relative to the beam depth or when the beam is sized based on serviceability rather than strength criteria. Moving from ASTM A325 bolts to A490 bolts might also offer some relief from this requirement. Because all of the tests directly related to bolt plowing utilized A325 bolts, the plowing behavior of A490

bolts has not been established, but it seems reasonable to believe that due to its greater strength, an A490 bolt would be capable of plowing through a greater length or thickness of plate before rupturing.

Edge Distance Requirements

The AISC *Manual* design procedures for single-plate connections had not included a provision requiring that the horizontal edge distance be twice the bolt diameter prior to the 13th edition. This requirement comes from the original Richard et al. (1980) research. It was included in the AISC book *Engineering for Steel Construction* (1984). It was not included in the Astaneh et al (1988, 1989) procedure, which was the basis of the procedure in the 9th edition (ASD), 2nd edition (LRFD), and 3rd edition (LRFD) *Manuals*. Rather than requiring a horizontal edge distance twice the bolt diameter, Astaneh et al.'s procedure recommended a horizontal edge distance 1.5 times the bolt diameter.

The intent of the twice the bolt diameter requirement seems to be to ensure that the bolts will bear without tearing through the edge of the material. However, bolt tear-out never occurred in any of the testing nor was any tearing between the edge of the hole and the edge of the plate observed that might indicate bolt tear-out was imminent. The maximum relative horizontal movement required to develop the simple beam end rotation of 0.03 radian is 0.495 in., as previously discussed. Based on this fact, and considering the fact that it was not required by the Astaneh et al. work (which was the basis for single-plate shear connection design in the United States for 20 years), the edge distance requirement of twice the bolt diameter would seem to be overly conservative and unnecessary.

DESIGN OF THE BOLT GROUP

It is intuitive to assume that the bolt group in a single-plate shear connection, being offset from the face of the support, will experience some eccentricity. The effective, or design, eccentricity, however, is not necessarily equal to the distance from the weld group to the bolt group, as might be assumed. A significant end moment might develop when a stiff plate connection is attached to a rigid support. In such cases, the inflection point of the beam might be moved considerably into the span, resulting in an effective eccentricity higher than the distance from the weld group to the bolt group. Conversely, the presence of short slots or bolt plowing might reduce the effective eccentricity on the bolt group. Both of these possibilities were reflected in the design procedures used prior to the 13th edition *Manual*. The LRFD 3rd edition *Manual* (AISC, 2001), for instance, calculated the effective eccentricity on the bolt group as:

$$e_b = \left|(n-1)-a\right| \text{ for connections using standard holes} \quad (3)$$

or

$$e_b = \left|\frac{2n}{3}-a\right| \text{ for connections using short-slotted holes} \quad (4)$$

When attached to a flexible support, the effective eccentricity, e_b, could not be less than the distance from the weld group to the bolt group. Assuming a practical range of 2½ in. to 3½ in. for a, the 3rd edition LRFD *Manual* equations would predict an effective eccentricity on the bolt group of between about 5 to 267% of the distance from the weld group to the bolt group. Where the predicted effective eccentricity exceeded the a dimension, this was presumably done to account for potentially large moments occurring at the support, which could result in a larger moment at the bolt group. Though this large effective eccentricity will occur early in the loading history, the tests indicate that the reduction in stiffness due to bolt plowing reduced the eccentricity at ultimate loads as was intended.

Reanalysis of existing data and further testing (Creech, 2005; Baldwin Metzger, 2006) led to a less conservative requirement for the 13th edition *Manual* in which, for most cases, eccentricity was neglected. Though the tests did not indicate that there was no eccentricity on the bolt group, the 20% reduction in the bolt strength inherent in the 2005 *Specification* allowed the conclusion that the eccentricity could safely be neglected.

Because many of the tests were configured such that the bolts governed the capacity of the connection, there is a relative wealth of data on which to base the design procedure for the bolts. Of 31 tests considered here, the bolts governed the strength of 20 of the connections. These 20 connections also contained a good mix of connection depths, hole types and support rigidities.

The approach taken in developing a design methodology for the bolt group followed the historical precedent of determining the effective eccentricity to which the bolt group was subjected. Only the effective eccentricity at ultimate load was considered in developing the design procedure, although effective eccentricities were often reported throughout the loading. There is no evidence in the testing that these larger effective eccentricities applied in conjunction with lesser loads can govern the strength of a single-plate shear connection meeting the dimensional requirements laid out in the procedure. A summary of the test data and the analysis is provided in Table 3.

In Table 3, the predicted bolt group strength without eccentricity values (column 11) were calculated by multiplying the number of bolts in the connection (column 2) by the bolt shear strength (column 4). Where the bolt shear strengths were measured and reported in the available reports, these values were used. Where measured bolt strengths were not reported, the bolt strength was assumed to be 26.5 kips for ASTM A325-N bolts and 33.2 kips for ASTM A325-X and

Table 3. Summary of Test Data

	(1) Test ID	(2) Bolts (All bolts are ¾-in. dia.)	(3) Hole Type	(4) Bolt Strength (kips)	(5) a (in.)	(6) Weld Size (in.)	(7) Plate F_y[b] (ksi)	(8) Plate F_u[b] (ksi)	(9) Tested Strength (kips)	(10) θ (rad.)	(11) Predicted Bolt Group Strength w/o Ecc. (kips)	(12) Test/ Predict	(13) Eff. e = %a	(14) Failure Mode
Astaneh and Colleagues														
1	1	(7)-A325-N	STD	26.5[a]	3	¼	35.3	61	160	0.026	186	0.860	1.02	Bolt
2	2	(5)-A325-N	STD	26.5[a]	3	¼	35.3	61	137	0.054	133	1.03	0	Bolt
3	3	(3)-A325-N	STD	26.5[a]	3	¼	35.3	61	94	0.056	79.5	1.18	0	Bolt
4	4	(5)-A490-N	STD	33.2[a]	2.75	7⁄32	35.3	61	130	0.053	166	0.783	1.07	Bolt
5	5	(3)-A490-N	STD	33.2[a]	2.75	7⁄32	35.3	61	79	0.061	99.6	0.994	0.585	Weld and bolt
Baldwin Metzger														
6	31C-3⅜	(3)-A325-N	STD	27.0	3	3⁄16	68.1	97.5	81	0.032	81	—	—	Beam
7	4B1C-3⅜	(4)-A325-N	STD	27.0	3	3⁄16	68.1	97.5	110	0.027	108	—	—	Beam
8	51C-3⅜	(5)-A325-N	STD	31.0	3	3⁄16	68.1	97.5	146	0.030	155	0.942	0.407	Bolt
9	71C-3⅜	(7)-A325-N	STD	27.0	3	3⁄16	68.1	97.5	173	0.018	189	0.915	0.740	Bolt
Creech														
10	S1-RSS-3-A325-N	(3)-A325-N	SSL	30.3	3	—	39.6	62.1	78.8	0.036	90.9	—	—	Beam
11	S2-RST-3-A325-N	(3)-A325-N	STD	30.3	3	—	39.6	62.1	90.7	0.027	90.9	0.998	0	Bolt
12	S3-FSS-3-A325-N	(3)-A325-N	SSL	30.3	3	—	39.6	62.1	71.8	0.039	90.9	0.790	0.55	Bolt
13	S4-FST-3-A325-N	(3)-A325-N	STD	30.3	3	—	39.6	62.1	61.4	0.023	90.9	0.675	0.82	Bolt
14	S5-FSS-3-A325-N-SR	(3)-A325-N	SSL	30.3	3	—	39.6	62.1	75.6	0.031	90.9	0.832	0.43	Bolt
15	S6-FST-2-A325-N	(2)-A325-N	STD	30.3	3	—	39.6	62.1	44.2	0.012	60.6	0.729	0.44	Bolt
16	S7-FSS-2-A325-N	(2)-A325-N	SSL	30.3	3	—	39.6	62.1	45.5	0.011	60.6	0.751	0.40	Bolt
17	S8-FSS-2-A325-N-SR	(2)-A325-N	SSL	30.3	3	—	39.6	62.1	47.9	0.013	60.6	0.790	0.34	Bolt
18	S9-RSS-7-A325-N	(7)-A325-N	SSL	30.3	3	—	44.4	66.3	166.5	0.028	212	—	—	Beam
19	S10-FSS-7-A325-N-SR	(7)-A325-N	SSL	30.3	3	—	44.4	66.3	202.5	0.027	212	0.955	0.40	Bolt
Sarkar and Wallace														
20	1a-North End	(2)-A325-X	STD	33.2[a]	3.5	—	47.4	—	41.7	0.033	66.6	—	—	PI yielding
21	1a-South End	(2)-A325-X	STD	33.2[a]	3.5	—	47.4	—	64.3	0.025 (0.043)	66.6	—	—	PI distortion
22	1b-North End	(2)-A325-N	STD	26.5[a]	3.5	—	47.4	—	60.8	0.028	53	1.15	0	Weld
23	1b-South End	(2)-A325-N	STD	26.5[a]	3.5	—	47.4	—	51.8	0.033	53	0.977	0.032	Weld
24	2a-North End	(4)-A325-N	STD	26.5[a]	3.5	—	47.4	—	93 (66.4)	0.028 (0.32)	106	0.877	0.41	No failure (bolt)
25	2a-South End	(4)-A325-N	STD	26.5[a]	3.5	—	47.4	—	93 (81.6)	0.32 (0.38)	106	0.877	0.41	No failure (bolt)
26	2b-North End	(4)-A325-N	SSL	26.5[a]	3.5	—	47.4	—	129	0.042	106	1.22	0	Bolt
27	2b-South End	(4)-A325-N	SSL	26.5[a]	3.5	—	47.4	—	129	0.042	106	1.22	0	Bolt
28	3a-North End	(6)-A325-N	STD	26.5[a]	3.5	—	47.4	—	119 (102)	0.027 (0.014)	159	0.748	1.14	Bolt
29	3a-South End	(6)-A325-N	STD	26.5[a]	3.5	—	47.4	—	119 (109)	0.027 (0.019)	159	0.748	1.14	Bolt
30	3b-North End	(6)-A325-N	SSL	26.5[a]	3.5	—	47.4	—	168	0.030	159	1.06	0	Bolt
31	3b-South End	(6)-A325-N	SSL	26.5[a]	3.5	—	47.4	—	194	–(0.030)	159	—	—	No failure

Notes:
a. Theoretical bolts strength with no end load reduction, based on nominal strength from the appropriate ASTM standard
b. All plates ⅜ in. thick measured yield and ultimate stresses as shown.
c. Indicates that the data are not available

A490-N bolts. Inherent in these values are the same assumptions made in the 2010 AISC *Specification* that the bolt strengths equal the minimum specified tensile strength given in the ASTM standards, the ratio of bolt shear strength to bolt tensile strength is 0.62 and ratio of effective thread root area to shank area is 0.80.

Once a predicted strength neglecting eccentricity was established, the effect of the eccentricity could be determined. Calculating the ratio of the tested strength (column 9) to the predicted strength (column 11) provided the efficiency of the bolt group in resisting the applied shear (column 12), which is essentially the C-value from the eccentrically loaded bolt group tables in Part 7 of the *Manual*. Using the instantaneous center of rotation method described in Part 7, an effective eccentricity corresponding to the bolt group efficiency could be determined and expressed as a percentage of the *a* dimension (column 13).

It can be seen that seven of the tests (tests 2, 3, 11, 22, 26, 27 and 30) indicate that the strength of the bolt group is best predicted by neglecting the eccentricity. The number of bolts for these tests ranged from two to six installed in both standard and short-slotted holes. There are eight tests (tests 8, 14, 15, 16, 17, 19, 24 and 25) that indicate that the strength of the bolt group is best predicted by assuming an eccentricity equal to 0 to 50% of the *a* distance. The number of bolts for these tests ranged from two to seven installed in both standard and short-slotted holes. Six of the tests (tests 1, 4, 9, 13, 28 and 29) indicate that the strength of the bolt group is best predicted by assuming an eccentricity equal to 74 to 114% of the *a* distance. In every case, where the best predictor of bolt group strength was based on an effective eccentricity exceeding one half the *a* distance, standard holes were used. Four of the tests were either six- or seven-row connections.

The remaining two tests were treated as outliers. One of the tests was a three-row connection in which the support girder was yielded during testing, which was considered unusual. The other outlier was a test in which the applied rotation was 0.053 radian, considerably more than the target. Other connections were subjected to similarly large rotations but did not show an increase in the effective eccentricity. It should be noted that when these two data points are compared to the 14th edition *Manual* design procedure there is still good agreement, even though an eccentricity less than that predicted by the test is used in the 14th edition *Manual* design procedure. This can be explained in part by the 10% reduction in bolt value inherent in the 2010 *Specification*.

In cases where bolt strengths were not reported, it is likely that the actual bolt strengths were greater than the nominal strengths used to calculate the predicted strength of the connection. Underestimating the predicted strength of the connection would lead to an overestimation of the bolt group efficiency and a lower corresponding effective eccentricity. There were 17 tests for which bolt strengths were not reported; of these, the bolt group governed the strengths of 12 tests. Therefore, nearly half of the tests potentially underestimate the effect of the eccentricity. However, in 7 of the 12 cases (tests 2, 3, 24, 25, 26, 27 and 30), the calculated effective eccentricity is more than 20% lower than the recommended eccentricity used in the 14th edition *Manual* design procedure, a considerably larger margin than the reported overstrength of the tested bolts. In 3 of the remaining tests (tests 1, 28 and 29), where the predicted effective eccentricity exceeds the recommended eccentricity used in the 14th edition *Manual* design procedure, the 14th edition *Manual* design procedure limits the plate thickness to less than the tested configuration to increase the ductility of the bolt group. In the final 2 of the 12 tests for which no bolt data were available (tests 4 and 5), the rotational demand on the connection during testing was approximately twice the expected simple beam end rotation.

The use of slip-critical connections should also be addressed. The design procedure contained in the 14th edition *Manual* follows the precedent set by previous editions of the *Manual* in allowing slip-critical connection design values to be used with single-plate shear connections. Because only standard and short-slotted holes are allowed and accommodation of the end rotation is required, the use of slip-critical connections would never be required per the *Specification* for these connections, and AISC discourages the use of slip-critical connections unless required by the *Specifications*. However, the use of slip-critical connection design values was not felt to be detrimental to the performance of the connection, so they have been allowed. Even when designed using slip-critical design values, the bolts in a single-plate shear connection will likely slip into bearing when large end rotations are required.

DESIGN OF THE WELD GROUP

Just as the ratio between the bolt diameter and plate thickness is intended to allow ductile redistribution of moments and accommodation of the simple beam end rotation, the weld is also sized to promote ductile behavior. The *Manual* design procedure requires that the weld size be equal to ⅝ of the plate thickness. A derivation of the weld requirement has been provided by Muir and Hewitt (2009), so only a brief discussion will be provided here. The derivation assumes that the plate must yield prior to weld rupture to ensure ductile behavior. Though most single-plate connections tested had a weld size equal to at least ¾ of the plate thickness, Baldwin Metzger (2006) ran several single-plate connection tests, both extended and conventional configurations, with welds sized to one-half the plate thickness, which confirmed the suitability of the current ⅝ of the plate thickness requirement.

DESIGN OF THE PLATE

Only two of the tests listed in Table 3 were governed by the strength of the plate, and the governing limit states were listed as shear yielding and shear distortion (Sarkar and Wallace, 1992). However, it is clear that the plate must have sufficient strength to resist the required design loads, as required by the *Specification*. The applicable limit states from Section J4 of the *Specification* are shear yielding (Equation J4-3) shear rupture (Equation J4-4) and flexural yielding. Flexural yielding should be checked using the plastic section modulus (Mohr and Murray, 2008). Block shear may also be a governing limit state if the horizontal edge distance does not exceed the vertical edge distance. Buckling will not occur in the plate, because the distance from the weld to the bolt group cannot exceed 3½ in. This can be proven as follows (Muir and Thornton, 2004):

Assuming a = 3.5 in. (the maximum permissible dimension), L = 36 in. for a 12-row connection, F_y = 50 ksi, and t_p = 0.25 in.:

$$\lambda = \frac{L\sqrt{F_y}}{t_p\sqrt{47{,}000 + 112{,}000\left(\frac{L}{2a}\right)^2}}$$

$$= \frac{36\sqrt{50}}{0.25\sqrt{47{,}500 + 112{,}000\left(\frac{36}{2(3.5)}\right)^2}}$$

$$= 0.587 < 0.7$$

Therefore, buckling will not govern.

COMPARISON TO TEST RESULTS

A comparison of the 14th edition *Manual* design procedure to the test results is given in Figures 2 and 3. Figure 2 compares the 14th edition *Manual* design procedure to test run with an a dimension equal to 3 in. Figure 3 makes the comparison to test run with an a dimension equal to 3½ in. There appears to be good agreement, and there is only one data point for which the 14th edition *Manual* procedure appears slightly nonconservative.

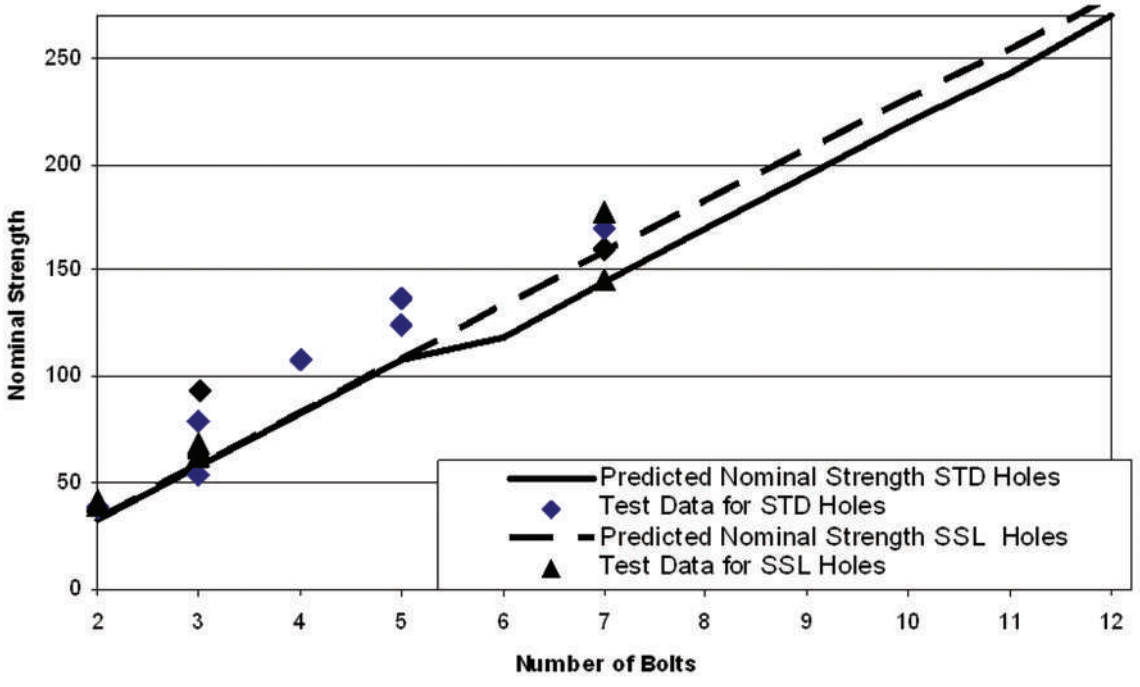

Fig. 2. Comparison of design procedure to test results for a = 3.0 in.

DESIGN EXAMPLE

Given:

Beam: W24×76 (A572 Grade 50); $t_w = 0.44$ in.
Bolts: Six ⅞-in. A325-N (STD holes)
Plate: A572 Grade 50; $t_p = 0.375$ in.; $d_p = 18$ in.

Verify that the plate satisfies the requirements for design as a conventional single-plate shear connection:

Verify number of bolts: $2 \le n = 6 \le 12$
Verify distance between the bolt and the weld: $a \le 3.5$ in.
Verify plate or web thickness: $t_p = 0.375$ in. $\le d_b/2 - 1/16$ in. $= (0.875 \text{ in.})/2 - 1/16$ in. $= 0.375$ in.
Verify horizontal edge distance: $L_{eh} = 1.75$ in. $\ge 2d_b = 2(0.875 \text{ in.}) = 1.75$ in.

Determine shear strength of a single bolt:

$$\phi r_b = \phi \frac{d_b^2}{4} \pi F_{nv} = 0.75 \left[\frac{(0.875 \text{ in.})^2}{4} \right] \pi (54 \text{ ksi}) = 24.4 \text{ kips}$$

Determine bolt bearing strength of plate per bolt:

First determine clear distance, L_c, to edge of plate:

$$L_c = L_e - \frac{d_h}{2} = 1.5 \text{ in.} - \frac{0.9375 \text{ in.}}{2} = 1.03 \text{ in.}$$

$$\phi r_{brg} = \min\left(\phi 2.4\, d_p t_p F_u,\ \phi 1.2 L_c t_p F_u\right)$$
$$= \min\left(0.75(2.4)(18 \text{ in.})(0.375 \text{ in.})(58 \text{ ksi}),\ 0.75(1.2)(1.03 \text{ in.})(0.375 \text{ in.})(58 \text{ ksi})\right)$$
$$= \min\left(38.4 \text{ kips},\ 22.6 \text{ kips}\right)$$

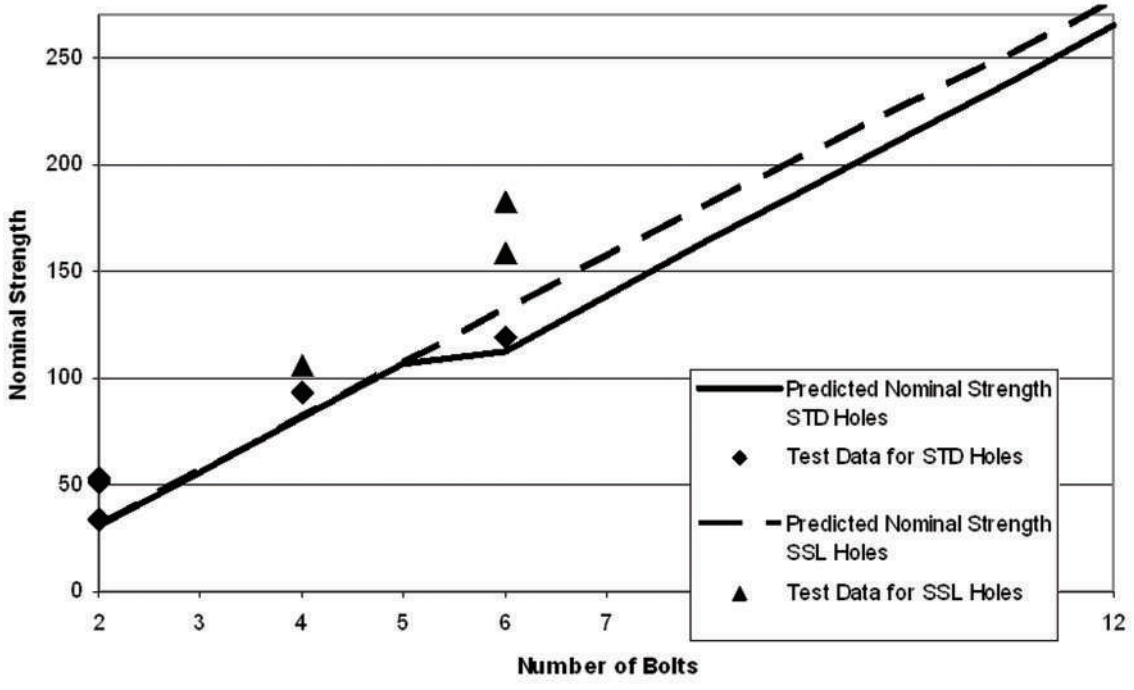

Fig. 3. Comparison of design procedure to test results for a = 3.5 in.

It should be noted that calculating the bearing strength based on lesser of the horizontal and vertical edge distances is conservative and other more exact methods are also acceptable. Because the thickness of the beam web is greater than the thickness of the plate, bearing on the plate will govern.

Determine strength of bolt group:

Because there are six rows of bolts in standard holes, the eccentricity shall be taken as the full distance between the bolts and the weld, 3 in.

From Table 7-7, $C = 4.98$

$$\begin{aligned}\phi R_b &= \min\left(\phi r_b, \phi r_{brg}\right) C \\ &= 22.6 \text{ kips}(4.98) \\ &= 113 \text{ kips} > 100 \text{ kips} \qquad \textbf{o.k.}\end{aligned}$$

Determine the shear yielding strength of the plate:

$$\begin{aligned}\phi R_{vy} &= \phi 0.6 F_y d_p t_p \\ &= 1.0(0.6)(50 \text{ ksi})(18 \text{ in.})(0.375 \text{ in.}) \\ &= 203 \text{ kips} > 100 \text{ kips} \qquad \textbf{o.k.}\end{aligned}$$

Determine the shear rupture strength of the plate:

$$\begin{aligned}A_n &= t_p\left[d_p - n\left(d_b + 0.125 \text{ in.}\right)\right] \\ &= 0.375 \text{ in.}\left[18 \text{ in.} - 6\left(0.875 \text{ in.} + 0.125 \text{ in.}\right)\right] \\ &= 4.5 \text{ in.}^2\end{aligned}$$

$$\begin{aligned}\phi R_{vr} &= \phi 0.6 F_u A_{net} \\ &= 0.75(0.6)(65 \text{ ksi})(4.5 \text{ in.}^2) \\ &= 132 \text{ kips} > 100 \text{ kips} \qquad \textbf{o.k.}\end{aligned}$$

Determine flexural strength of the plate:

As noted earlier, the check should be performed using the gross plastic section modulus and buckling of the plate will not govern.

$$Z_g = \frac{t_p d_p^2}{4} = \frac{(0.375 \text{ in.})(18 \text{ in.})^2}{4} = 30.4 \text{ in.}^3$$

$$\begin{aligned}\phi R_f &= \frac{\phi F_y Z_g}{e} \\ &= \frac{0.9(50 \text{ ksi})(30.4 \text{ in.}^3)}{3 \text{ in.}} \\ &= 456 \text{ kips}\end{aligned}$$

Size the weld:

$w = \frac{5}{8} t_p = \frac{5}{8}(0.375 \text{ in.}) = 0.234 \text{ in.}$

Therefore, use a ¼-in. weld each side.

Because the horizontal edge distance is greater than the vertical edge distance block shear will not govern.

CONCLUSION

The design procedure for conventional single-plate shear connections contained in the 14th edition of the AISC *Manual* has been revised to accommodate a change in the nominal bolt strength presented in the AISC *Specification*. The new procedure represents a safe and economical approach to these connections based on rational design methods and confirmed by testing.

ACKNOWLEDGMENTS

The authors would like to acknowledge the participation of the AISC Committee on Manuals and Textbooks in developing the design procedure presented in this paper with special thanks to Charlie Carter, Patrick Fortney, William Lindley and Clifford Schwinger, who, along with the authors, comprised the task group that worked to distill the available data into a clear and user-friendly procedure.

SYMBOLS

F_y	Minimum specified yield stress, ksi
L_{eh}	Horizontal edge distance, in.
L_{ev}	Vertical edge distance, in.
R	Simple beam end reaction, kips
R_{ult}	Ultimate shear strength of the bolt, kips
a	Distance from the face of the support to the vertical line of bolts
b	Spacing between rows of bolts
d	Plate depth
d_b	Bolt diameter
e_b	Effective (design) eccentricity of the bolt group
n	Number of rows
t_p	Plate thickness, in.
t_w	Beam web thickness, in.
w	Weld leg size, in.
δ	Relative horizontal movement of the bolts and the connected materials, in.
Δ	Deformation of the bolt, in.
λ	Slenderness parameter, dimensionless

REFERENCES

AISC (1984), *Engineering for Steel Construction*, American Institute of Steel Construction, Chicago, IL.

AISC (2001), *Manual of Steel Construction: Load and Resistance Factor Design*, 3rd ed., American Institute of Steel Construction, Chicago, IL.

AISC (2005a), *Steel Construction Manual*, 13th ed., American Institute of Steel Construction, Chicago, IL.

AISC (2005b), *Specification for Structural Steel Buildings*, ANSI/AISC 360-05, American Institute of Steel Construction, Chicago, IL.

AISC (2010), *Specification for Structural Steel Buildings*, ANSI/AISC 360-10, American Institute of Steel Construction, Chicago, IL.

Astaneh, A., Call, S.M. and McMullin, K.M. (1988), "Design of Single Plate Framing Connections," Report No. UCB/SEMM-88/12, Department of Civil Engineering, University of California, Berkeley.

Astaneh, A., Call, S.M. and McMullin, K.M. (1989), "Design of Single Plate Shear Connections," *Engineering Journal*, AISC, Vol. 26, No. 1.

Astaneh, A., McMullin, K.M. and Call, S.M. (1993), "Behavior and Design of Steel Single Plate Shear Connections," *Journal of Structural Engineering*, ASCE, Vol. 119, No. 8, pp. 2421–2440.

Astaneh, A. and Porter, K.A. (1990), "Design of Single Plate Connections with Snug-Tight Bolts in Short Slotted Holes," Report No. UCB/SEMM-90/23, Department of Civil Engineering, University of California, Berkeley.

Astaneh, A. and Shaw, A.L. (1992), "Experimental Study of Single-Plate Steel Beam-to-Girder Connections," Report No. UCB/SEMM-92/13, Department of Civil Engineering, University of California, Berkeley.

Baldwin Metzger, K.A. (2006). "Experimental Verification of a New Single Plate Shear Connection Design Model," Master's Thesis, Virginia Tech, Blacksburg, VA.

Creech, D. (2005), "Behavior of Single Plate Shear Connections with Rigid and Flexible Supports,: Master's Thesis, North Carolina State University, Raleigh, NC.

Hormby, D.E., Richard, R.M. and Kreigh, J.D. (1984), "Single-Plate Framing Connections with Grade-50 Steel and Composite Construction," *Engineering Journal*, AISC, Vol. 21, No. 3.

Lipson, S.L. (1968), "Single-Angle and Single-Plate Beam Framing Connections," Canadian Structural Engineering Conference, Toronto, ON, Canada, pp. 141–162.

Mohr, B.A., and Murray, T.M. (2008), "Bending Strength of Steel Bracket and Splice Plates," *Engineering Journal*, AISC, Vol. 45, No. 2.

Muir, L.S. and Hewitt, C. (2009), "Design of Unstiffened Extended Single-Plate Shear Connections," *Engineering Journal*, AISC, Vol. 46, No. 2.

Muir, L.S. and Thornton, W.S. (2004). "A Direct Method for Obtaining the Plate Buckling Coefficient for Double Coped Beams," *Engineering Journal*, AISC, Vol. 41, No. 3.

Richard, R.M., Gillet, P.E., Kreigh, J.D. and Lewis, B.A. (1980), "The Analysis and Design of Single Plate Framing Connections," *Engineering Journal*, AISC, Vol. 17, No. 2.

Richard, R.M., Kreigh, J.D. and Hormby, D.E. (1982), "Design of Single Plate Framing Connections with A307 Bolts," *Engineering Journal*, AISC, Vol. 19, No. 4.

Sarkar, D. and Wallace, B. (1992), "Design of Single Plate Framing Connections," Draft Research Report, Report No. FSEL/AISC 92-01, University of Oklahoma, Norman, OK.

White, R.N. (1965), "Framing Connections for Square and Rectangular Structural Tubing," *Engineering Journal*, AISC, Vol. 2, No. 3.

TECHNICAL NOTE

NewZ-BREAKSS: Post-tensioned Rocking Connection Detail Free of Beam Growth

DANIEL M. DOWDEN and MICHEL BRUNEAU

ABSTRACT

This technical note concisely presents the details of a post-tensioned rocking moment connection (PT-RMC) concept that could be implemented in steel plate shear wall (SPSW) and moment-resisting frame (MRF) systems, along with preliminary results from limited SAP2000 cyclic nonlinear static pushover and time-history analyses that verify its anticipated behavior. The partial research results presented here could be of benefit in ongoing discussions about practical implementation and design codification of PT-RMCs [aka post-tensioned energy dissipating (PTED) or self-centering moment-resisting (SC-MRF) connections].

Keywords: rocking connection; self-centering frame; steel plate shear wall; moment frame.

Post-tensioned rocking moment connections (PT-RMCs) in steel frames have been proposed by many researchers (e.g., Ricles et al., 2002; Christopoulos et al., 2002a, 2002b; Garlock et al., 2005; Rojas et al., 2005) as an alternative moment-resisting frame (MRF) connection that provides frame self-centering and limits hysteretic damage to designated energy dissipating elements during earthquakes. This connection, which is appealing for many reasons, requires careful and nonconventional floor diaphragm detailing to account for interaction effects of the PT frame with the gravity system. In particular, issues with PT frame expansion (Garlock, 2003), often referred to as "beam growth," arise associated with the opening of the rocking beam joint. Garlock and Li (2008) and Iyama et al. (2009) proposed some innovative floor slab diaphragm details for specific plan layouts to accommodate the beam growth that occurs in the PT frames relative to the other gravity frames in building structures and, more challengingly, when beam growth develops in both orthogonal plan directions. Apart from floor slab issues, in taller frames having larger columns, because columns must flexurally deform to accommodate beam growth at subsequent stories, the large stiffness of these columns may become overwhelming and prevent beam growth to the point where PT-RMC systems may not work properly.

Here, a type of rocking connection is proposed, inspired by a moment-resisting connection developed and implemented in New Zealand (Clifton, 1996, 2005; MacRae et al., 2007; Clifton et al., 2007; MacRae, 2008; MacRae et al., 2009), to achieve the advantages of a PT-RMC system without beam growth. This is done as part of an ongoing research project on steel plate shear walls (SPSWs) having rocking beam connections (e.g., Berman et al., 2010); consequently, the focus of this technical note is primarily on SPSW systems. However, while this technical note illustrates how a rocking connection of the type proposed here could be detailed for SPSW systems, it is presented with the understanding that, with minor changes, it could also be a workable solution for rocking MRF as a method to eliminate beam-growth issues, while providing in both cases the benefit of frame recentering while eliminating the need for special detailing of the diaphragm to accommodate beam growth.

NEWZ-BREAKSS ROCKING CONNECTION

For convenience, the proposed connection is called the "New Zealand-inspired—Buffalo Resilient Earthquake-resistant Auto-centering while Keeping Slab Sound (NewZ-BREAKSS) Rocking Connection." This proposed rocking connection is shown in Figure 1 for the particular detail that would be used in a self-centering SPSW system (the detail shown is for a ⅓-scale frame considered for possible testing).

In Figure 1, VBE is the vertical boundary element and HBE is the horizontal boundary element in keeping with the nomenclature used for conventional SPSW systems. The proposed rocking connection essentially eliminates the beam

Daniel M. Dowden, P.E., S.E., Ph.D. candidate, Department of Civil, Structural, and Environmental Engineering, University at Buffalo, Buffalo, NY. E-mail: dmdowden@buffalo.edu

Michel Bruneau, P.Eng., Ph.D., Professor, Department of Civil, Structural, and Environmental Engineering, University at Buffalo, Buffalo, NY (corresponding). E-mail: bruneau@buffalo.edu

growth typically encountered in the previously researched connections that rock about both of their beam flanges by, instead, maintaining constant contact of the beam top flange with the column during lateral drift. Additionally, this connection provides a large moment arm from the rocking point to the centroid of the post-tension for maximizing the PT elongation desired for self-centering connections. However, in a given beam, because the top flange of the beam is in constant contact with the columns at both ends of the beam, as the frame drifts, when one of the rocking joint "opens" and induces PT elongation, the rocking joint at the opposite end of the beam "closes" and induces PT decompression. Thus, the two PT elements need to be anchored independently along the length of the beam as shown in Figure 1; if a single PT element was used to span across the entire beam and was anchored only to the columns, its net elongation would be zero over the full length of the beam. Note that the stress concentrations at the rocking point for this connection are not significantly different than for the condition for post-tensioned moment-resisting rocking steel frames, in that a flange reinforcement plate will also typically be needed to accommodate stress demands on the rocking beam flanges as shown in Figure 1.

The location of the PT anchor point along the beam will depend on the strain demands of the PT elements at the maximum target drift. The anchor location should be provided to ensure that the PT strains remain elastic up to that drift demand. Either steel or fiber-reinforced polymer (FRP) tendons or rods could be used, depending on the level of PT strain anticipated. One other notable characteristic with the proposed detail is that because one joint closes, the recentering capability of the PT at the closing joint diminishes as the PT element is "relaxed"; if, at certain drifts, the initial elongation of the PT tendon or rod is overcome, the PT element will become fully relaxed and only the PT element at the opening joint will contribute to recentering the frame. Thus, the opening joint will always contribute to frame recentering, while the closing joint may or may not contribute depending on whether the PT element loses its pretension at the maximum target drift level. In the example presented subsequently, eventually, at large drifts, only the opening joint contributes to frame recentering (the closing joint eventually does not contribute after the PT element at that joint has lost its pretension). However, preliminary results show that this phenomenon has been found to be of no significant detrimental effect on structural behavior and can be accommodated by design.

To better understand the behavior of the proposed detail, the moment relationship along the length of the beam was obtained from first principles based on the free body diagram shown in Figure 2 using a capacity design approach for a self-centering SPSW. Here, it is assumed that the boundary frame and PT remain elastic and only the web plate yields. Note that vertical HBE reactions develop as shown in Figure 2, which is resisted by a shear tab connection as shown in Figure 1. However, for clarity, the shear tab detail is not shown in the free-body diagram illustrated in Figure 2.

In Figure 2, V_i is the story shear force, W_{bx} is the web plate horizontal yield force resultant along the length of the HBE, W_{by} is the web plate vertical yield force resultant along the length of the HBE, $P_{HBE(VBE)}$ is the horizontal reaction at the rocking point of the yield force resultant of the web plate acting on the VBE, P_s is the PT force, P_{sVBE} is the horizontal reaction of the post-tension force at the rocking point, y is the distance from the HBE neutral axis to the centroid of the PT, d is the depth of the HBE, R is the length of the radius corner cut-out of the web plate, and L is the clear span of the HBE. Note that the subscripts 1 and 2 indicate

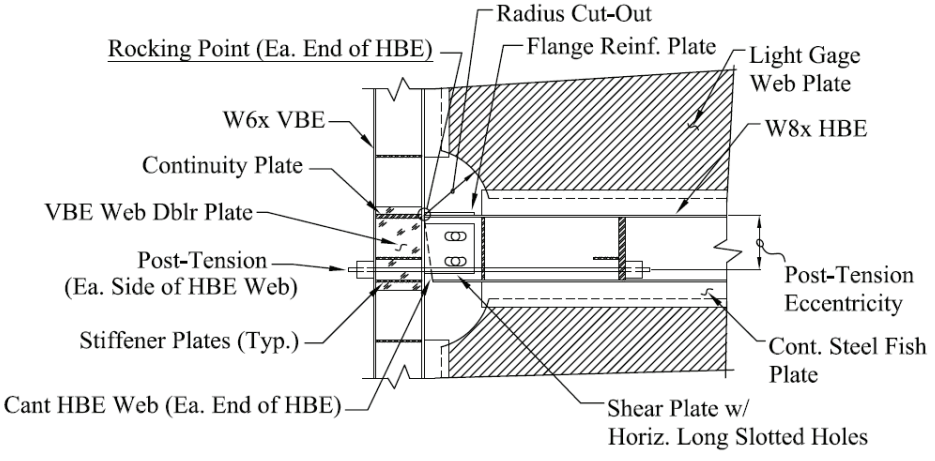

Fig. 1. Self-centering SPSW rocking connection.

that the force components shown are of different magnitude. In particular, it is assumed that the web plate below the HBE flange is thicker than the web plate above the HBE. By static equilibrium at sections 1 to 5 (points of applied load changes), the moment distribution along the length of the HBE is determined as follows:

$$M_1 = P_{s1VBE}\left(\frac{d}{2}\right) - P_{s1}\left(\frac{d}{2L}x + \frac{y}{L}x\right) + P_{s2}\left(\frac{y}{L}x + \frac{d}{2L}x\right) + \left(\omega_{by1} - \omega_{by2}\right)\left(\frac{L}{2}x - Rx\right) + \left(\omega_{cx1} + \omega_{cx2}\right)\left(\frac{dh}{4} - \frac{d^2}{4} - \frac{dR}{2}\right) + \omega_{bx1}\left(\frac{2dR}{L}x - dx\right) + V_i\left(\frac{d}{4}\right) \quad (1)$$

$$M_2 = P_{s1VBE}\left(\frac{d}{2}\right) - P_{s1}\left(\frac{d}{2L}x + \frac{y}{L}x\right) + P_{s2}\left(\frac{y}{L}x + \frac{d}{2L}x\right) + \left(\omega_{by1} - \omega_{by2}\right)\left(\frac{L}{2}x - \frac{x^2}{2} - \frac{R^2}{2}\right) + \left(\omega_{cx1} + \omega_{cx2}\right)\left(\frac{dh}{4} - \frac{d^2}{4} - \frac{dR}{2}\right) + \omega_{bx1}\left(\frac{2dR}{L}x - \frac{d}{2}x - \frac{dR}{2}\right) + \omega_{bx2}\left(\frac{d}{2}x - \frac{dR}{2}\right) + V_i\left(\frac{d}{4}\right) \quad (2)$$

$$M_3 = P_{s1VBE}\left(\frac{d}{2}\right) + P_{s1}\left(y - \frac{d}{2L}x - \frac{y}{L}x\right) + P_{s2}\left(\frac{y}{L}x + \frac{d}{2L}x\right) + \left(\omega_{by1} - \omega_{by2}\right)\left(\frac{L}{2}x - \frac{x^2}{2} - \frac{R^2}{2}\right) + \left(\omega_{cx1} + \omega_{cx2}\right)\left(\frac{dh}{4} - \frac{d^2}{4} - \frac{dR}{2}\right) + \omega_{bx1}\left(\frac{2dR}{L}x - \frac{d}{2}x - \frac{dR}{2}\right) + \omega_{bx2}\left(\frac{d}{2}x - \frac{dR}{2}\right) + V_i\left(\frac{d}{4}\right) \quad (3)$$

$$M_4 = P_{s1VBE}\left(\frac{d}{2}\right) + P_{s1}\left(y - \frac{d}{2L}x - \frac{y}{L}x\right) + P_{s2}\left(\frac{y}{L}x + \frac{d}{2L}x - y\right) + \left(\omega_{by1} - \omega_{by2}\right)\left(\frac{L}{2}x - \frac{x^2}{2} - \frac{R^2}{2}\right) + \left(\omega_{cx1} + \omega_{cx2}\right)\left(\frac{dh}{4} - \frac{d^2}{4} - \frac{dR}{2}\right) + \omega_{bx1}\left(\frac{2dR}{L}x - \frac{d}{2}x - \frac{dR}{2}\right) + \omega_{bx2}\left(\frac{d}{2}x - \frac{dR}{2}\right) + V_i\left(\frac{d}{4}\right) \quad (4)$$

$$M_5 = P_{s1VBE}\left(\frac{d}{2}\right) + P_{s1}\left(y - \frac{d}{2L}x - \frac{y}{L}x\right) + P_{s2}\left(\frac{y}{L}x + \frac{d}{2L}x - y\right) + \left(\omega_{by1} - \omega_{by2}\right)\left(\frac{L^2}{2} + Rx - \frac{L}{2}x - LR\right) + \left(\omega_{cx1} + \omega_{cx2}\right)\left(\frac{dh}{4} - \frac{d^2}{4} - \frac{dR}{2}\right) + \omega_{bx1}\left(\frac{2dR}{L}x - dx + \frac{dL}{2} - dR\right) + \omega_{bx2}\left(\frac{dL}{2} - dR\right) + V_i\left(\frac{d}{4}\right) \quad (5)$$

where h is the story height; ω_c and ω_b are the force per unit length of the horizontal and vertical components of the yielded web plate along the height and length of the VBE and HBE, respectively (Berman and Bruneau, 2008; Sabelli and Bruneau, 2007); x is the distance from point C along the length of the HBE; and P_{s1VBE} is the horizontal reaction at the rocking point, which is a fraction of P_{s1} and calculated as follows:

$$P_{s1VBE} = P_{s1}\left(\frac{h-y}{h+\frac{d}{2}}\right) \quad (6)$$

In addition, V_i, the story shear force assumed to be applied equally at each end of the frame for the condition considered, is given by:

$$V_i = \frac{1}{2}\left(t_1 - t_2\right)F_{yp}\left(L - 2R\right)\sin 2\alpha \quad (7)$$

where t_1 and t_2 are the thickness of the web plate below and above the HBE, respectively; F_{yp} is the anticipated yield strength of the web plate; and α is the angle of inclination of the tension field of the web plate with respect to a vertical axis. Note that for use with multistory frames, the

additional lateral story shear force at each HBE level due to multistory PT frame stiffness would have to be considered for preciseness in calculating the HBE demands. These equations would be considerably simpler for the case of a self-centering moment-resisting frame because there would be no contribution from the yielding SPSW web plate in the preceding equations, but rather a small contribution due to the type of energy dissipation element introduced in the connection (to reflect the schemes considered in research on PTED or SC-MRF).

SAP2000 ANALYTICAL MODEL COMPARISON

To verify the behavior of the proposed rocking connection and the hysteretic response of SPSWs having NewZ-BREAKSS connections, cyclic nonlinear static pushover analysis was first conducted using the computer program SAP2000 (CSI, 2009). The analytical model used consisted of a single-bay, single-story frame with a bay width of 20 ft and story height of 10 ft. The SPSW web plate consisted of a 16 gage steel plate with assumed expected yield strength of 46.8 ksi. A total of eight ½-in.-diameter grade 270-ksi steel tendons were provided at each end of the HBE with a distance of 6 in. below the neutral axis of the HBE to the centroid of the tendons (here, it is assumed the tendons would be placed equally along each side of the HBE web in a grouping of 2 × 2). An initial post-tensioning force of approximately 20% of the assumed yield strength of the PT was provided. The depth of the HBE was taken to be 18 in., representing the use of a W18 beam section.

A strip model was used for the SPSW web plate (Sabelli and Bruneau, 2007). Because the hysteretic behavior of SPSW relies on yielding of the web plate through diagonal tension field action, the web plate was modeled by using a series of tension-only strips. Each of the strips was assigned an axial plastic hinge model assuming an elastic perfectly plastic response to account for nonlinear hysteretic behavior. The thickness of the web plate was provided to ensure that the boundary frame and post-tension elements remained elastic. A combination of nodal joint constraints and SAP2000 gap link elements was also required to properly model the rocking joint behavior.

For the current example, the designed SPSW is used to avoid abstract complexities in keeping the problem parametric. Additionally, the boundary frame members are assumed rigid here such that PT force losses due to HBE axial shortening can be ignored, because this has a negligible impact on the results and keeps the conceptual illustration manageable. Ongoing research accounts for those effects that are secondary for the purpose of this technical note. However, the formulations developed earlier are applicable regardless of whether PT force losses are considered. Only the P_{s1} and P_{s2} terms in the moment equations are affected and would need to consider PT force losses due to axial shortening of the HBE due to the axial compression forces along the length of the HBE shown in Figure 2.

The comparison of the formulations developed describing the moment distribution along the HBE and also the system hysteretic response with the NewZ-BREAKSS connection is shown in Figure 3. It is observed that the proposed rocking connection provides recentering capability as observed by the hysteresis plots. A maximum displacement of approximately 3.6 in. was reached corresponding to a drift of 3%. The corresponding maximum base shear was approximately 256 kips. Note that because the boundary frame was modeled as rigid, this will lead to nearly simultaneously yielding of the web strips, which translates into the bilinear hysteresis loops observed (versus multilinear hysteresis loops that would be representative of a progression of web plate strip yielding, which would be observed in a boundary frame with flexibility).

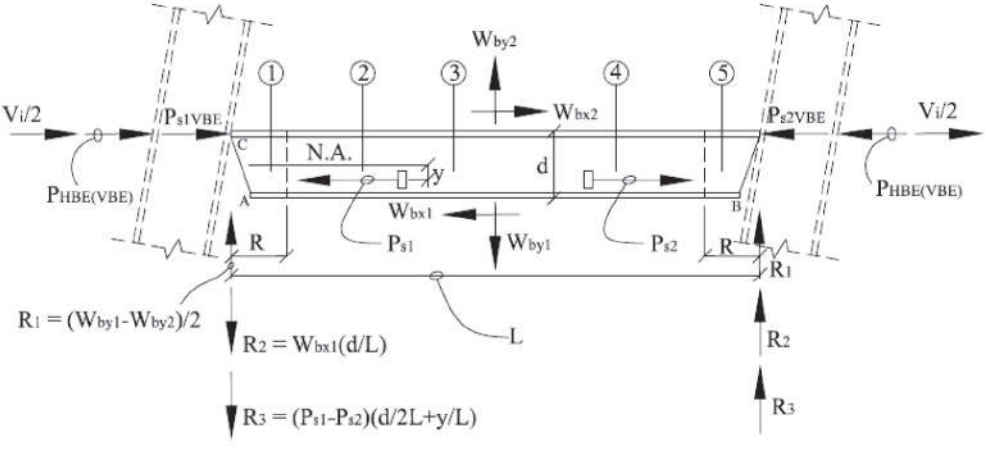

Fig. 2. Free-body diagram on HBE for rightward drift.

Additionally, the moment distribution obtained from the theoretical and analytical models are comparable. Note that the moment diagram shown is for a rightward 3% drift condition. From observation of the moment distribution, it can be seen that the PT force at the "opened" joint results in a vertical "step" in the moment diagram at the PT anchor location, as observed in Figure 3. The PT at the "closed" joint—for the condition shown—has become fully relaxed at this particular drift, and therefore no vertical step in the moment diagram is present at that location (which would not be the case otherwise).

Second, SAP2000 nonlinear time-history analysis was performed to verify the performance of the self-centering SPSW system with the NewZ-BREAKSS rocking connection under a more realistic loading environment due to a ground motion excitation. The same model was used as that for the cyclic nonlinear static pushover analysis, but a total frame tributary seismic weight of 350 kips was considered. For illustrative purposes only, the SAC LA14 ground motion was used as the ground motion input and is shown in Figure 4. The LA14 record is taken from the M6.7 Northridge earthquake record and is part of the Los Angeles suite of historical earthquake recordings, which were scaled to match the 10% in 50-year earthquake hazard for Los Angeles, California, as part of the 1997 SAC Joint Venture Project.

It is observed in Figure 4 that recentering under dynamic ground motion loading occurs for the given earthquake record as observed by the hysteresis plots. A maximum displacement of approximately 4 in. was reached, corresponding to a drift of approximately 3.4%. The corresponding maximum base shear was approximately 262 kips.

Note that a different hysteretic behavior would be obtained for a moment-resisting frame having the NewZ-BREAKSS rocking connections and would depend on the type of energy dissipation elements used in conjunction with the rocking beams (per the references cited earlier). Typically, those energy dissipation elements are weaker than the web plate of an SPSW but are able to dissipate energy in a repeatable manner. However, regardless of the different energy dissipation mechanism, the favorable characteristic of no beam growth would remain.

CONCLUSION

The NewZ-BREAKSS rocking connection provides the advantage of essentially no beam growth, thus mitigating damage to the floor diaphragm and beams while keeping

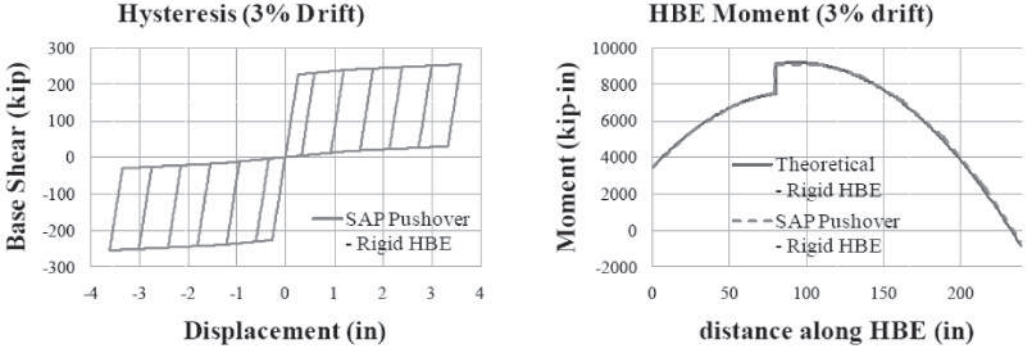

Fig. 3. SAP2000 pushover analytical versus theoretical comparison.

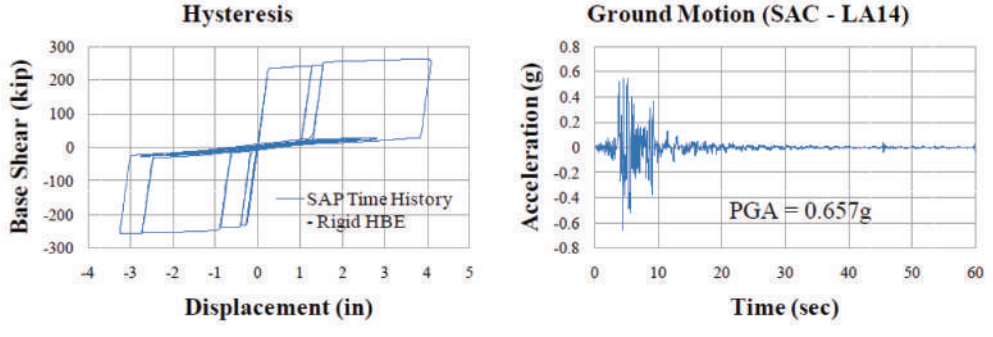

Fig. 4. SAP2000 nonlinear time history.

the desirable benefits of PT frames—namely, self-centering after an earthquake and limiting inelastic deformations to replaceable elements while the surrounding boundary frame remains elastic. Analytical modeling for use with self-centering SPSW systems was presented. Preliminary results from SAP2000 cyclic nonlinear static push-over and time-history analyses indicate that the NewZ-BREAKSS connection could be a viable option for self-centering systems. Future research is needed to further validate the connection, including experimental work to investigate its behavior and self-centering characteristics in a physical model.

ACKNOWLEDGMENTS

Support was provided in part by the National Science Foundation as part of the George E. Brown Network for Earthquake Engineering Simulation under award CMMI-0830294. Any opinions, findings and conclusions presented in this technical note are those of the writers and do not necessarily reflect the views of the sponsors.

REFERENCES

Berman, J. and Bruneau, M. (2008), "Capacity Design of Vertical Boundary Elements in Steel Plate Shear Walls." *Engineering Journal*, AISC, First Quarter, pp. 57–71.

Berman, J., Lowes, L., Bruneau, M., Fahnstock, L. and Tsai, K.C. (2010), "An Overview of NEESR-SG: Smart and Resilient Steel Walls for Reducing Earthquake Impacts," *Proc. Joint 9th US and 10th Canadian Conference on Earthquake Engineering,* Toronto, Canada, July 2010.

Christopoulos, C., Filiatrault, A. and Folz, B. (2002a), "Seismic Response of Self-Centering Hysteretic SDOF Systems," *Earthquake Engineering and Structural Dynamics,* Vol. 31, pp. 1131–1150. (DOI: 10.1002/eqe.152)

Christopoulos, C., Filiatrault, A., Uang, C.M. and Folz, B. (2002b), "Posttensioned Energy Dissipating Connections for Moment-Resisting Steel Frame," *Journal of Structural Engineering*, ASCE, Vol. 128, No. 9, pp. 1111–1120.

Clifton, GC. (1996), "Development of Perimeter Moment-Resisting Steel Frames Incorporating Semi-Rigid Elastic Joints," *Proc. New Zealand National Society for Earthquake Engineering Conference,* pp. 177–184.

Clifton, G.C. (2005), "Semi-Rigid Joints for Moment Resting Steel Framed Seismic Resisting Systems," Ph.D. Thesis, Department of Civil and Environmental Engineering, University of Auckland, New Zealand.

Clifton G.C., MacRae G.A., Mackinven H., Pampanin S. and Butterworth J. (2007), "Sliding Hinge Joints and Subassemblies for Steel Moment Frames," *Proc. New Zealand Society of Earthquake Engineering Annual Conference,* Paper 19, Palmerston North, New Zealand.

CSI (2009), "SAP2000: Static and Dynamic Finite Element Analysis of Structures (Version 14.1.0)," Computers and Structures Inc., Berkeley, CA.

Garlock, M. (2003), "Design, Analysis, and Experimental Behavior of Seismic Resistant Post-Tensioned Steel Moment Frames," Ph.D. Thesis, Department of Civil and Environmental Engineering, Lehigh University, Bethlehem, PA.

Garlock, M. and Li, J. (2008), "Steel Self-Centering Moment Frames with Collector Beam Floor Diaphragms," *Journal of Constructional Steel Research*, Vol. 64, No. 5, pp. 526–538.

Garlock, M., Ricles J. and Sause R., (2005), "Experimental Studies of Full-Scale Posttensioned Steel Connections." *Journal of Structural Engineering,* ASCE, Vol. 131, No. 3, pp. 438–448.

Iyama, J., Seo, C-Y., Ricles, J. and Sause R., (2009), "Self-Centering MRFs with Bottom Flange Friction Devices under Earthquake Loading," *Journal of Constructional Steel Research*, Vol. 65, pp. 314–325.

MacRae, G.A. (2008), "A New Look at Some Earthquake Engineering Concepts," Nigel Priestly Symposium, August, King's Beach, CA.

MacRae, G.A., Clifton, G.C. and Butterworth, J.W. (2009), "Some Recent New Zealand Research on Seismic Steel Structures," STESSA09, August, Philadelphia, PA.

MacRae, G.A., MacKinven, H., Clifton, G.C., Pampanin, S., Walpole, W.R. and Butterworth, J. (2007), "Tests of Sliding Hinge Joints for Steel Moment Frames," *Proc. Pacific Structural Steel Conference*, Wairakei, NZ.

Ricles J., Sause R., Peng, S. and Lu, L., (2002), "Experimental Evaluation of Earthquake Resistant Posttensioned Steel Connections." *Journal of Structural Engineering,* ASCE, Vol. 128, No. 7, pp. 850–859.

Rojas, P., Ricles, J. and Sause, R. (2005), "Seismic Performance of Post-tensioned Steel Moment Resisting Frames with Friction Devices," *Journal of Structural Engineering,* ASCE, Vol. 131, No. 4, pp. 529–540.

Sabelli, R. and Bruneau, M. (2007), "Steel Plate Shear Walls." *AISC Steel Design Guide 20*, American Institute of Steel Construction, Chicago, IL.

Current Steel Structures Research

No. 26

REIDAR BJORHOVDE

This quarter's paper focuses on a selection of current research projects at some of the leading Chinese universities. The descriptions will not discuss all of the current projects at the schools. Instead, selected studies provide a representative picture of the research efforts and demonstrate the importance of the schools to the country and indeed to the efforts of industry and the profession worldwide.

The universities and many of their structural steel researchers are very well known in the world of steel construction: Tsinghua University in Beijing, Tongji University in Shanghai and the Polytechnic University of Hong Kong. Some other projects at these institutions have been discussed in previous "Current Steel Structures Research" papers, but the studies that are presented here reflect major, long-time efforts in a number of areas of industry and transportation systems of the country. Much of the work is tied to the aggressive programs of the government of China to improve and expand the infrastructure, including electrical power stations and related structures, and, of course, highways and railroads and numerous bridges to span the rivers of China. Some of the design work for various structures has been performed by prominent international companies, including many American firms. A number of the technical solutions have certainly been based on the results of international research, including many American projects, but over the past several years, the magnitude of the Chinese research efforts within universities and governmental organizations has been very significant.

In true forward-looking fashion, the researchers at the institutions that are featured here have been active for many years, as evidenced by their leading roles in the design standards development efforts of China, including the independent codes of Hong Kong. Large numbers of English-language technical papers and conference presentations have been published, contributing to a collection of studies that continue to offer practical solutions to complex problems for designers as well as fabricators and erectors. Not the least important, these efforts complement and expand on ongoing work in other areas of the world. Thus, the collaboration between Chinese researchers and their colleagues in Australia, Japan, Korea, Singapore and the United States (to mention just a few countries) is extensive. The broad sharing of knowledge that is taking place promises significant results, not the least of which will be related to of issues of finance and the sheer cost of research.

References are provided throughout the paper, whenever such are available in the public domain. However, much of the work is still in progress, and in some cases reports or publications have not yet been prepared for public dissemination.

Reidar Bjorhovde, Dr.-Ing., Ph.D., P.E., Research Editor of the *Engineering Journal.* Tucson, AZ. Email: rbj@bjorhovde.com

SOME CURRENT RESEARCH WORK AT TSINGHUA UNIVERSITY IN BEIJING, CHINA

For many years Tsinghua University has been one of the leaders in many areas of structural engineering research. The university is sometimes referred to as the "MIT of China." There have been numerous principal contributors, and the faculty of the Department of Civil Engineering of Tsinghua University, now with the leadership of Professor Lin-Hai Han as chair, has been very active in the development of solutions to many technical problems. In particular, since 2005 Professor Han and his colleagues have conducted extensive studies of the performance of concrete-filled steel tubular (CFST) members, including the response of columns and beam-columns and beam-to-column connections subjected to seismic effects as well as fire temperatures. Numerous papers have been published, some very recent (Han et al., 2011; Li and Han, 2011; Tao et al., 2011). Funded by the National Natural Science Foundation of China (NSFC), initially the program examined the behavior and strength under monotonic as well as cyclic loads, including the important issue of residual strength following fire exposure. Long-term effects such as concrete creep have been examined, along with the influence of member preloading.

Major efforts are currently under way at Tsinghua and Tongji universities addressing the strength and behavior of very high strength members. These studies will be addressed here.

Performance of CFST Beam-to-Column Connections: The current focus of the research program examines the behavior of CFST columns connected to steel beams and steel-reinforced concrete (SRC) columns to SRC beams. Both of these options reflect typical construction practice in China. The developments examine the lifetime behavior

of such elements and connections, using a loading sequence that includes initial loading, heating, cooling and postfire loading on the assembly. Figure 1 provides a schematic of the full-scale testing arrangement.

Using finite element modeling and parametric evaluations, the model results were verified by the full-scale tests. The computational results were then used to analyze the mechanical characteristics of the connections, including stress distributions, stress resultants and moment-rotation data. These evaluations have been utilized to develop simplified formulations for the residual stiffness and strength ratios for the assemblies.

Subsequent to the first series of tests and evaluations, the response of the composite connections under seismic loading was also studied. This work focused on CFST columns with steel beams, using external diaphragms for stiffening and load transfer mechanisms. CFST columns connected to reinforced concrete beams were included in these tests and analyses. Figure 2 shows the full-scale test setup for the latter. The accuracy of the finite element models was verified by the tests, including the cyclic behavior performance, following extensive parametric analyses. The studies now aim to determine the behavior and strength under the combined effects of fire and structural loading, including seismic loads, for structures that have survived a fire. The concepts and approaches will be extended to full composite frames.

Performance of High-Strength Steel Structures: This is a long-term (since 2006) research effort that has been funded by the National Natural Science Foundation of China (NSFC). The project directors have been Professors Yongjiu Shi and Gang Shi.

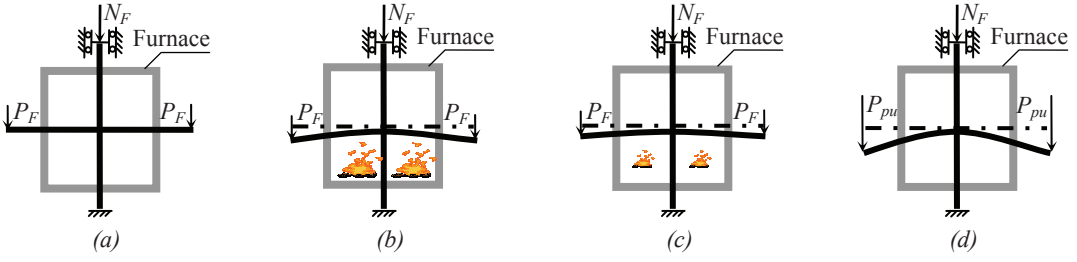

Fig. 1. Lifetime loading sequence for composite beam and column and beam-to-column connection tests: (a) initial loading; (b) heating; (c) cooling; (d) postfire loading. (Drawing courtesy of Professor L.-H. Han)

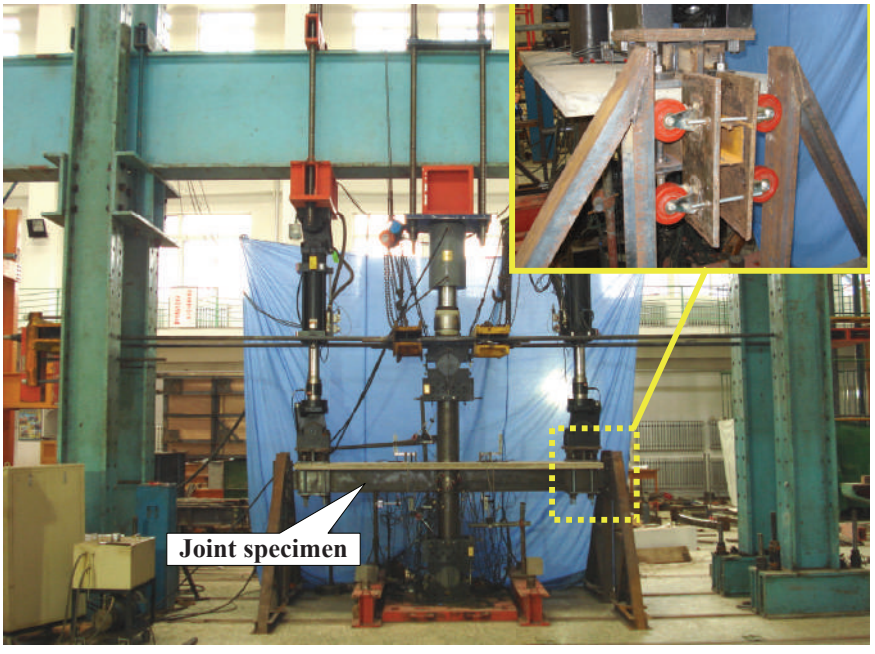

Fig. 2. Test assembly for CFST column and reinforced concrete beam in a beam-to-column connection test. (Photo courtesy of Professor L.-H. Han)

As in other areas of the world, the most common grades of steel for building and bridge structures in China have been 250 to 350 MPa (36 to 50 ksi) yield stress materials, with the occasional use of higher grades [up to 460 MPa (65 ksi)] for certain applications. For the past few years, there has been great interest in using steels with higher yield stress levels, but at the same time it has been recognized that the design code criteria have been based on tests and analyses with yield stress values at lower levels. This is, of course, the same situation as is found in other areas of the world. The current multiyear project is an aggressive effort to establish performance criteria for steels with yield stress larger than 460 MPa (65 ksi). The database has been extended to include tests of columns and connection elements in 690 and 960 MPa (100 and 140 ksi) yield stress steel (Girao and Bijlaard, 2008), with additional examinations of the performance capacities of very high strength connections (Bjorhovde, 2008). The work is now being extended to assess the strength and behavior data for members and connections under fire and seismic conditions.

It should also be noted that significant studies on the same subjects are being conducted at Tongji University in Shanghai. These will be detailed later in this paper.

Because there are no hot-rolled shapes available in the higher grades of steel, welded built-up shapes are used. The current studies include residual stress measurements, using the well-known sectioning method, and full-scale tests of stub columns as well as long columns are conducted. Local and overall buckling limit states are established, with extensive parametric evaluations using finite element modeling. The tests have verified the analytical results. Figure 3 shows a stub column test in 65 ksi steel; Figure 4 shows a long column test.

Certainly, the types and details of the individual tests and the analytical results that have been established agree with compression member studies conducted elsewhere, but the performance of all of the high-strength members do provide new data.

Fig. 3. Stub-column test of shape with slender web and flange elements in 65-ksi yield stress steel. (Photo courtesy of Professor Gang Shi)

Fig. 4. Long column test of welded built-up shape in 65-ksi yield stress steel. (Photo courtesy of Professor Gang Shi)

The physical testing and finite element analyses have been extended to welded and bolted connections, including limit states, deformation capacities, ductility and robustness. The work is now being extended to seismic effects and will include the development of suitable constitutive models for the steel, accounting for the gradual deterioration of the members and the connection elements.

SOME CURRENT RESEARCH WORK AT TONGJI UNIVERSITY IN SHANGHAI, CHINA

Tongji University is another major Chinese research university, with extensive programs in all areas of construction. The researchers in the building and bridge research groups are very well known internationally, and the analytical and physical testing facilities are excellent. Numerous papers have been published in international journals and conferences; the following is but a small example (Li and Mativo, 2000; Li, 2004; Wang and Li, 2008).

Analysis and Design of High-Strength Steel-Fabricated Columns: This long-term project has been directed by Professor G.-Q. Li.

Using 65-ksi yield stress plates, welded built-up H-shapes and box shapes were fabricated for the physical testing, and the residual stress distributions were determined using the hole-drilling method as well as the sectioning method. The distributions were used as imperfections for the analytical examinations.

A total of 26 full-scale columns were fabricated, using 11-mm (7⁄16-in.) and 21-mm (approximately 7⁄8-in.) plates. With centrally and eccentrically loaded specimens, using slenderness ratios of 35 to 70 for the square box sections and 40 to 80 for the H-shapes, the agreement with the finite element solutions was very good. Additional evaluations are now being conducted to develop improved column strength criteria for static loads.

In addition to the various tests and analyses for compression behavior, a total of eight columns were tested for constant axial load and cyclic bending. The test setup is shown in Figure 5. The hysteretic responses of columns with varying slenderness ratios were determined by tests; these data were used together with analytical results to arrive at the cyclic behavior of the high-strength columns. Seismic code criteria are currently being developed.

Fatigue Performance of Welded H-Beam with Corrugated Web: This project has been directed by Professor G.-Q. Li.

Beams with corrugated webs have become very attractive for bridge girders as well as for crane girders, for reasons of structural strength and stiffness as well as construction economy. The contribution of the web is a major consideration, and the resistance to local buckling that is afforded by the corrugated web is very significant. But the questions related to the fatigue performance of dynamically loaded members are very important, considering the geometry of the web and some of the welding details that may offer limited dynamic resistance.

Four girders were fabricated as test specimens, using trapezoidal corrugations. Figure 6 shows the test setup. During the testing, the webs were subjected to concentrated cyclic loads with a constant stress amplitude, applied at midspan. The tests were designed to adhere to the criteria of the Chinese steel design code. The girders had the same overall and cross-sectional dimensions; the corrugation profiles varied, with different symmetries. Specifically, one of the specimens was designed with a 10-mm (3⁄8-in.) deviation away from the centerline of the web, aiming to take into

Fig. 5. Testing for seismic behavior of welded H-shape column. (Photo courtesy of Professor G.-Q. Li)

consideration how the performance would be affected by the installation of a crane girder. All of the tests are conclusive—to the effect that the fatigue life of a girder with a trapezoidal corrugated web is significantly longer than that of a girder with a traditional flat web.

The findings and the design recommendations have now been incorporated into the Chinese code for steel structures.

Construction Process Analysis of Large and Complex Spatial Steel Structures: This project has been directed by Professor Y.-F. Luo.

Professor Luo makes the observation that state-of-the-art steel structures are often large in dimensions and scale with complex and distinctive structural systems. Further, and very importantly, the researchers note that

- The construction process is complicated and time-dependent on the system and its elements.
- The magnitude and distribution of the loading on the structure is highly nonlinear and time-dependent.
- The construction process has a significant influence on the final loading behavior and indeed the strength and behavior of the structure.

However, in spite of these facts, current analysis techniques usually do not take into account the variations of the nonlinear response of the structure during the construction process. Two early studies did just that, but they were not expanded (Griffis, 1986; Vallenilla and Bjorhovde, 1990).

Fig. 6. Testing of girder with trapezoidal corrugated web. (Photo courtesy of Professor G.-Q. Li)

To resolve these issues, Professor Luo's study aims at developing analytical procedures that will recognize the effects of the time-dependent response to provide an approach for how to predict the loading behavior and how to control the construction process. The examination will proceed in the following steps:

1. Identify the main construction process parameters and the roles they play at various stages of construction.
2. Using the initial numerical model for the structure, update the real-time model for the during construction.
3. Examine the limit states of the structure during construction and the potential "prewarning" indicators for the structural behavior.

Behavior, Strength, and Construction of Cold-Formed Steel Structures: This project is a long-duration, comprehensive study of cold-formed steel structures and the standards that are needed for the Chinese industry. The project directors are Professors Z.-Y. Shen and Y.-Q. Li.

The original Chinese cold-formed steel structures design and fabrication industry was based on very small thickness materials that were also typical in the United States and other countries. Steel grades with yield stresses of 36 and 50 ksi were preferred, and material thicknesses between 2 and 6 mm (approximately 0.1 and 0.25 in.) were the norm. Local and overall buckling, effective widths and local material property variations were, therefore, paramount considerations for the design codes. Today's materials for cold-formed elements use thicknesses less than 1 mm (0.04 in.) and up to 20 mm (¾ in.), and steel grades are available with yield stress up to 550 MPa (80 ksi), albeit with ductility limitations. This is the situation that is also the case for the rest of the world. The development of the Chinese cold-formed steel structures design standard was largely based on the American Iron and Steel Institute's *Specification* and *Manual* (AISI, 2007; 2008), as is actually the case for most such codes in the world today. It is now been revised to reflect the housing needs of the population as well as the expansion of the construction industry in general. It is anticipated that the new code will be adopted soon.

Responding in particular to the needs for residential construction in many areas of China, the project focuses on the following engineering and construction needs:

- Testing and analytical evaluation of the mechanical behavior, strength and stability of the typical thin-walled (less than 2 mm) cold-formed cross-sections, including some built-up members (double Cs) as well as thin-walled tubular shapes.
- Development of reliability and limit states design criteria for such cold-formed members.

- Development of the characteristics of strength, behavior and design of cold-formed steel trusses.
- Testing of single shear connections with self-drilling screws and various dimensions of plates, fastener patterns and grades of steel.
- Performing monotonic and cyclic shear tests of 16 composite wall specimens with different aspect ratios, types of sheathing, grades of steel and sizes of openings to assess ductility and seismic energy dissipation.
- Shaking table tests for three full-scale models of two-story residential buildings, using different grades of steel for the studs and different sheathing boards.

Figure 7 shows one of the buildings that will be tested.

The evaluation of the larger thickness (6 to 20mm) cold-formed elements is proceeding, aiming for the development of the following data:

- Material property variations and residual stress distributions for various open and closed cross-sections.
- Analytical and experimental data for the strength and behavior of typical members and cross-sections.

Fig. 7. Full-scale two-story building to be tested on shaking table. (Photo courtesy of Professors Z.-Y. Shen and Y.-Q. Li)

- Hysteretic behavior of bracing members and eccentrically loaded columns.
- Cyclic behavior, strength and limit states for typical connections between thick-walled cold-formed members.

SOME CURRENT RESEARCH WORK AT HONG KONG POLYTECHNIC UNIVERSITY IN HONG KONG, CHINA

The Hong Kong Polytechnic University is one of the premier universities in Hong Kong. With a large academic staff, good laboratories and especially fine computational facilities, this school has a first-class reputation for advanced graduate and undergraduate programs. Like a number of the major Chinese universities, the graduate courses in some areas of study are offered in English, lending significant advantages to its graduates. In addition, the university enjoys very close collaboration with the many national and international design firms with offices in the city. Equally important are the joint efforts between the university and the highly competent staff of the Hong Kong Buildings Department (HKBD), through which an outstanding limit states steel design code was developed (HKBD, 2005).

Direct Analysis for Structures in Steel, Composite and Reinforced-Concrete Construction: This is a major project that has been led by Professors S.-L. Chan and Y.-P. Liu.

Following the 2005 publication of the new steel design code for Hong Kong, direct analysis has been used extensively for the design of steel structures. The approach that was developed for the code is highly reliable and efficient, just as has been found for the direct analysis method of the AISC *Specification* in the United States. The research team at HKPU has now extended the method to hybrid steel and concrete frames, where the approach is applied to bare steel, composite steel-concrete and reinforced-concrete systems. Using a single code, originally developed for steel, structural analysis is now performed without the use of several codes—thus becoming safer, more efficient and more economical. This is accomplished in true, efficient hybrid form in terms of strength, stiffness and structural robustness. Of course, individual limit states for members and connections in the different materials still have to be checked.

Time will tell whether the combined application of the code will succeed in broadly applicable fashion, but the initial responses from the design community are favorable. The key is the consideration of member as well as structural second-order effects, because these do not depend on the construction material (Chan, 2001; 2006). Thus, biaxial stress resultant surfaces can be formulated for steel or concrete, as required, and the resulting capacity surfaces can be incorporated directly into practical second-order analysis and design procedures.

Modeling of Long-Span Composite Beams with High-Performance Materials and Deformable Shear Connectors: This is a long-duration project under the direction of Professor K.-F. Chung and his research team. Previous work by Professor Chung reflects much of the initial thinking (Chung, 2006). At this stage, the project aims for improved structural accuracy and efficiency of long-span composite beam design, incorporating practical construction features.

Using test data for simply supported and continuous beams, suitable two- and three-dimensional models have been developed. The models have the following features:

- Geometric and material nonlinearities are represented, including initial geometric and mechanical imperfections.
- Deformable shear connectors with limited ductility are represented, including nonlinearity at the interface of steel and concrete.
- The steel is modeled as an elastoplastic high-performance material, including various levels of strain hardening.
- Advanced reinforced-concrete models reflect normal weight material, with normal to high-strength concrete.
- Complete ranges for different failure criteria of the materials are represented, including steel stress levels, concrete strains, overall beam deflections and slip of the shear connectors.
- Effects of shoring during construction are incorporated.

Figure 8 illustrates the undeformed and the deformed two- and three-dimensioanl models, including distributions and intensities of the von Mises stresses.

Following extensive parametric evaluations, the major findings of the study are as follows:

1. For beams with 100% shear connection, the full flexural capacity is developed, and the shear connector slip is generally less than 1 mm (0.04 in.).
2. For beams with a partial shear connection, the shear connector slip is typically in the range of 2 to 5mm (0.08 to 0.2 in.) when the requisite moment capacity has been reached. As expected, the slip will be smaller for unshored beams.
3. For partially composite beams with spans larger than 20 ft and deep, wide-flange shapes ($d > 18$ in.), slip in the range of 5 to 10mm (0.2 to 0.4 in.) will occur when the shear connection is less than 50%. The moment capacity is typically reduced by 5 to 10% of the design values.
4. For composite beams with 100% shear connection and different material grades for the concrete and steel, the moment capacity is increased by 20 to 70% if the yield stress of the steel is increased from 50 to 65 ksi and 100 ksi. The self-weight is not increased.
5. The common plastic moment stress block gives accurate moment capacities for a wide range of steel and concrete materials.

The researchers are currently developing improved composite beam design expressions for use with the design

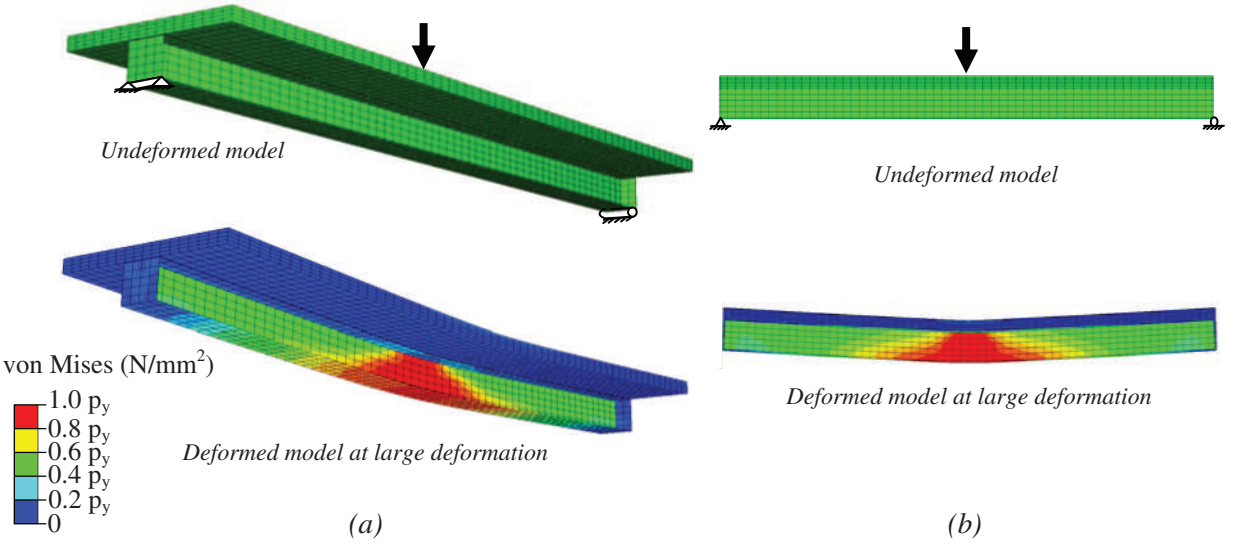

Fig. 8. Two- and three-dimensional composite beam models: (a) three-dimensional model; (b) two-dimensional model. (Drawing courtesy of Professor K.-F. Chung)

standards. In addition, vibrations induced by foot traffic are examined, with the aim of providing suitable methods of analysis and realistic performance criteria.

Enhancing the Performance of Steel Structures with Fiber-Reinforced Polymers (FRPs): This project is a wide-ranging investigation with Professor J.-G. Teng as the director. While the original work focused on the use of FRPs to improve the response characteristics of reinforced-concrete structures, for the past number of years, in-depth studies have been addressing a range of subjects aimed at enhancing the performance of steel structures. The project has focused on the strengthening of existing steel structures, but also providing for the efficient use of FRPs and steel in hybrid applications. Several subprojects have been undertaken, as follows:

Strengthening of Steel Structures with FRP:

1. *Debonding failures in FRP-strengthened steel structures:* Typically, the FRP has been bonded to the steel through some form of adhesive. The subject has been addressed in a number of studies, including
   a. An experimental evaluation of the effect of the surface preparation of the steel.
   b. a combined experimental and analytical examination of the full range of behaviors for the FRP-to-steel interface, using linear and nonlinear adhesives.

   The key results have shown that adhesion failure can be avoided if the steel surface is grit-blasted before bonding. Using finite element analysis, reliable bond-slip models have been developed for the linear as well as the nonlinear adhesives. The agreement with the experimental results is very good.

2. *FRP confinement of hollow and concrete-filled steel tubes:* These types of elements are commonly used in various structural applications. One of the governing limit states for columns is local buckling of the tube wall near the member end, and FRP jackets have sometimes been used to prevent this type of failure. The project was a combination of testing and analytical evaluations, which demonstrated that the confinement of the steel by the FRP could be an effective solution. Basically, the FRP jacket delayed or completely suppressed the local buckling failure, while also providing for a significant improvement of the column behavior and strength. As part of the study, an accurate stress-strain model was developed for use with monotonic as well as cyclic loading for the confined concrete.

Hybrid FRP-Concrete-Steel Double-Skin Tubular Members: Figure 9 shows typical examples of the cross sections of some double-skin tubular members (DSTMs). The use of FRPs for such members was invented by Professor Teng; it has attracted significant attention.

Briefly, as can be seen, the outer tube is FRP and the inner tube is steel. The tube can be left unfilled (as shown in Figure 9) to maintain a lower mass. Briefly, the FRP provides the confinement for the concrete as well as additional shear strength of the member. These members may be precast or built on site.

In addition to the high corrosion resistance of the member as provided by the FRP skin, these members offer high ductility, a high weight-to-strength ratio, and ease of construction. Beam-to-column connections can be built relatively easily by removing the FRP in the immediate area and connecting directly to the steel through the concrete.

The DSTM researchers have performed a number of full-scale member tests for axial compression, bending and eccentric compression. The results have demonstrated effective confinement of the concrete between the outer FRP tube and the inner steel tube. Further, the members are highly ductile under pure compression as well as combined bending and compression. Finally, a simple and practical design procedure has been developed; it has been adopted by the Chinese code for infrastructure application of FRP composite materials.

Currently, the behavior and strength of DSTM members under cyclic loading is being examined, using full-scale tests as shown in Figure 10. Conclusions will be forthcoming.

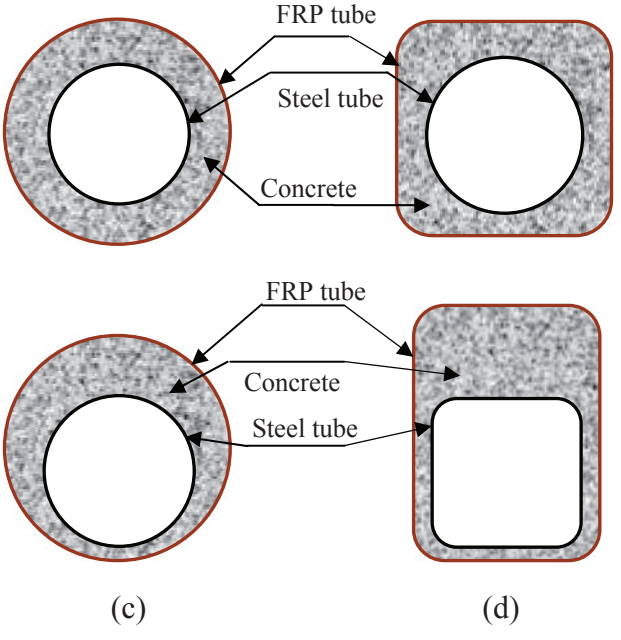

Fig. 9. Typical double-skin tubular member (DSTM) cross-sections. (Drawing courtesy of Professor J.-G. Teng)

ACKNOWLEDGMENTS

Significant assistance has been provided by Professor S.-L. Chan, Hong Kong Polytechnic University, and Professor G.-Q. Li, Tongji University, both members of the International Structural Steel Research Advisors (ISSRA). Additional assistance was provided by Professors L.-H. Han and Gang Shi of Tsinghua University; Professors Y.-F. Luo, Z.-Y. Shen and Y.-Q. Li of Tongji University; and Professors K.-F. Chung and J.-G. Teng of Hong Kong Polytechnic University. Their efforts are sincerely appreciated.

REFERENCES

AISI (2007), *North American Specification for the Design of Cold-Formed Steel Structural Members*, ANSI/AISI Standard S100-2007, American Iron and Steel Institute, Washington, D.C.

AISI (2008), *Manual for Cold-Formed Steel Design*, American Iron and Steel Institute, Washington, D.C.

Bjorhovde, R. (2008), "Performance and Design Issues for High Strength Steel in Structures," *International Symposium on Innovative Design of Steel Structures*, University of Hong Kong, December 5, pp. 1–14.

Chan, S.-L. (2001), "Non-Linear Behavior and Design of Steel Structures," *Journal of Constructional Steel Research*, Vol. 63, No. 7, pp. 961–969.

Chan, S.-L. (2006), "Codified Second-Order Analysis and Design of Steel Structures," *International Symposium on Worldwide Trend and Development in Codified Design of Steel Structures*, Singapore Structural Steel Society, 2–3 October, pp. 101–111.

Chung, K.-F. (2006), "Developing a Performance-Based Design Code for Steel and Composite Structures in Asia," *International Symposium on Worldwide Trend and Development in Codified Design of Steel Structures*, Singapore Structural Steel Society, 2–3 October, pp. 35–45.

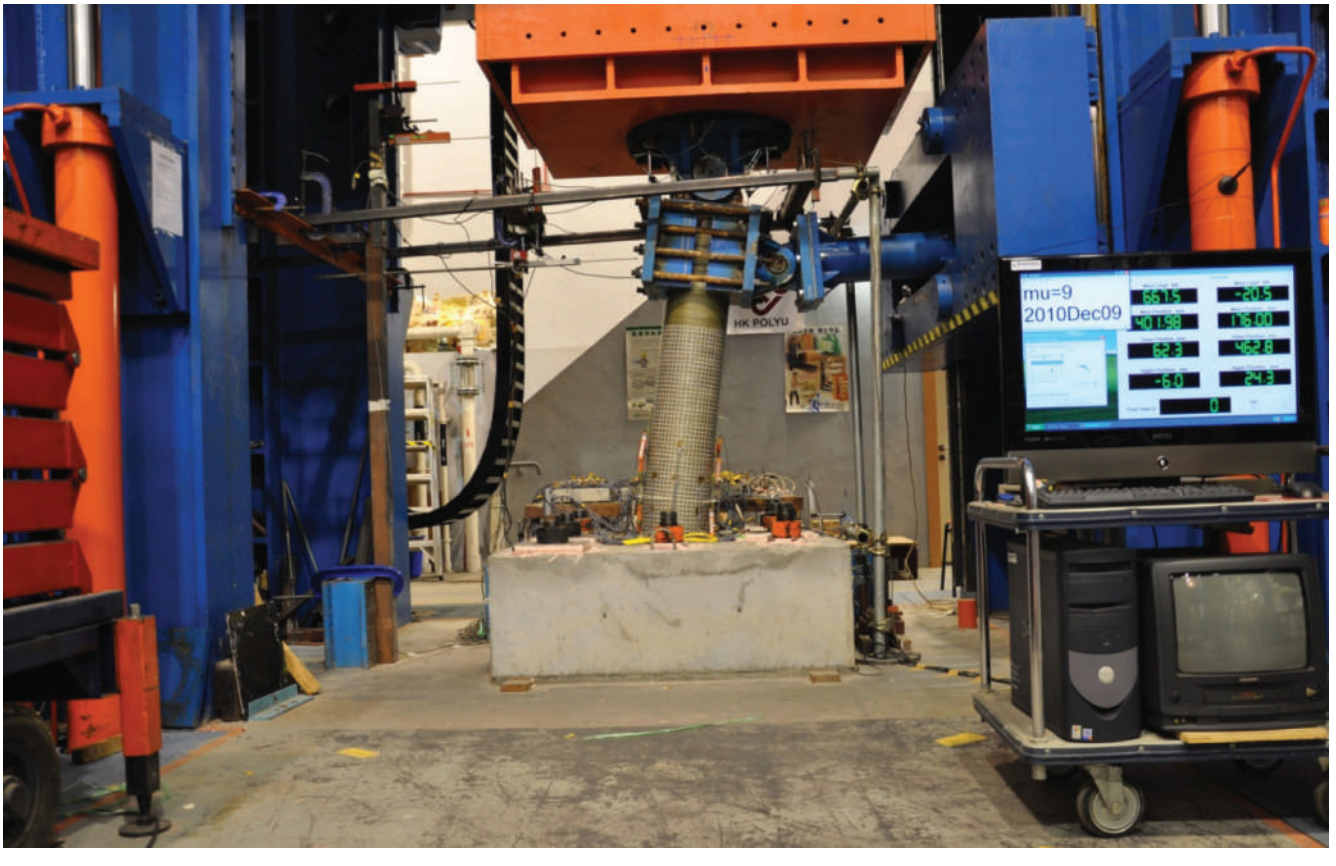

Fig. 10. Full-scale cyclic lateral loading test of a hybrid DSTM. (Photo courtesy of Professor J.-G. Teng)

Girao, A. and Bijlaard, F.S.K. (2008), "High Strength Steel in Buildings and Civil Engineering Structures," *International Symposium on Innovative Design of Steel Structures*, University of Hong Kong, December 5, pp. 15–42.

Griffis, L.G. (1986), "Some Design Considerations for Composite Frame Structures," *Engineering Journal*, AISC, Vol. 23, Second Quarter, pp. 59–64.

Han, L.-H., Wang, W.-D. and Tao, Z. (2011), "Performance of Circular CFST Column to Steel Beam Frames under Lateral Cyclic Loading," *Journal of Constructional Steel Research*, Vol. 67, No. 5, pp. 876–890.

HKBD (Hong Kong Buildings Department) (2005), *Code of Practice for the Structural Use of Steel (Limit State Approach)*, Hong Kong, China.

Li, G.-Q. (2004), "Aseismic Design of Steel Structures in China," *International Symposium on Worldwide Codified Design and Technology in Steel Structures*, Hong Kong Institute of Steel Construction, Hong Kong, 9–10 February, pp. 69–78.

Li, G.-Q. and Mativo, John (2000), "Approximate Estimation of the Maximum Load of Semi-Rigid Steel Frames," *Journal of Constructional Steel Research*, Vol. 54, No. 2, pp. 213–225.

Li, W. and Han, L.-H. (2011), "Seismic Performance of CFST Column to Steel Beam Joints with RC Slab: Analysis," *Journal of Constructional Steel Research*, Vol. 67, No. 1, pp. 127–139.

Tao, Z., Han, L.-H., Uy, B. and Chen, X. (2011), "Post-Fire Bond between the Steel Tube and Concrete in Concrete-Filled Steel Tubular Columns," *Journal of Constructional Steel Research*, Vol. 67, No. 3, pp. 484–496.

Vallenilla, C.R. and Bjorhovde, R. (1990), "Behavior of Composite Frames during Construction," *Journal of Constructional Steel Research*, Vol. 15, No. 1, pp. 3–21.

Wang, J.-F. and Li, G.-Q. (2008), "A Practical Design Method for Semi-Rigid Composite Frames under Vertical Loads," *Journal of Constructional Steel Research*, Vol. 64, No. 2, pp. 176–189.